

New Achievements and Configurations of Helical Resonator Filters for
Space Applications –Theory and Design

Giuseppe Salza

Submitted for the degree of Doctor of Philosophy

Heriot-Watt University

School of Engineering & Physical Sciences

January 2018

The copyright in this thesis is owned by the author. Any quotation from the thesis or use of any of the information contained in it must acknowledge this thesis as the source of the quotation or information.

ABSTRACT

The satellite for communication uses frequencies from UHF band (300MHz to 3 GHz) up to Ka band (40GHz). The dimensions of the components in the satellite transponder, usually decrease with the frequency increment. For the Ka band typical dimensions of the microwave components are in the order of 10mm while for lower frequencies such as UHF band, the dimensions are in the order of 100mm. For this last case, there is the necessity of the reduction of the size of the component to save mass and minimize the footprint in the satellite transponders.

This work focuses on the filters that compose the input and output multiplexer (IMUX and OMUX) for the UHF band applications. In particular, the OMUX manage several hundred of watts of RF power, so, in this case, the filters has to be designed for high power, maintaining the small dimensions and low mass. In the thesis, prototypes waveguide filters loaded by single helical resonator were designed and manufactured. The prototypes were tested for high power in ESA-VSC High Power RF Laboratory in Valencia to verify their power handling characteristics.

For the IMUX, the thesis concentrates on the mass and dimensions saving due to the fact that, for UHF band, typical size of waveguide filters is higher than 100mm. the proposed solution is to use a dual mode concentric helices filters. The novelty of this kind of solution required the development of the mathematical background for the first dimensioning and analysis of filter characteristics. All the theory developed is reported in this work. The output of this procedure is the design and simulation of a very compact dual mode concentric helices filter (28.08mmx28.08mmx10.36mm). A prototype is produced using 3D additive manufacturing technique and the test campaign is in progress.

In conclusion, for the helical resonator filter in OMUX, the high power test confirms that this technology is promising for power handling purposes and gives some suggestions for future development such as changing the helix geometry and loading the helices with dielectrics. For the dual mode concentric helices filter, the hope is that the test campaign will confirm the designed results and after, the possible next step is to improve the design for high power applications.

DEDICATION

To My Family: Without them I would not have come anywhere.

To Savvas and George for believing in my skills.

My wife for the constant and loving support

ACADEMIC REGISTRY

Research Thesis Submission


Name:	Giuseppe Salza		
School:	Engineering and Physical Science		
Version: <i>(i.e. First, Resubmission, Final)</i>	Final	Degree Sought:	PHD

Declaration

In accordance with the appropriate regulations I hereby submit my thesis and I declare that:

- 1) the thesis embodies the results of my own work and has been composed by myself
- 2) where appropriate, I have made acknowledgement of the work of others and have made reference to work carried out in collaboration with other persons
- 3) the thesis is the correct version of the thesis for submission and is the same version as any electronic versions submitted*.
- 4) my thesis for the award referred to, deposited in the Heriot-Watt University Library, should be made available for loan or photocopying and be available via the Institutional Repository, subject to such conditions as the Librarian may require
- 5) I understand that as a student of the University I am required to abide by the Regulations of the University and to conform to its discipline.
- 6) I confirm that the thesis has been verified against plagiarism via an approved plagiarism detection application e.g. Turnitin.

* Please note that it is the responsibility of the candidate to ensure that the correct version of the thesis is submitted.

Signature of Candidate:		Date:	07/05/2018
-------------------------	-------------------------------------------------------------------------------------	-------	------------

Submission

Submitted By <i>(name in capitals)</i> :	
Signature of Individual Submitting:	
Date Submitted:	

For Completion in the Student Service Centre (SSC)

Received in the SSC by <i>(name in capitals)</i> :			
Method of Submission <i>(Handed in to SSC; posted through internal/external mail):</i>			
E-thesis Submitted (mandatory for final theses)			
Signature:		Date:	

TABLE OF CONTENTS

CHAPTER 1	INTRODUCTION	4
1.1	GENERAL INTRODUCTION	4
1.1.1	<i>Introduction on satellite communication systems.....</i>	4
1.1.2	<i>Previous work on helical resonator filters</i>	9
1.1.3	<i>Motivations and Objectives</i>	10
1.1.4	<i>Description of the chapters in the thesis</i>	11
CHAPTER 2	- HELICAL RESONATORS THEORY	14
2.1	ANALYSIS AND NUMERICAL TECHNIQUES OF UNIFORM RADIUS HELIX	14
2.1.1	<i>The helical structure.....</i>	14
2.2	NUMERICAL TECHNIQUES FOR HELICAL RESONATOR.....	16
2.3	DESIGN OF HELICAL RESONATOR	19
2.4	FILTER SYNTHESIS	22
2.4.1.1	Transfer function.....	22
2.4.1.2	Prototype circuit.....	27
2.4.2	<i>Coupling determination.....</i>	30
CHAPTER 3	- LARGE GAP CONCEPT FOR OMUX HELICAL FILTERS.....	36
3.1	INTRODUCTION	36
3.2	PRESENTATION OF DESIGNED PROTOTYPES	39
3.2.1	<i>REXOLITE 1422™ characteristics</i>	41
3.2.2	<i>The Long Length Cavity Case</i>	41
3.2.2.1	Cylindrical helical resonator filters without REXOLITE 1422™	42
3.2.2.2	Step conical helical resonator filters without Rexolite 1422™	43
3.2.2.3	Cylindrical helical resonator filters with Rexolite 1422™	44
3.2.2.4	Step conical helical resonator filters with Rexolite 1422™	44
3.2.3	<i>The Small Length Cavity Case</i>	46
3.2.3.1	Cylindrical helical resonator filters without Rexolite 1422™	47
3.2.3.2	Step conical helical resonator filters without Rexolite 1422™	48
3.2.3.3	Cylindrical helical resonator filters with Rexolite 1422™	48
3.2.3.4	Step conical helical resonator filters with Rexolite 1422™	49
3.2.4	<i>The Medium Length Cavity Case</i>	51
3.2.4.1	Cylindrical helical resonator filters without Rexolite 1422™	52
3.2.4.2	Step conical helical resonator filters without Rexolite 1422™	52
3.3	MULTIPACTOR ANALYSIS	54
3.3.1	<i>The Long Length Cavity Case</i>	56
3.3.2	<i>The Medium and Short Length Cavity Cases</i>	58
3.3.3	<i>Small length cavity with rexolite</i>	64
3.3.4	<i>Designed prototypes and multipaction analysis results</i>	65
CHAPTER 4	- TEST CAMPAIGN OF OMUX STUDY	69
4.1	MANUFACTURING OF THE PROTOTYPES	69
4.1.1	<i>Prototype manufacturing.....</i>	69
4.1.1.1	Cavity.....	70
4.1.1.2	Helix	77
4.1.1.3	Tuning.....	78
4.1.1.4	Assembly and plating.....	80
4.1.2	<i>Low Power test.....</i>	81
4.1.2.1	RF test campaign.....	81
4.1.3	<i>High Power test.....</i>	84
4.1.3.1	High power test premises	84
4.2	DISCUSSION	89
4.2.1	<i>Conclusion.....</i>	89
CHAPTER 5	- IMUX.....	92
5.1	INTRODUCTION	92
5.1.1	<i>Potential applications of the dual mode concentric helices</i>	92

5.1.2	<i>Dual mode helical resonator filters</i>	95
5.1.3	<i>The evolution of the helical structures: Higher order modes of the concentric helices</i>	97
5.1.4	<i>The concentric helix structure</i>	98
5.2	FILTER DESIGN	102
5.2.1	<i>Synthesis and Analysis of dual mode filter</i>	102
5.3	DESIGN EXAMPLES 4TH ORDER FILTER.....	108
5.3.1	<i>4th order</i>	108
5.4	DISCUSSION	112
CHAPTER 6 – CONCLUSIONS AND FINAL CONSIDERATION		116
6.1	GENERALS	116
6.2	OUTPUT FILTERS – THE OMUX	116
6.3	INPUT FILTERS – THE IMUX	117
6.4	CONCLUSIVE REMARKS.....	118
APPENDIX		121
FORMULAS IN CHAPTER 2		121
	<i>Field Inside Helix</i>	121
FORMULAS IN CHAPTER 5		122
	<i>Fields inside concentric helix</i>	122
	<i>Analysis and numerical techniques of concentric helix</i>	123
	<i>Coefficients of the Fields of concentric helices</i>	129

LIST OF PUBLICATIONS BY THE CANDIDATE

1. **Giuseppe Salza**, George Goussetis, Carlos Vicente, Marta Reglero, Mariam Taroncher, Vicente Boria, Nikolas Sidiropoulos, Jaione Galdeano, Marco Guglielmi, Efstratios Doumanis, Savvas Kosmopoulos – “Helical resonator with modulated radius for improved multipactor threshold: Numerical and experimental results” - 46th European Microwave Conference (EuMC), London, UK, 2016
2. **Giuseppe Salza**, George Goussetis, Jaione Galdeano, Marco Guglielmi – “Quality factor of helical coaxial cavity resonators with modulated radius” - 44th European Microwave Conference (EuMC), Rome, Italy, 2014
3. **Giuseppe Salza**, Jaione Galdeano, Dr. George Goussetis, Carlos Vicente, Ivàn Arregui, Vicente Boria Esbert, Dr. Savvas A. Kosmopoulos, Dr. Nikolas Sidiropoulos, Marco Guglielmi – “On the design of space qualified uhf high power helical resonator filters: a comparison among simulated and experimental electrical performance” - 6th CNES/ESA International Workshop on Microwave Filters, Toulouse, France, 2015
4. **G. Salza**, C. Vicente, I. Arregui, M. TaroncherCalduch, M. Reglero, J. Galdeano, M. Guglielmi, V.BoriaEsbert, G. Goussetis, S.A. Kosmopoulos - “Multipactor Analysis of Helical Resonator Filters with Improved Power Handling Capability” - International workshop on Multipactor, Corona and Passive Intermodulation (MULCOPIM), ESA High Power Lab., Valencia, 2014.
5. **Giuseppe Salza**, George Goussetis, Carlos Vicente, Savvas Kosmopoulos, Marta Reglero, Máriam Taroncher, Vicente E. Boria, Nikolas Sidiropoulos, Jaione Galdeano – “Helical Resonator Filters with Improved Multipactor Performance Exploiting Rigorous Modeling and the Large Gap Approach”, Submitted to IET Microwaves, Antennas & Propagation.

CHAPTER 1 INTRODUCTION

1.1 General introduction

1.1.1 Introduction on satellite communication systems

A satellite communication system can be considered as a platform that allows two or more users to communicate, so to exchange information in a variety of ways. Differently from other communication systems, the satellite is a unique system of its kind: in fact, the transponder is housed on the satellite orbit around the earth, so the satellite "sees" a large terrestrial ground at once. A key parameter relating to a satellite system is the operating orbit; typically a telecommunications satellite occupies special orbits. Examples of common orbit for telecommunication purposes are:

- Geostationary orbit (GEO)
- Geosynchronous orbit (GSO)
- Elliptic Synchronous orbit

In general, a satellite in one of these orbits maintains a precise synchronization with the Earth's rotation so that the satellite always sees the same point on the Earth's surface. A system of three GEO orbit satellites, each separated by 120° longitude, can receive and send radio signals so that they have full coverage of the globe, with the exception of small regions around the North and South poles (see Figure 1.1.1-1). The distance of the GEO satellite from the Earth's surface is at least 36000km, which makes the design of the microwave communication link very difficult mainly in the size of the signal power received.

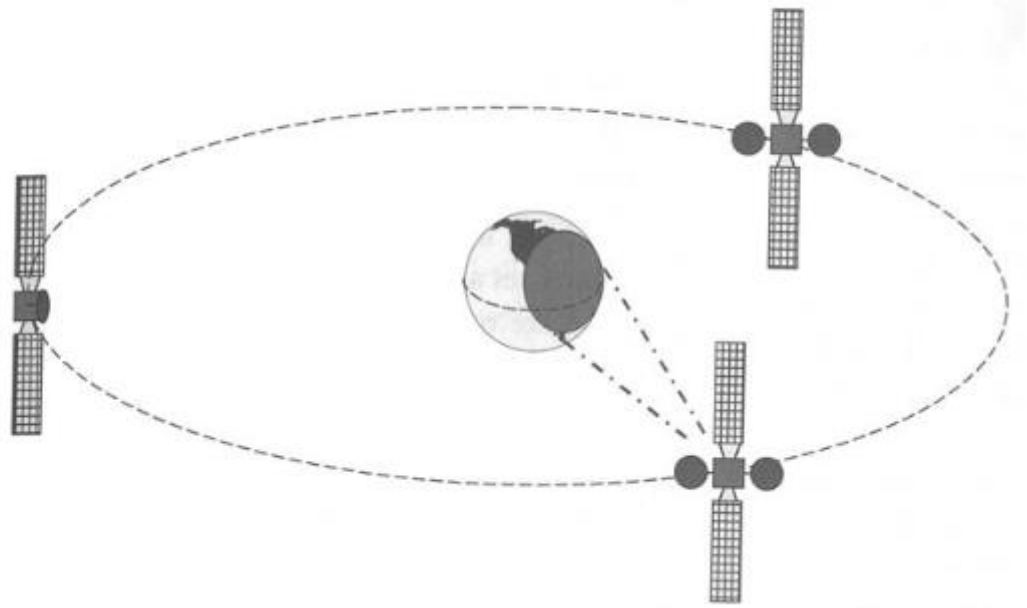


Figure 1.1.1-1: A system of three geostationary communication satellites provides nearly worldwide coverage.

In general, a telecommunications satellite brings specific advantages compared to other wireless communication platforms and installations. A key benefit arises due to the fact that the satellite manages to "see" an important terrestrial area at one time. Thus, as a result of this observation, the advantages of a telecommunications satellite can be summarized as follows:

- **Mobile communications independent of the location**

Any user with a suitable ground station can connect via satellite while it is in its footprint. This way, a radio communication link between the satellite and the user can be established. The user can be stationary, or fixed, or moving, or mobile.

- **Wide coverage area: Regions, continents, globe**

The coverage of a satellite serves whole areas as extensive as continents. In fact, when properly designed, a satellite can serve any kind of region it can see.

- **Extensive bandwidth**

The availability of spectrum frequencies for satellites is ample and satellite service users have access to an extended bandwidth, mainly for fixed services. It should be remembered

that bandwidth is the measure of the capacity of communication channels. Most satellite communications occur at microwave frequencies from the UHF band (from 300 MHz to 3 GHz) to the Ka band (from 27 GHz to 40 GHz).

- **Independence from Earth Infrastructure**

Since a satellite can be seen as a repeater in space, a satellite creates a microwave connection for ground stations. Then, installing earth stations directly at the application points allows users to communicate without external connections. This feature can be attractive for those regions where terrestrial infrastructures are poor or non-existent.

Now focusing the attention on payloads, general definitions to define telecommunication payload components are provided. The satellite transponder performs receiving, processing and retransmission functions. Receiving the ground signal at the satellite is referred to as Uplink, while satellite-to-ground broadcasting defines Downlink. The following Figure 1.1.1-2 shows a diagram of a simplified block of a typical telecommunications payload.

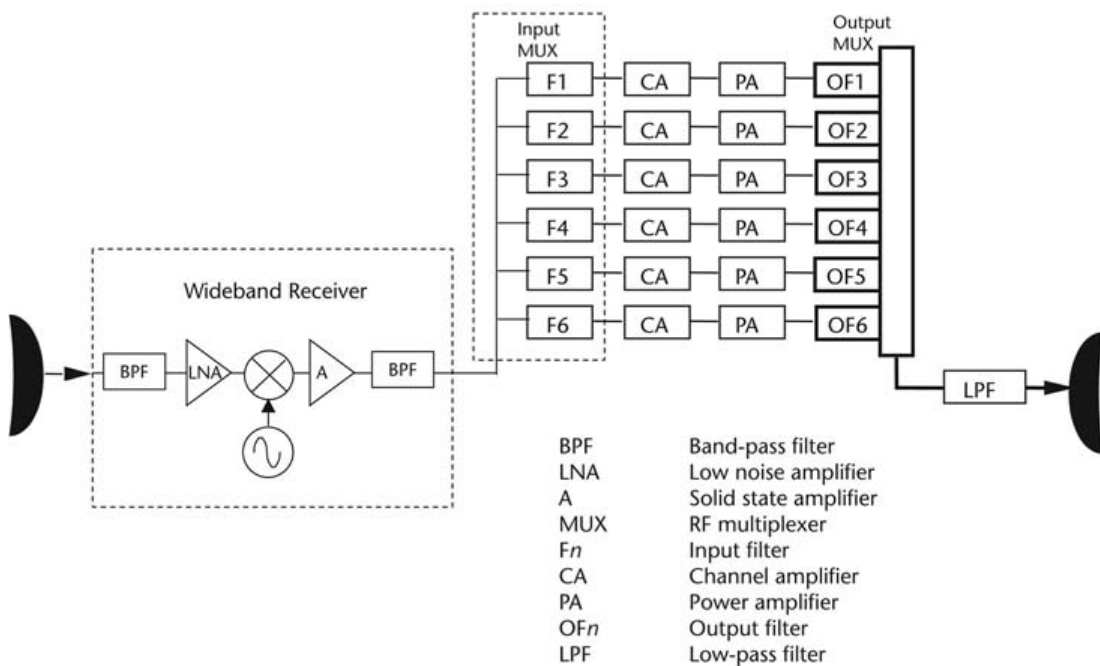


Figure 1.1.1-2: Simplified block diagram of telecommunication payload [RD.01]

The diagram in the figure shows a payload that can handle a multitude of channels in Uplink and Downlink by operating only frequency translations and amplifications. In detail, all uplink signals are first amplified (LNA) and then transmitted in frequency

(Mixer) from Uplink band to Downlink band; This operation is performed by the Wideband Receiver. Next, after the Wideband Receiver, there is the Input Multiplexer (IMUX), Power Amplifiers (PAs) and Multiplexer Outputs (OMUX). All the complete set of amplified channels output from the OMUX is then passed from the payload transmission antenna.

As it is understood, the IMUX separates the channels to be amplified, while the OMUX recombines them for transmission. The received signal from earth to satellite (uplink), is composed by several carriers that share the same band; in this way, a large number of intermodulation products is introduced into the system. When the level of the noise, generated by this intermodulation, becomes extremely high for a single wide band amplification, the system frequency band is divided into several sub bands. This operation of frequency division is called channelization and the sub bands are called channels. The splitting of the band into channels produces distortions that are minimized by using filters which restricts the channel widths. In order to have a good level of the signal, a channel amplification occurs for the maximization of the ratio between signal respect to noise ([RD.02]). A typical multiplexer contains a microwave filter for each channel, to filter the bandwidth for that channel and reject all the other. Since the interest of this work is the UHF / VHF telecommunication payloads, and in particular the IMUX and OMUX in these bands, the features of these components at the frequencies of interest will now be described.

UHF/VHF OMUX

As can be seen from previous considerations, OMUX components are often subject to a very high input power that can be up to hundreds of Watts. For a UHF payload, typical high power levels can be considered an input power to the device ranging from 60W to 100W[RD.03]. In addition, to ensure sufficient signal quality to be transmitted, filters in the OMUX need very low insertion losses, which result in the requirement for a high quality factor. For UHF / VHF filters, high quality factors are in the order of magnitude ranging from 1000 to 2000 [RD.04]. In addition, and once the cost of launching is considered, limited volume and mass budgets are critical. Therefore, the desirable features for an OMUX filter are:

- High power management capabilities

- High quality factor
- Reduced weight
- Limited dimensions and mass

The considerations that have been made on power and quality factor exclude the use of lumped element filter filters and SAW filters. Instead the best performance in terms of quality factor and power management, would be distributed filters such as, for example, waveguide filters. However, considering that frequencies are being considered in the UHF / VHF band, the dimensions and weights of this type of filters are excessive. The real challenge is therefore to get working filters that best meet the features mentioned above. In this work, we have tried to give a promising alternative to current technologies: filters composed by waveguide cavity that host helices have been designed and implemented. In fact, helical resonators can be a promising quality factor (1300 @ 300MHz) and size and weight, while being critical to power management. In this thesis, various strategies have been evaluated to contain and limit the deleterious phenomena related to power by making prototypes that have been tested.

UHF/VHF IMUX

Respect to the OMUX, the component filters are not subject to high powers; However, even in this case, the desirable features are:

- High quality factor
- Reduced weight
- Dimensions contained

In this work, however, the helix technology is designed to produce a very compact filter. The method used was to implement a dual mode configuration, much used to make the filters more compact.

The electromagnetic design of this innovative filter has been concluded; and the real challenge is to implement the solution using the right manufacturing technique. Due to the particular geometry, the strategy is to using a 3D additive manufacturing technique. The realized prototype has to be assembled and it has to perform the RF measurements test campaign.

1.1.2 Previous work on helical resonator filters

Initial work on helices were done in [RD.05]. In this work, the basic equation of the helix for traveling wave tube were derived and analyzed.

Coaxial resonators with helical inner conductor were studied in [RD.06]. In this work, a quarter-wave helical resonator inside a below-cutoff metallic cavity were investigated. This work, that uses results of [RD.05], reports simple equations and charts that are useful for the designer for the dimensioning of the helical resonator. Measured results are also presented for the unloaded Q as a function of certain design parameters as well as for resonant frequencies from a few MHz up to 500 MHz. The limitation of this work is that only resonators with shield of circular cross sections are analyzed. The first filter realization using helical resonators was performed in [RD.06] while the first documented work on the interdigital helical resonator filters is reported in [RD.07]. All the results presented here are derived using empirical relation for the filter realization. Some attempt using a more structured design was tried in works [RD.08] – [RD.13], where the properties of the helical structure is theoretically and experimentally explored.

A practical helical resonator filter using an improved design procedure is given in [RD.14]. The filter was at the output of a low-power UHF land mobile transmitter. Also a theoretical approach for the determination of unloaded Q is given. Experimental results for a 3-pole filter are presented. A new helical resonator, resonant for lengths of approximately half wavelength is presented in [RD.15]. A prototype is shown where the resonator consists of a helical transmission line wound between two SMA connectors with a portion of the coil connected to the ground at each end. An equivalent lumped element circuit is also given. The unloaded Q for the resonator at a resonant frequency of 900 MHz is measured to be 582.

All the filters reported until now were designed considering single mode operations and are collected and rationalized into [RD.17].

Finally works in [RD.18] explores the helical resonator filters for high power applications.

New attempt considering dual mode operations were tried in [RD.19] but, as described in that work, the concept seems to be not well understand. In order to move from the described dual mode operations in [RD.19] to totally new concept, works from [RD.20] to [RD.23] on concentric helices is studied.

1.1.3 Motivations and Objectives

This thesis starts from what has been done in [RD.18]; the authors recognizes the importance of a more critical and not empirical approach in the helical resonator design, but a direct approach using the EM simulator for the design is preferred. In this way, the synthesis process results not very efficient and requires time consuming procedure. In this work, when it is possible, a rigorous theoretical approach is followed and mathematic expressions were extensively explored and explained. The use of this way to proceed permits to explore different topologies of helical resonators geometries suitable for power handling for single helices in OMUX. So, the work in the first part could be divided as follows:

- 1) Description of theoretical and mathematical approach for the single helix
- 2) Design of helical resonator filters in single mode operation
- 3) Test campaign

For the second part of the work, the same rigorous approach is used in order to design the dual mode filter using concentric helices. This way to proceed is necessary for this totally new filter concept proposed here.

The objective of the thesis could be summarized in the following few points:

- Using theory for the design of filters
- Design filters for high power operation
- Tests the filter for multipaction

- Propose improvements for future work
- Design dual mode concentric helix
- Propose a solution for the physical manufacturing of the dual mode filter.

1.1.4 Description of the chapters in the thesis

The Objectives of this thesis work are divided, as natural, in the development of the filters for Input Multiplexer (IMUX) and Output Multiplexer (OMUX). In particular for the IMUX, the work is focused on the reduction of the mass and size; in fact this point is crucial for components in satellite payload: the mass and dimensions savings permits to increment the functionalities of the payload. For passive microwave band pass filters, The most common technique used to meet the requirement of mass reduction and size saving is to realize a dual mode topology: in some particular conditions (mainly due to a symmetry of the filter geometry) two modes resonate in the same cavity; in this way, at one single physical cavity corresponds to two electromagnetic cavities. Using this technique, it is possible to obtain an high order filter with reduced numbers of cavities.

For the OMUX, the work concentrates on the improvement of the power handling characteristics much more than the dimensions and mass savings. Different prototypes are studied and optimized in order to meet high power in transmission. The structure of the cavity that host the helices and the helices shapes are optimized to meet the multipaction characteristics. The filter topology is a classical Chebichev filter.

Normally, an high rejection in the upper frequency bandwidth is desirable filter characteristics. In order to improve this, is common practice to increase the number of resonators in the filter; this means that the order of the filter will increase. With the increment of the filter order, the dimensions of a filter becomes larger. If there are requirements in the filter dimensions, it is possible to improve the far out of band response by using a transmission zero properly allocated in the higher frequency band. This kind of filter topology is called pseudo-elliptic or generalized Chebichev. The filters in the IMUX and OMUX implement this last solution.

In this first chapter there are a very brief introduction of the satellite communication systems and the importance of the multiplexing. After that, the focus is on the filters for IMUX and OMUX in UHF/VHF band. The chapter is completed by a review of the previous work related to the argument.

In second chapter there is the description of the helical resonators filter Used for the OMUX. First of all it is presented the theoretic background related to the characteristics of helical structure. The Eigenmode equation used for the determination of the propagation constant, is described and solved using a semi-analytic technique developed by the author of this thesis. The calculated values of the propagation constant is used for the calculation of the quality factor. After the description of these numerical techniques, a review regarding the design on the filter synthesis is presented. The chapter is concluded by the design of a single mode pseudo-elliptic helical resonator filter.

In chapter 3 is presented the design of the filter prototypes that potentially could be used for high power application. All the designed prototypes are simulated for multipactor effect in order to make a choice of the filters eligible for manufacturing. At the end of the chapter, the final choice for the manufacturing is presented.

Chapter 4 starts from the filters presented in the previous chapter and shows all the manufacturing and silver plating process. Also the low power RF test for all filters is explained. The chapter is concluded by the presentation of high power test in VAL SPACE premises.

The second part of the thesis starts from Chapter 5. It presents a brief introduction on potential applications of dual mode filters. The dual mode concept applied in helical resonator filters is described and it is improved in the new conception of concentric helices. All the theory of the concentric helices is developed and described in details. Using the developed theoretical background, the synthesis and analysis of a second order dual mode filter with concentric helices is performed. At the end of the chapter, a 4th order pseudo-elliptic helical resonator filter with concentric helices is presented.

In last chapter 6 there are the conclusions and the lessons learnt during all the test campaign (OMUX) and the presentation of a possible technique (3D additive

manufacturing) for the realization of the 4th order dual mode concentric helices filter. Possible future development are explained at the end of the chapter.

CHAPTER 2 - HELICAL RESONATORS THEORY

2.1 Analysis and numerical techniques of uniform radius helix

2.1.1 The helical structure

The first researches about the electromagnetic fields associated with a coaxial line with a helical inner conductor were intimately connected with the development of traveling wave tubes (TWT). Although the requirements for a TWT are different compared to those of a resonator filter in a helix at a quarter wavelength, the basic assumptions in assessing the electromagnetic fields of a transmission line in the helix are applicable to both. The fundamental problem involves the search for explicit expressions, or methods to evaluate the behavior of electromagnetic fields in a helical structure.

The reasons why the knowledge of electromagnetic fields is important are essentially two. First of all, the knowledge of the propagation constant leads to the determination of the electrical length and binds the size of a line in helix to $\lambda/4$ at its resonant frequency. In addition, the knowledge of electromagnetic fields is necessary to know the quality factor Q . Second, the form field indicates which is the dominant component for coupling mechanisms, thus giving an estimate of what extent, location and orientation must have an element of coupling, such as for example, an iris, a post or an opening.

The reference model for the calculation of electromagnetic fields is that of Sheath helices. This is the model in which the helix is represented by a cylinder which leads only along a specified direction by the angle ψ of the pitch of the helix. No current can flow perpendicular to this direction. In the following Figure 2-1 you can see the dimensions sheath helix characteristics, inside a cylindrical cover.

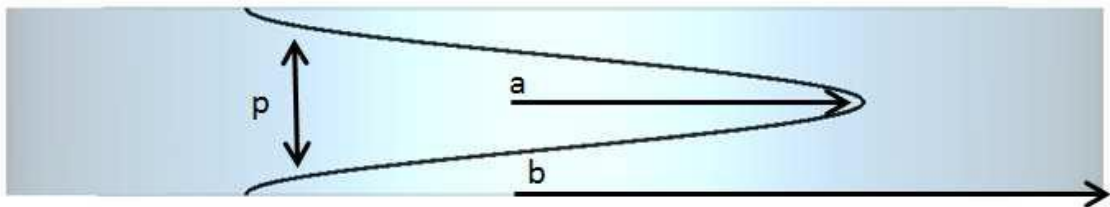


Figure 2-1: Definition of Sheath helix dimensions

A solution of Maxwell's equations in cylindrical coordinates, for the helix problem sheath inside a cylindrical cover ([RD.17]), needs to satisfy the following boundary conditions:

1. The helix is a surface that conducts only along the direction specified by the angle of the pitch; whereby the tangential electric field is perpendicular to the helix when $r = a$

$$E_z^i \sin \psi + E_\theta^i \cos \psi = 0 \quad (2-1)$$

$$E_z^o \sin \psi + E_\theta^o \cos \psi = 0 \quad (2-2)$$

2. Component of the tangential electric field is normal to the direction of ψ is continuous along the cylinder $r = a$

$$E_z^i \cos \psi - E_\theta^i \sin \psi = E_z^o \cos \psi - E_\theta^o \sin \psi \quad (2-3)$$

3. tangential component of the magnetic field along ψ must be continuous for $r = a$

$$H_z^i \sin \psi + H_\theta^i \cos \psi = H_z^o \sin \psi + H_\theta^o \cos \psi \quad (2-4)$$

4. In $r = b$ the tangential electric field and the normal magnetic field must be zero:

$$E_z^o = 0 \quad (2-5)$$

$$E_\theta^o = 0 \quad (2-6)$$

$$H_r^o = 0 \quad (2-7)$$

These boundary conditions lead to express the components of the electric and internal and external magnetic field by the helix in the fundamental mode, as reported in APPENDIX (formulas pag.121).

This set of equations therefore allow to determine the electric and magnetic fields of an infinitely long helix inside a cylindrical cover. To determine total fields, one has to first determine the propagation constant γ . It is shown that the propagation constant γ is related to β_0 as reported below (from [RD.25] to [RD.27]):

$$(\beta_0 a \cot \psi)^2 = (\gamma a)^2 \frac{I_0(\gamma a) \Delta_1}{I_1(\gamma a) \Delta_0} \quad (2-8)$$

This equation is very important and it is called Eigenvalue Equation; it relates the frequency to wave length λ_g and the propagation constant β . Using this information, one can calculate all the other quantities that are characteristic of a microwave resonator.

Among all these quantities, an important role plays the quality factor Q_u . It defines the quality factor of a resonator, the ratio between the stored energy density compared to that dissipated for losses in a resonator:

$$Q_u = \omega \frac{W_E + W_M}{P_{loss}} \quad (2-9)$$

Where expressions of power stored in electric and magnetic field (W_E, W_M) and power dissipation are:

$$W_E = \frac{\epsilon}{4} \iiint E \cdot E^* r dr d\theta dz \quad (2-10)$$

$$W_M = \frac{\mu}{4} \iiint H \cdot H^* r dr d\theta dz \quad (2-11)$$

$$P_{loss} = \frac{R_s}{2} \iint H_t^2 dS \quad (2-12)$$

$$R_s = \frac{\sqrt{2}}{2} \sqrt{\frac{\omega\mu}{\sigma}} \quad (2-13)$$

Since, as can be seen from the equations, the expressions of the fields change depending on the considered region (internal or external by the helix), the expressions of the terms of dissipated power and stored power will be given by the following expressions:

$$W_E = W_E^i + W_E^o \quad (2-14)$$

$$W_M = W_M^i + W_M^o \quad (2-15)$$

$$P_{loss} = P_{loss}^h + P_{loss}^c \quad (2-16)$$

where superscripts "i" and "o" are to be understood as the internal and external components, respectively, while with the superscripts "h" and "c" are understood as the components on the helix the outer surface and inner surface of the cylindrical cover.

The expression of losses due to dissipation is given by the following expressions([RD.24])

$$P_{loss}^h = \pi R_s \int_0^z H_t^2 a dz \quad (2-17)$$

$$P_{loss}^c = \pi R_s \int_0^z H_t^2 (b - a) dz \quad (2-18)$$

where, H_t It is the expression of the tangential magnetic field.

From these expressions is the ratio of the energy stored with respect to the power dissipation can be estimated as the sum of the same ratio in each revolution of the helix by normalizing with respect to the total number of laps. The calculation can be performed with a semi-analytical technique. In particular, numerically integrating the components of the fields can provide the total power stored. Considering the particular geometry of the problem, the integration is conveniently performed in a cylindrical co-ordinate system, as shown by the following equations

$$W_E^i = \frac{\epsilon}{4} \int_0^{2\pi} d\theta \int_0^z dz \int_0^a E^i \cdot E^{i*} r dr \quad (2-19)$$

$$W_M^i = \frac{\epsilon}{4} \int_0^{2\pi} d\theta \int_0^z dz \int_0^a H^i \cdot H^{i*} r dr \quad (2-20)$$

$$W_E^o = \frac{\epsilon}{4} \int_0^{2\pi} d\theta \int_0^z dz \int_a^b E^o \cdot E^{o*} r dr \quad (2-21)$$

$$W_M^o = \frac{\epsilon}{4} \int_0^{2\pi} d\theta \int_0^z dz \int_a^b H^o \cdot H^{o*} r dr \quad (2-22)$$

In the next section, we will illustrate the technique used for the calculation of the dispersion and the quality factor report

2.2 Numerical Techniques for helical resonator

As specified previously, the calculation of the dispersion relation provides the essential elements to determine the characteristics of the resonator in the helix. To obtain a numerical solution of the equation, a routine that solves the problem by using a technique

SOR (successive over-relaxation) can be employed ([RD.25]). This numerical method, specialized for this case is expressed as follows

$$f_{n+1} = B \left[\frac{c}{2\pi} \sqrt{\frac{\gamma_{n+1}^2 I_0(\gamma_{n+1} a) \Delta_1}{\cot \psi I_1(\gamma_{n+1} a) \Delta_0}} \right] + (1 - B)f_n \quad (2-23)$$

Where "n" is the index of the iteration and "B" is the SOR parameter that is $0 < B < 2$. A numerical routines for the calculation has been developed and the results were verified by a full wave commercial software (CST TM).

In particular, the structure that has been simulated as follows (see Figure 2-2)

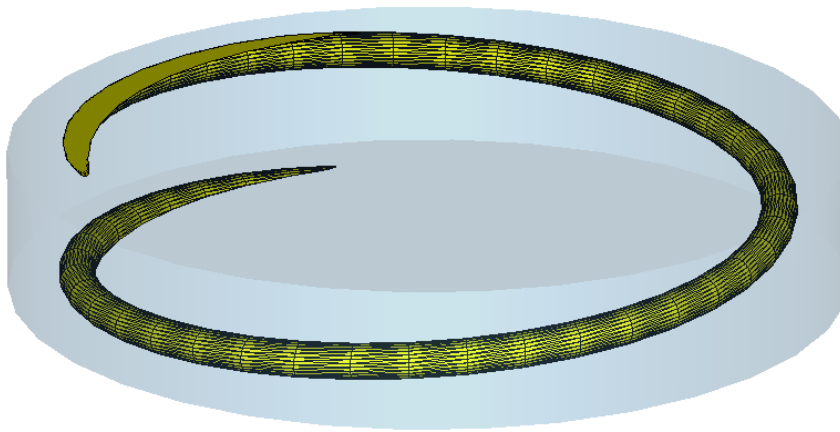


Figure 2-2: Helix Geometry

This model is then simulated using an eigenmode solver and the geometric parameters that were used in the analysis are shown in the table below

Parameter	Value	Description
d	32 [mm]	External Helix diameter
p	6.53 [mm]	Internal Helix pitch
b	38.3 [mm]	External Cylindrical sheath

Table 2-1 : Geometric parameters

The theoretical analysis results were verified with those obtained using electromagnetic simulation and are shown in the Figure 2-3 .

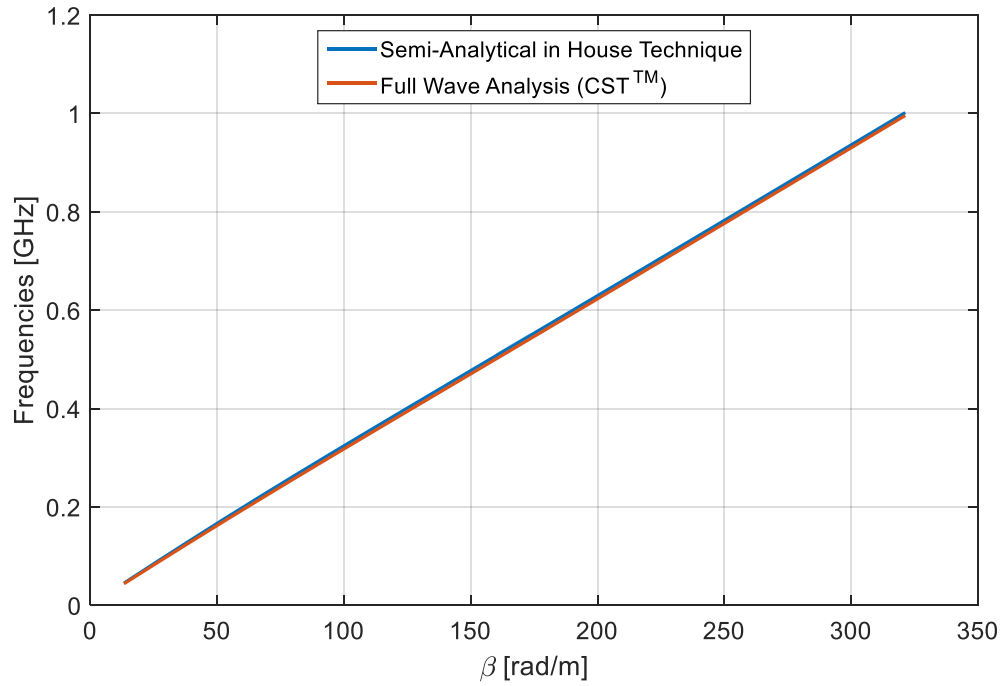


Figure 2-3: Comparison between theoretical and real model

As can be seen, the agreement between the two techniques is sufficiently similar, which confirms:

- the theoretical model helices sheath is sufficiently accurate to describe the helix behavior.
- theoretical model is used to determine the propagation constant for each frequency, for each way in a very short time.
- from the determination of the propagation constant it is possible to calculate the value of the electric and magnetic fields
- from determination of electric and magnetic fields, it is possible to evaluate the quality factor of the resonator

Using the techniques outlined in the previous section, one can then calculate the quality factor in an analytical way. Q analysis was conducted by varying the helix diameter, and the results were verified with CST TM. Below are the results of the analysis and the comparison with those obtained by electromagnetic simulation (Figure 2-4). Based on this agreement, it can be concluded:

- The sheath helices theoretical model is accurate sufficiently to describe the helix behavior

- The theoretical model could be used to determinate the propagation constant for each frequency
- From the propagation constant it is possible to calculate the electrical and magnetical fields
- From electric and magnetic fields it is possible to calculate the Q factor.

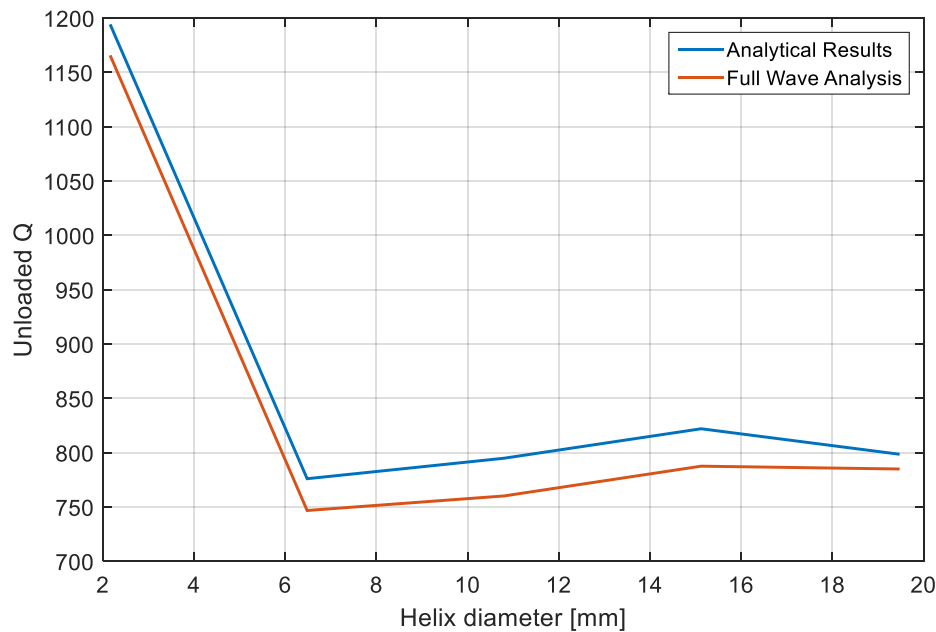


Figure 2-4: Q factor of helical resonator comparison between analytical results and full wave analysis.

The previous Figure 2-4 shows the comparison between the unloaded quality factor calculated with the analytical technique and with full wave simulation. The behaviour of the Unloaded Q is correctly represented: the value tend to decrease with the increasing of the helix diameter, because obviously the losses tend to increase. The slight differences between the analytical and full wave simulation in the figure are mainly related to the fact that the results calculated with closed formulas does not consider the wire thickness while the full wave analysis is obtained using an EM simulator where the more realistic model is realized.

2.3 Design of helical resonator

We face now the problem of filter design. We begin with the determination of the size of single-stranded and then proceed to the tuning procedure of the entire filter. The manufacturing techniques are essentially of two types:

- Procedure via closed formulas using approximate relations ([RD.26])
- procedure through analytical technique.

We will begin with the deal with the case of the synthesis via closed formulas. This kind of technique has been introduced by Zeverev ([RD.26]) and the system of equations which has been obtained is the optimal empirical description of a spiral resonator which maximizes the quality factor.

The formulas that are used in the sizing of helical filters involve the following quantities:

- S that is the amplitude of the rectangular resonant cavity (in meters)
- H is the height of the rectangular resonant cavity (in meters)
- B that is the height of the resonator in the helix (in meters)
- d which it is the helix diameter (in meters)
- N which is the number of helix revolutions
- Z_0 which is the characteristic impedance of the transmission line in the helix of the cavity
- δ which it is the skin depth.

The optimal values of the parameters of the resonator in the helix and of the cavity are as follows:

Cavity

$$\bullet \quad d = 0.66S \quad (2-24)$$

$$\bullet \quad B = S \quad (2-25)$$

$$\bullet \quad H = 1.6S \quad (2-26)$$

$$\bullet \quad Q_0 = 2363S\sqrt{f} \quad (2-27)$$

Cavity

$$\bullet \quad N = \frac{40.6}{S \cdot f} \quad (2-28)$$

$$\bullet \quad \delta = \frac{6.6 \cdot 10^{-5}}{\sqrt{f}} \quad (2-29)$$

$$\bullet \quad Z_0 = \frac{2070}{S \cdot f} \quad (2-30)$$

The circuital value of the helical filter:

$$\bullet \quad L = \frac{0.025}{25.4} n^2 d^2 \left[1 - \left(\frac{d}{D} \right)^2 \right] \left[\frac{\mu h}{mm} \right] \quad (2-31)$$

$$\bullet \quad C = \frac{0.75}{25.4 \log_{10} \left(\frac{L}{d} \right)} \left[\frac{\mu f}{mm} \right] \quad (2-32)$$

The circuital equivalent s reported in the following Figure 2-5

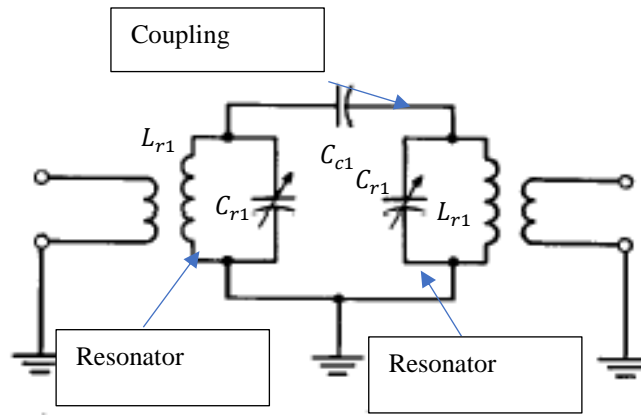


Figure 2-5: circuital equivalent ([RD.26])

At this point it is easy to calculate the circuit parameters that are used to filter design.

In fact, we see that the resonance frequency is expressed as:

$$f_0 = \frac{1}{2\pi\sqrt{LC}} \quad (2-33)$$

So, one can optimize various sizes introduced in order to match as the value of f_0 ; the values obtained provide the magnitudes C_{r1} e L_{r1} . with a total different case is considered for the value C_{c1} ; in fact, the value of the capacitance which provides the coupling, in the case of capacitive coupling, can be obtained by means of a parametric analysis via circuit simulator.

A more complete procedure, which involves an analysis on the helix physical model, rather than the circuit, is referred to as the analytical technique. It consists in analyzing the single resonator in the helix and then to evaluate the coupling which must be implemented by means of a full wave analysis. The advantage of this technique lies mainly in the fact that, working directly with the physical model of the filter, it is also possible to explore very complicated solutions or coupling methods that otherwise could not be evaluated.

All the analysis starts by determining, by means of the techniques developed and explained earlier, the propagation constant of a helix through the dispersion analysis. In the analysis of the fields the following assumptions are employed:

- The configurations of the fields are of type TEM
- The helix internal fields are not disturbed by the external cavity
- Because the components of the fields have the form of traveling waves, the resonator of a quarter of a wavelength can be considered as a section of transmission line which is an open circuit at one end and a short circuit in the other.

This latter point highlights the fact that a uniform helix section, short-circuited on one side and open on the other, it behaves as a resonator to $\lambda/4$. In this way, it is possible to tune all the filter components using common techniques that will be explained in the next paragraph.

First, however, to enter the field of the helix of the filter tuning, it is useful and appropriate, invoke the filter synthesis technique.

2.4 Filter Synthesis

2.4.1.1 Transfer function

The generalized Chebyshev filters, are today among the most used ([RD.27]). The properties that have made their popularity, mainly, the ability to arbitrarily distribute the zeros in transmission and have a steady ripple band.

The S-parameters of a filter (seen as a 2-port network), are the relations between the incident waves and reflected power at its gates. S_{11} will be the relationship between the incident wave and reflected to port 1, while S_{21} is the ratio of the reflected wave at the port 2 and the incident wave at port 1. Both of these terms, for an RF filter, can be expressed as relationship between complex polynomials, according to the following form:

$$S_{11}(s) = \frac{F(s)/\epsilon_r}{E(s)}, S_{21}(s) = \frac{P(s)/\epsilon_r}{E(s)} \quad (2-34)$$

Both $F(s)$ that $E(s)$, have degree N , where N is the filter order, ie the number of resonators from which it is composed. $E(s)$, must be a polynomial of Hurwitz, ie, it must have complex roots only placed in claims quadrants of the complex plane, this, because the network two ports represented by the filter, is supposed without losses. $P(s)$, instead it is a polynomial of degree n_z , the number of zeros in transmission at finite frequencies, and its zeros, are precisely the transmission zeros. The number of zeros at infinity is therefore

N-nz. Combining the orthogonality conditions, unity and reciprocity, it is demonstrated that the following relation must hold for any value of the variable s:

$$-\theta_{n21}(s) + \frac{\theta_{n11}(s) + \theta_{n22}(s)}{2} = \frac{\pi}{2}(2k \pm 1) \quad (2-35)$$

where θ_n is the phase of the polynomial at numerator of S_{21} , S_{11} e S_{22} expressed as phase and modulus: $|S_{11}|e^{j\theta_{n11}}$. Now, we extrapolate that the zeros of the numerator of S_{11} , S_{22} e S_{21} , They must lie in the axis imaginary, or at most, be specularly symmetrical with respect to the imaginary axis, as shown in Figure 2-6. So for the zeros of S_{11} e S_{22} these relations are valid:

$$S_{22i} = -S_{11i}^* \quad (2-36)$$

$$S_{21i} = -S_{21i}^* = S_{21i+1} \quad (2-37)$$

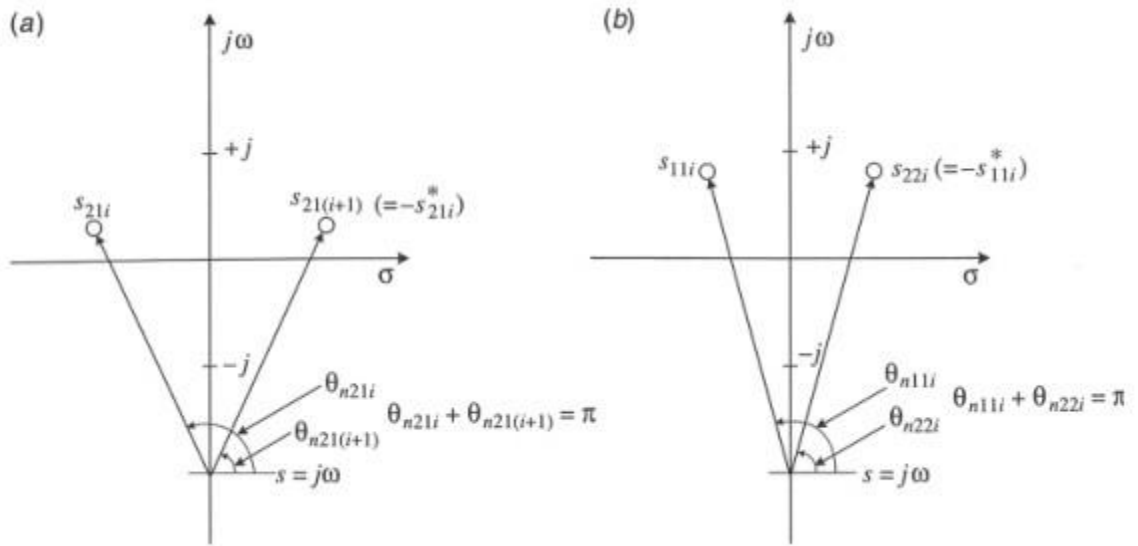


Figure 2-6 Disposition of the S_{21} zeros (a) and disposition of S_{11} e S_{22} zeros (b).

[RD.28]

The expression of the F_{22} , from the zeros of S_{11} is:

$$F_{22}(s) = (-1)^N \prod_{i=1}^N (s - s_{11i})^* = (-1)^N F(s)^* \quad (2-38)$$

Let us now consider the angle of S_{21} , because of the symmetry condition mentioned above, regardless of the nz value and s should be a multiple of $\pi/2$. So, we get:

$$\theta_{n21}(s) = \frac{nz\pi}{2} + k_1\pi \quad (2-39)$$

$$\frac{(N-nz)\pi}{2} - k_1\pi = \frac{\pi}{2}(2k \pm 1) \quad (2-40)$$

In order to satisfy this equation, and then the condition of orthogonality, (N-nz) must be odd. In the case where (N-nz) is equal, then you must add a term $\pi/2$ to the left side. This

means adding $\pi/2$ to θ_{21} that is you must multiply $P(s)$ for j ! Summarizing this information in the scattering matrix, we obtain that:

$$\begin{bmatrix} S_{11} & S_{12} \\ S_{21} & S_{22} \end{bmatrix} = \frac{1}{E(s)} \begin{bmatrix} \frac{F(s)}{\epsilon_r} & \frac{P(s)}{\epsilon} \\ \frac{P(s)}{\epsilon} & \frac{(-1)^{nz+1}F(s)^*}{\epsilon_r} \end{bmatrix} \quad (2-41)$$

From the condition of unity ($SS^* = I$), 2 properties can be derived. One binds the constant of normalization of $F(s)$ and $P(s)$, i.e. ϵ and ϵ_r . The other, is the principle of alternating poles, with which it will be possible to reconstruct one of the three polynomials $E(s)$, $F(s)$ and $P(s)$, knowing the two other (will be used to find $E(s)$). The 2 normalization constants, should be chosen such that the S-parameters are always less than or equal to 1. In addition, it is assumed that the three polynomials E , F and P , have unitary coefficient for the highest degree term. Determining ϵ exploits the knowledge of the value of S_{21} and S_{11} (e.g. for Chebyshev filters), which is known for $s = \pm j$, and is the specified ripple. If $N = nz$, one will have to use the conservation of energy, so:

$$S_{21}^2 + S_{11}^2 = \frac{F(j\infty)F(j\infty)^*}{\epsilon_r^2 E(j\infty)E(j\infty)^*} + \frac{P(j\infty)P(j\infty)^*}{\epsilon^2 E(j\infty)E(j\infty)^*} = \frac{1}{\epsilon_r^2} + \frac{1}{\epsilon^2} = 1 \quad (2-42)$$

However, we recall that the previous relation is only valid for "fully canonical" filters, ie with $N = nz$. The value for ϵ is obtained by evaluating the polynomials at the points where you know the values for the S_{11} and S_{21} parameters, and then forming a system the two expressions and elide the polynomial $E(s)$, still unknown:

$$\epsilon = \frac{1}{\sqrt{10^{RL/10}-1}} \left| \frac{P(\omega)}{F(\omega)} \right|_{\omega=\pm 1} \quad (2-43)$$

$$\epsilon_r = 1, N \neq nz \quad (2-44)$$

$$\epsilon_r = \frac{\epsilon}{\sqrt{\epsilon^2-1}}, N = nz \quad (2-45)$$

Suppose we have already the polynomial $F(s)$, since the transmission zeros are imposed at the outset. Then we also have $P(s)$ (built by the product data monomials by transmission zeros). Therefore, $E(s)$ is obtained using the conservation of energy:

$$\frac{F(s)F(s)^*}{\epsilon_r^2} + \frac{P(s)P(s)^*}{\epsilon^2} = E(s)E(s)^* \quad (2-46)$$

Note, however, that from the previous equation we get the product between $E(s)$ and $E(s)^*$ which will prove to be a polynomial with $2N$ roots. These roots, will be arranged in a symmetrical manner with respect to the imaginary axis.

Extracting the $2N$ roots, recalling that $E(s)$ is a Hurwitz polynomial, and then having roots with negative real part, will provide the physical solutions.

Once the total zeros have been calculated, it is possible to generate the monomials dependent on these zeros and by making the products of these monomials it is possible to calculate the $E(s)$ as in [RD.28].

Although this is a general and mathematically valid procedure, it may happen that for high order filters the roots tend to be more dense towards $s = \pm j\omega$, with consequent loss of precision in the numerical search of zeros. To deal with this you can find a viable alternative, called "method of alternating poles." This is summed up in the following steps::

- Building the complex polynomial $P(\omega) / \varepsilon - jF(\omega) / DK$ and find its zeros
- Conjugate all places zeros in the lower half of the ω plane (equivalent to make the polynomial, a polynomial of Hurwitz), i.e. produce all zeros, negative real part.
- Rebuild $E(\omega)$, with the obtained zeros.

At this point, the polynomial $E(s)$ can be determined (Figure 2-7).

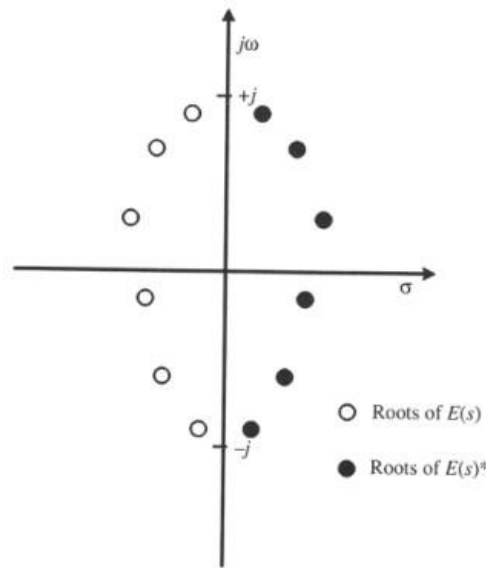


Figure 2-7: 2N zeros of $E(s)E(s)^*$ disposition [RD.28]

Next we address how to find the polynomial $F(s)$ and then perform the operations described above. It is shown that the following relationship is valid:

$$S_{21}(\omega)S_{21}(\omega)^* = \frac{P(\omega)P(\omega)^*}{\varepsilon^2 E(\omega)E(\omega)^*} = \frac{1}{\left[1 - j\frac{\varepsilon}{\varepsilon_r}k_{CN}(\omega)\right]\left[1 + j\frac{\varepsilon}{\varepsilon_r}k_{CN}(\omega)^*\right]} \quad (2-47)$$

where, for generalized Chebyshev filters, for C_N following relationships apply:

$$kC_N = \frac{F(\omega)}{P(\omega)} \quad (2-48)$$

$$C_N(\omega) = \cosh\left[\sum_{n=1}^N \cosh^{-1}(x_n(\omega))\right] \quad (2-49)$$

Considering $\cosh \theta = \cos j\theta$

$$C_N(\omega) = \cos\left[\sum_{n=1}^N \cos^{-1}(x_n(\omega))\right] \quad (2-50)$$

where $x_n(\omega)$:

$$x_n = \frac{\omega - \frac{1}{\omega_n}}{1 - \frac{\omega}{\omega_n}} \quad (2-51)$$

one may notice that when the zeros tend to infinite one obtains $x_n = \omega$ and returns to the case of a not generalized Chebyshev filter.

After various manipulations, one can write the following C_N

$$C_N(\omega) = \frac{1}{2} \left[\frac{\prod_{n=1}^N (c_n + d_n) + \prod_{n=1}^N (c_n - d_n)}{\prod_{n=1}^N \left(1 - \frac{\omega}{\omega_n}\right)} \right] \quad (2-52)$$

$$c_n = \left(\omega - \frac{1}{\omega_n}\right) \quad (2-53)$$

$$d_n = \omega \sqrt{1 - \frac{1}{\omega_n^2}} \quad (2-54)$$

By performing the calculations for $N = 1, 2, 3$ we note that there is an recursive pattern, which can be exploited to set up the algorithm that will generate the numerator of C_N , in fact:

$$N=1 \rightarrow \text{num}[C_1(\omega)] = c_1$$

$$N=2 \rightarrow \text{num}[C_2(\omega)] = (c_1)c_2 + (d_1)d_2$$

$$N=3 \rightarrow \text{num}[C_3(\omega)] = (c_1 c_2 + d_1 d_2)c_3 + (c_2 d_1 + c_1 d_2)d_3$$

Etc.

The numerator of the C_N can be expressed as the sum of two auxiliary functions in ω :

$$\text{num}[C_N(\omega)] = \frac{1}{2} [G_N(\omega) + G'_N(\omega)] \quad (2-55)$$

$$G_N(\omega) = \prod_{i=1}^N \left[\left(\omega - \frac{1}{\omega_n}\right) + \omega' \sqrt{1 - \frac{1}{\omega_n^2}} \right] \quad (2-56)$$

$$G'_N(\omega) = \prod_{i=1}^N \left[\left(\omega - \frac{1}{\omega_n}\right) - \omega' \sqrt{1 - \frac{1}{\omega_n^2}} \right] \quad (2-57)$$

It is noted that in order to obtain the numerator of the C_N method is recursive and it builds on the basis of polynomial $(n-1)$ -th as follows:

$$G_N(\omega) = U_N(\omega) + V_N(\omega) \quad (2-58)$$

$$U_N(\omega) = u_0 + u_1 \omega + \dots + u_N \omega^N \quad (2-59)$$

$$V_N(\omega) = \omega' (v_0 + v_1 \omega + \dots + v_N \omega^N) \quad (2-60)$$

This way you get the numerator is C_N and A , remembering that for Chebyshev filters its zeros are the zeros F_N . F_N is achieved by building it as a product of monomials of A zeros.

2.4.1.2 Prototype circuit

After introducing a synthesis method for the S-parameters, next we address the representation of the circuit model for a microwave filter.

The representation of a microwave filter by means of the couplings matrix (henceforth M), was introduced in 1970 by Atia and Williams and is of fundamental practical importance ([RD.29]). This is because, the individual elements of M have a correspondence with the characteristic physical parameters of the filter, such as the resonance frequencies of the individual resonators, the couplings between them and the quality factors Q of each. The generic filter template layout to which reference will be made, is that in Fig 2.3. Next we see how the filter is composed of a series of N resonators in cascade, coupled by means of transformers. Each resonator is composed of the capacitors in series with the inductances of the resonator and the mutual inductances of transformers. In addition, each circuit, is coupled to the other, through the crossed mutual inductances. The mutual inductances, corresponding to the pairs, and are M_{ij} calls. In each resonator, they have been included in frequency invariant reactances (FIR), which are necessary to obtain the asymmetric responses in the filters.

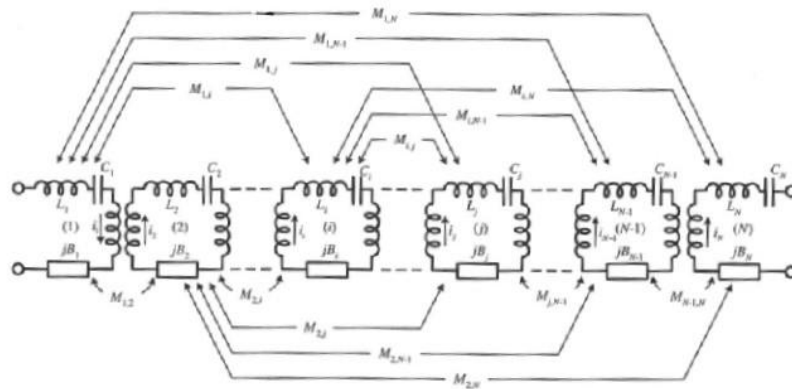


Figure 2-8: Lumped element model with FIR elements of a band pass filter [RD.29]

To proceed to the proper transformation, it is necessary to first replace all mutual inductances, with the impedance or admittance inverters of equal value. After applying the transformation, we obtain the circuit visible in Figure 2-8, which is the prototype lowpass with the inverters.

From the outside, the filter can be treated as a two-port network connected to a load R_L and a voltage generator e_g with internal impedance R_s .

Considering the network two ports and the two load impedances and source as a single impedance $[z']$, then we can write the matrix equation:

$$[e_g] = [z'] [i] \quad (2-61)$$

$$e_g[1,0,0, \dots]^T = [jM + sI + R][i_1, i_2, \dots, i_n]^T \quad (2-62)$$

Here, e_g is the vector containing the source voltages, $[i]$ contains the current in each of the N links that make up the network. The impedance matrix $[z']$, is instead composed of the sum of three matrices: jM , sI and R .

$$jM = j \begin{bmatrix} B_{11} & \dots & M_{1N} \\ \vdots & \ddots & \vdots \\ M_{N1} & \dots & B_{NN} \end{bmatrix} \quad (2-63)$$

$$sI = \begin{bmatrix} s & \dots & 0 \\ \vdots & \ddots & \vdots \\ 0 & \dots & s \end{bmatrix} \quad (2-64)$$

$$R = \begin{bmatrix} R_s & 0 & \dots & 0 \\ 0 & \dots & \dots & \vdots \\ 0 & \dots & \dots & R_L \end{bmatrix} \quad (2-65)$$

$$s = j \frac{\omega_0}{\omega_2 - \omega_1} \left[\frac{\omega_b}{\omega_0} - \frac{\omega_0}{\omega_b} \right] \quad (2-66)$$

$$\omega_0 = \sqrt{\omega_2 \omega_1} \quad (2-67)$$

$$\omega = 2\pi f. \quad (2-68)$$

The $N \times N$ diagonal matrix, sI contains the part in the frequency of the variable matrix, $s = j\omega$. M is a $N \times N$ matrix containing the values of the mutual coupling, in particular M_{ij} is the coupling between the i -th and the j -th resonator. $M_{i, i+1}$ are called direct couplings between adjacent cavities, while the others, are the cross couplings. M_{ii} is instead self-mating and is offset relative to the central frequency of the i -th resonator (the sign is opposite, so a negative M_{ii} indicates that the resonance frequency is higher than the central frequency). It should be noted, that this matrix M , being composed by the couplings between the various cavities of the filter, also has a direct correspondence with the size of the elements that physically implement the couplings, for example the classic irises. To this end, knowing the matrix M , for the designer means valuable information on how to size these coupling structures. In addition, the diagonal values provide the resonance frequencies of each resonator.

Finally, R is a $N \times N$ matrix containing only 2 non-zero values, R_s and R_L , placed respectively in the index elements 1,1 and N, N .

In order to find the connection between the M and the S -parameter matrix, first, we consider the admittance matrix Y , the network 2 described above. It shows that the four elements of this matrix are polynomials for which the following relationship holds:

For N , the filter order, of:

$$y_{21}(s) = \left(\frac{\frac{P(s)}{\epsilon}}{m_1(s)} \right) \quad (2-69)$$

$$y_{22}(s) = \left(\frac{n_1(s)}{m_1(s)} \right) \quad (2-70)$$

N odd:

$$y_{21}(s) = \left(\frac{\frac{P(s)}{\epsilon}}{n_1(s)} \right) \quad (2-71)$$

$$y_{22}(s) = \left(\frac{m_1(s)}{n_1(s)} \right) \quad (2-72)$$

Using the partial fraction expansion, we can convert y_{21} and y_{22} by the expression that involves the polynomials and residuals combinations, and obtain the following expression

$$Y_N = j \begin{bmatrix} 0 & K_{\infty} \\ K_{\infty} & 0 \end{bmatrix} + \sum_{k=1}^N \frac{1}{s-j\lambda_k} \begin{bmatrix} r_{11k} & r_{12k} \\ r_{21k} & r_{22k} \end{bmatrix} \quad (2-73)$$

where k is the k -th resonator. To then obtain the matrix Y of the entire filter just add up all the k matrices. Summing over all N resonators, one can obtain:

$$Y_N = j \begin{bmatrix} 0 & M_{SL} \\ M_{SL} & 0 \end{bmatrix} + \sum_{k=1}^N \frac{1}{sC_k - jB_k} \begin{bmatrix} M_{Sk}^2 & M_{Lk}M_{Sk} \\ M_{Lk}M_{Sk} & M_{Lk}^2 \end{bmatrix} \quad (2-74)$$

$$C_k = 1 \quad (2-75)$$

$$B_k (\equiv M_{kk}) = -\lambda_k \quad (2-76)$$

$$M_{Lk} = \sqrt{r_{22k}} \quad (2-77)$$

$$M_{Sk} = \frac{r_{21k}}{\sqrt{r_{22k}}} \quad (2-78)$$

Once the pairs of the M matrix have been determined, this can be transformed in the form that best represents the type of filter by means of matrix algebra similarity relations. The most common form of array is the so-called "folded". This allows to insert the "cross-coupling" between the not consecutive resonators, and therefore, can enable realization of different filters with transmission zeros. Figure 2-9 shows the structure of the filter "folded" and its mating matrix, we note that there are cross-coupling between non-adjacent resonators.

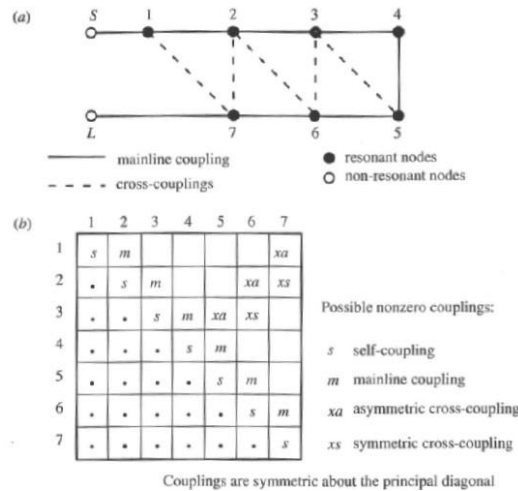


Figure 2-9: Folded configuration and the associated coupling matrix [RD.28].

2.4.2 Coupling determination

The tuning procedure for microwave filters is certainly a significant part of filter development. The determination of the resonant frequencies and coupling coefficients between coupled resonators are needed to minimize the efforts of the tuning.

In this section we will see a technique for tuning based on the group delay . The coupling between the input connecting lines and output from the filter, is determined by a value called an external quality factor Q_e , while the coupling between resonators is determined by k_{ij} which is linked to the M_{ij} values by the following relation

$$k_{ij} = M_{ij} \frac{BW}{f} \quad (2-79)$$

Once these values are set and coupling the resonators are all tuned to the center frequency, the filter will have the predicted response. The Q_e and k_{ij} values are determined from the reflected signal S_{11} when the resonators are tuned to resonance. These parameters are linked to each other by fairly simple equations involving the phase and group delay of S_{11} . The group delay of S_{11} is defined as:

$$GD = -\frac{1}{2\pi} \frac{d \arg(S_{11})}{df} \quad (2-80)$$

It is shown that the following relations apply:

$$M_{j,j+1} = \frac{1}{\sqrt{g_j g_{j+1}}} \quad (2-81)$$

$$R_1 = \frac{1}{g_0 g_1} \quad (2-82)$$

$$R_N = \frac{1}{g_N g_{N+1}} \quad (2-83)$$

Resonator Number	Group delay	
n=1	$\frac{4Q_e}{2\pi f}$	GD_0
n=2	$\frac{4}{\omega_0 Q_E K_{12}^2}$	GD_1
n=3	$GD_1 + \frac{4K_{12}^2 Q_E}{\omega_0 K_{23}^2}$	GD_2

This process can be repeated at each element added to the network. This tuning technique, which is strictly valid for in-line configuration filters can be applied as follows for the filters in helical topology. To simplify the concept we demonstrate an example considering a second-order filter ([RD.30]).

The theoretical group delay of the single resonator using data obtained from the synthesis can be calculated (see Figure 2-10)

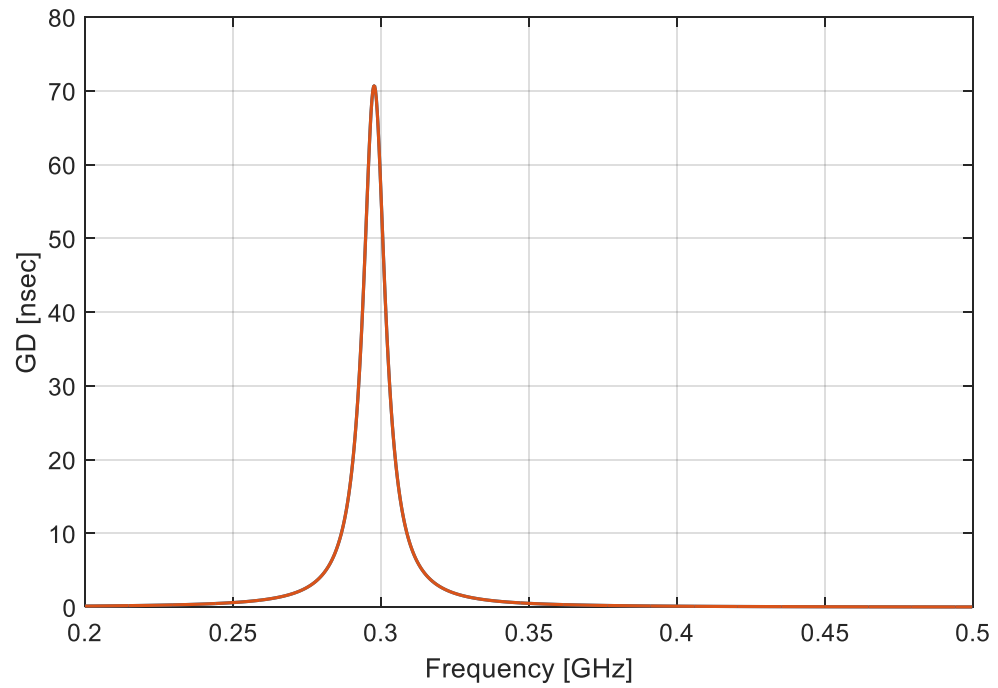


Figure 2-10: Group delay from the synthesis process.

The structure of the single resonator can be built and simulated in a fullwave software (See Figure 2-11)

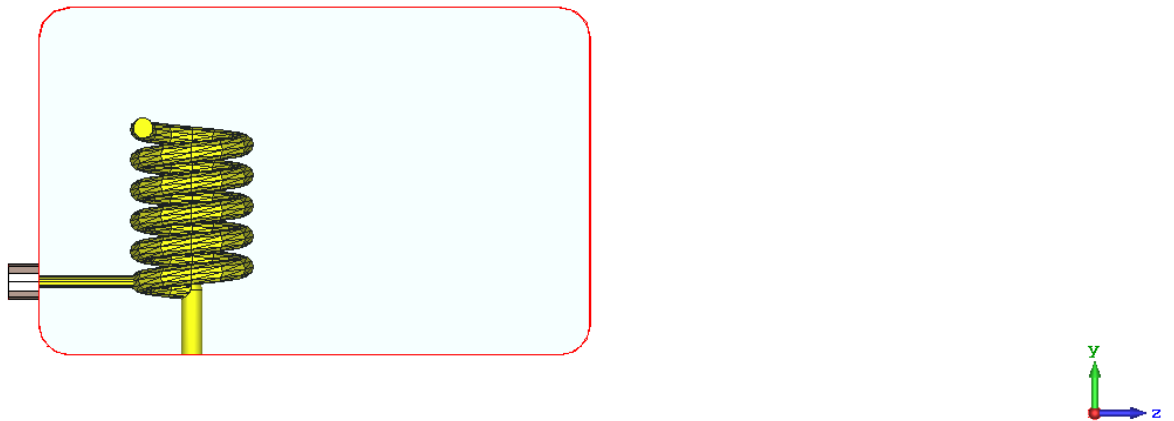


Figure 2-11: Physical model for Group Delay calculation.

Following Figure 2-12 shows the result for the simulated group delay

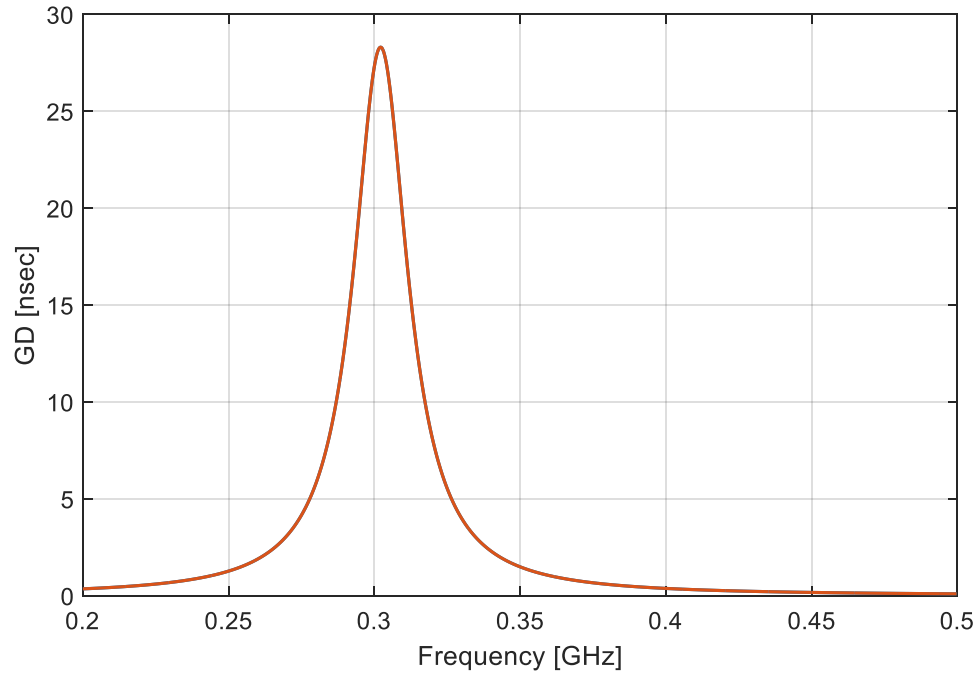


Figure 2-12: Group delay using software fullwave.

At this point, we optimize the size of the resonator to make so that the theoretical curves (Figure 2-10) and those calculated (Figure 2-12) go to coincide. In particular, the group delay depends on the contact point between the connectors and the helix and the length of the pin that connects the helix to the bottom wall of the cavity. Once the cavity dimension is established, the problem is reduced to the determination of few geometrical parameters.

As the structure has only two resonators, optimizing the results is fairly straightforward. In this regard, a simple optimization software was written. With few optimization steps, that touch the contact point with the connectors and length of the ground connection, it is possible to obtain a quasi perfect match between the theoretical group delay (red curve in Figure 2-13) and the results obtained using full wave analysis (green curve in Figure 2-13).

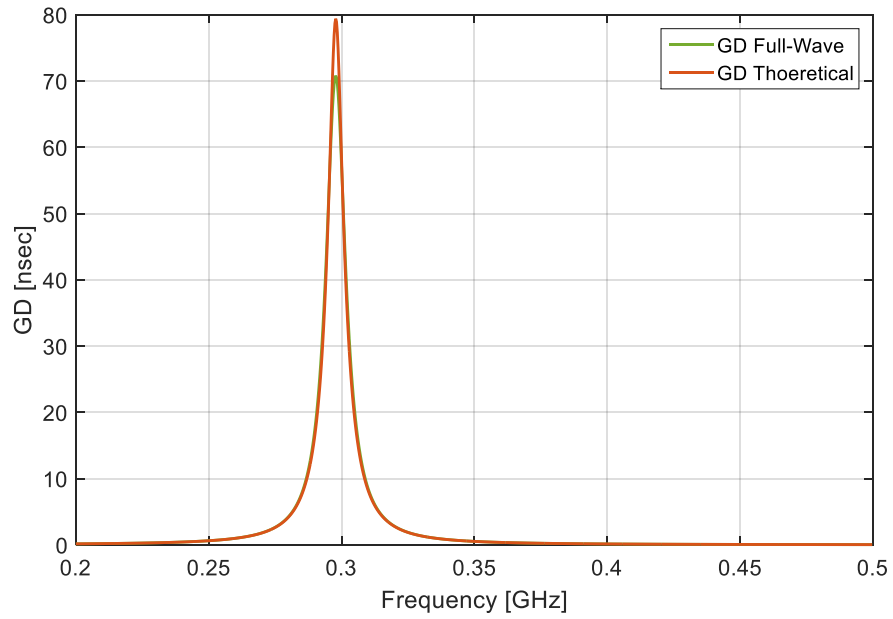


Figure 2-13: Group Delay comparison

The group delay of the full wave analysis is determined by numerical derivative of the unwrapped phase of S_{11} with respect to the simulated frequencies.

The same analysis could be developed for two resonators, as presented in Figure 2-14.

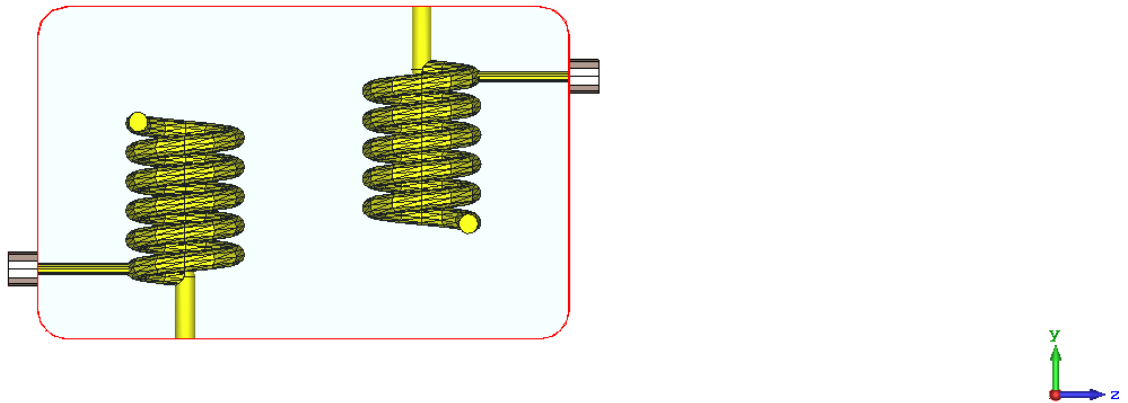


Figure 2-14: Physical structure of Group Delay of 2 resonators.

The results are presented in Figure 2-15 and Figure 2-16

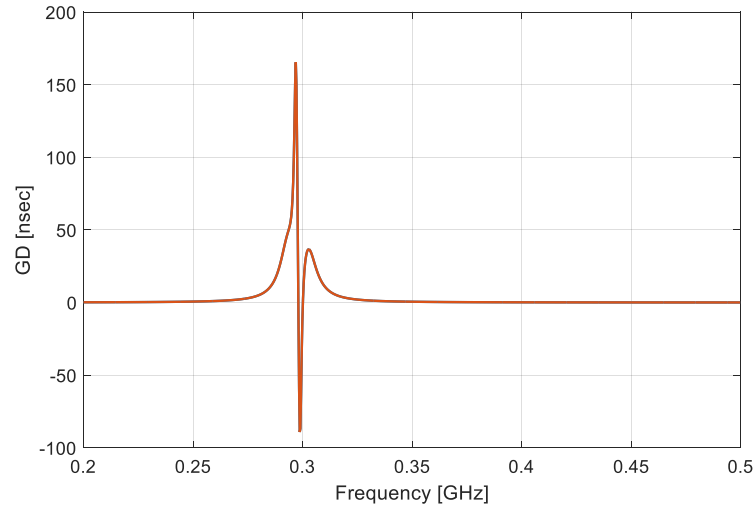


Figure 2-15: Group delay from synthesis 2nd order filter resonator.

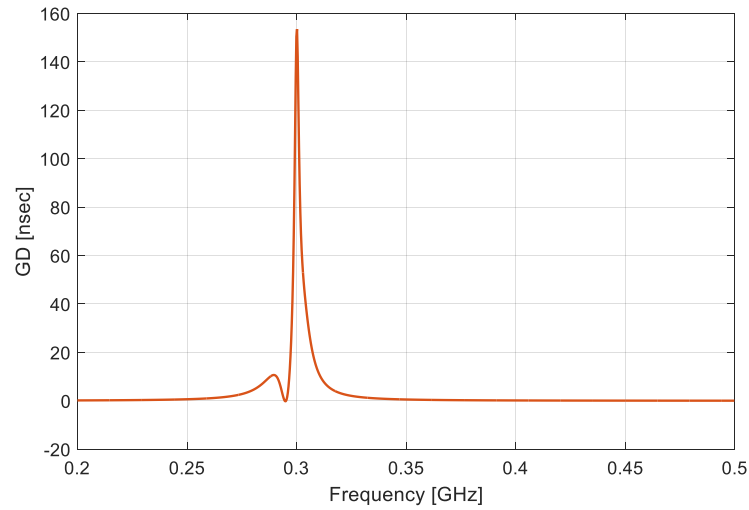


Figure 2-16: Group delay from full wave simulation of 2nd order filter resonator before tuning

The final results are reported in the following Figure 2-17: also in this case, an automated optimization routine is developed. With two resonators the parameters that are involved are the connector position, the grounding length and the relative distance between the two helices; in particular, once this distance is determined, a slight modification of the other parameter is performed. The tuning procedure, is very efficient and there is a quasi perfect matching between the theoretical (violet curve in Figure 2-17) and the full wave analysis (green curve in Figure 2-17)

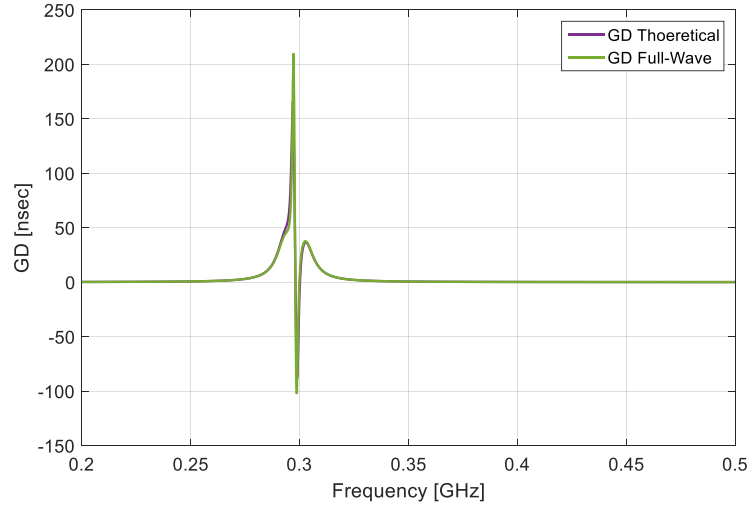


Figure 2-17: Group Delay comparison between synthesis and fullwave simulation

The filter performances, at the end of the tuning and without any further optimization are reported in the following Figure 2-18. In particular, the RF characteristics are:

- Center frequency $f_0=300\text{MHz}$
- Bandwidth $BW=10\text{MHz}$
- Transmission zeros around 360MHz .

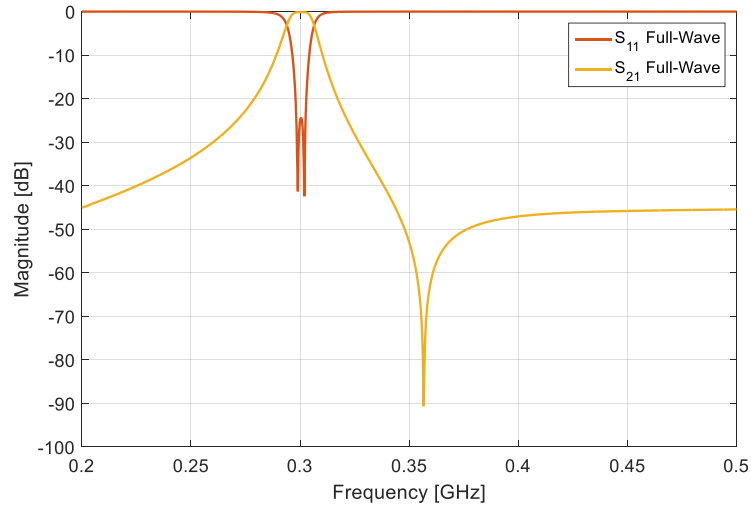


Figure 2-18: Near band filter performance

The position of the transmission zero and the level of in band S_{11} is considered for the the helical structures developed for high power application, explained in the next chapter.

CHAPTER 3 – LARGE GAP CONCEPT FOR OMUX HELICAL FILTERS

3.1 Introduction

On-board VHF/UHF OMUX filters pose significant engineering challenges. Power handling and Q-factor considerations exclude lumped or SAW filters. Meanwhile, traditional distributed filters (cavity or combline) are too bulky, and hence their use is impractical (e.g., very expensive particularly for the space segment). Helical resonators in evanescent mode cavity enclosures is a promising solution; with dimensions at a small fraction of the wavelength (typically wavelength/20) and relatively high Q-factor value (e.g. 1300 @ 300 MHz), they offer a valuable trade-off between volume/mass and electrical performance. Despite their favourable characteristics, the power handling capabilities of Helical Resonator Filters (HRF) can be limited by the power handling. Multipaction is a key phenomenon limiting the power handling for on-board filters. It is a phenomenon that occurs in the amplifier and waveguide; this is present when electrons accelerated by RF fields are self sustained in vacuum via an electron avalanche. The latter refers to secondary electron emission in resonance with an alternating electric field, leading to exponential electron multiplication, possibly damaging and even destroying the RF device. This can be prohibiting in employing HRF in the on-board downlink channel chain (from [RD.31] to [RD.37]).

The mechanism of multipaction is related to the RF electric field and its orientation with respect to the surface. The multipaction is divided into two different types: two surface multipaction and single surface multipaction. For the purpose of this work, the two surface multipaction is studied. This effect occurs in the gap between two metallic surfaces, where the electric field is normal to the surface. The development of the phenomenon is a combination of a resonance between the electron flight from a surface to another and RF field cycle. For the existence of multipaction three conditions are necessary [RD.31]:

- 1) The average number of electrons released has to be greater than 1 for incident electron depending on the secondary electron yield (SEY)
- 2) The time of the electron travel between the surfaces is an integer multiple of the RF period
- 3) The average SEY is greater than one.

From quantitative point of view, considering two infinite metallic plate, the following quantities could be defined:

- d distance between the surface
- ω angular frequency of the RF fields
- V_0 peak voltage between plates
- $E_0 = V_0/d$ peak electric field between plates

Consider that the RF voltage varies sinusoidally; at defined time the voltage in a plate passes from 0 value to negative value. From the first condition, almost one electron free near the plate starts to accelerate toward the other plate. The electron continues to accelerate and reach a maximum velocity at $\frac{1}{2}$ a cycle later just as the voltage at the second plate begins to become negative. If the electron from one plate strikes the other in this condition, it produces additional free electrons, that starts to accelerate from one plate to the other. The process may then repeat causing multiplication. The Equation of motions it could be used for the modeling of the multiplication process. For the free electrons the acceleration is:

$$a(t) = \frac{F(t)}{m} \quad (3-1)$$

$$\ddot{x} = \frac{qE_0}{m} \sin(\omega t) \quad (3-2)$$

That could be integrate and the solution is:

$$x = -\frac{qE_0}{m\omega^2} \sin(\omega t) + \frac{qE_0}{m\omega} t - \frac{d}{2} \quad (3-3)$$

Considering that the resonance happens if the electrons arrive at one plate after one half of the period of the field, $t = \frac{\pi}{\omega}$. Using this value into the solution obtained, it is possible to have the relation used for the multiplication calculation used normally.

$$\frac{d}{2} = -\frac{qE_0}{m\omega^2} \sin\left(\frac{\omega\pi}{\omega}\right) + \frac{qE_0}{m\omega} \frac{\pi}{\omega} - \frac{d}{2} \quad (3-4)$$

$$fd = \frac{1}{2\sqrt{\pi}} \sqrt{\frac{qV_0}{m}} \quad (3-5)$$

The product fd is called frequency-gap product.

The power imbalance between the Rx and Tx channels further poses the need for high out-of-band isolation. Although increasing the order of the filter is the traditional technique for improving out of band performance, this approach leads to increased volume and mass. Instead, selectively located transmission zeros in the stop-band can reduce cross-talk between two predetermined frequency bands without increasing the filter order and the associated volume/mass and loss. Such pseudo-elliptic response is increasingly becoming the preferred solution for high performance filters.

By using the HRF, it was possible to develop the capability to

- 1) increase the power handling qualification of HRF by over 25 dB (to values beyond 45 dBm) exploiting dielectric layers that cover the helices.
- 2) introduce selectively located transmission zeros in the lower or upper stopband of direct-coupled HRF without any auxiliary elements.

In particular, Figure 3-1 to Figure 3-2 illustrate the photos and the measured behaviour of some previously studied structures at Space Engineering. Figure 3-2 shows the simulated results obtained for a 2nd order BPF based on modified shape helical resonators which was developed at Space Engineering in collaboration with Heriot-Watt University (HW). The following figures show examples of the previous work realized in cooperation between Space Engineering and Heriot-Watt.

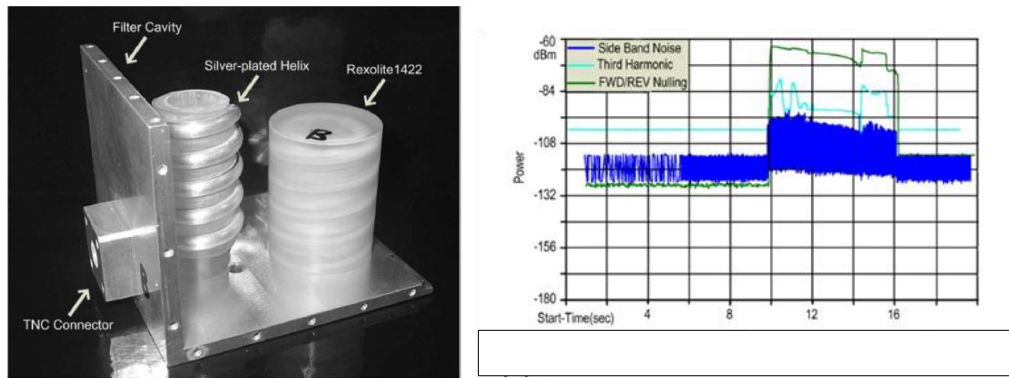


Figure 3-1: Photograph of a fabricated prototype and measured multipactor results for peak power up to 90W on 30% duty cycle [RD.32]

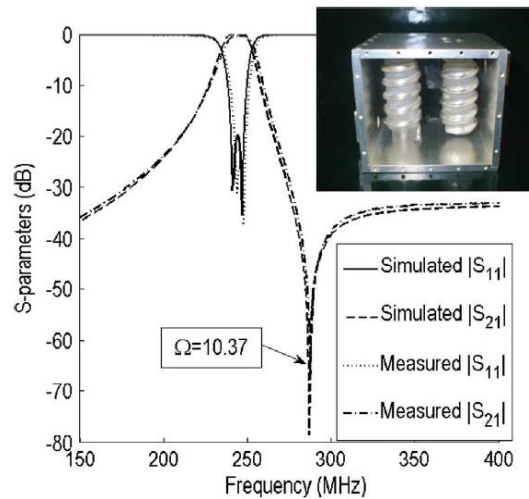


Figure 3-2: Photograph of an interdigitally coupled HRF and its measured response showing a transmission zero in the upper stop-band [RD.37]

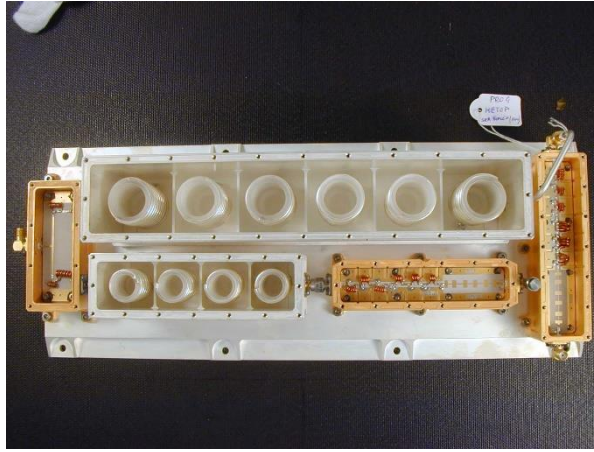


Figure 3-3: The photo of the HRF-base Diplexer, on-board the METOP-1 satellite
[RD.37]

Despite the significance of these results, HRF technology necessitates further increase in power handling capability if it is to become a viable proposition for demanding VHF/UHF satellite systems. In fact, while the power handling of helical resonator covered with dielectrics cap was proven in high power in vacuum test, other possibilities were never exploited. In particular for this study, to improve the power handling characteristics, was investigated the key novel concept of using helices with modified geometries, whereby the frequency-gap product at the most critical regions for multipactor to occur is increased without significantly affecting the resonator properties. In fact, the idea is that the multipaction occurs when the electric field is maximum between two conductors; in the helical resonator the electric field is maximum at the open end. In this condition, the gap between the resonator and side wall of the cavity housing the helices could produce the multipaction. In order to increase locally the gap between the helices and the cavity, the shape of the resonator is modified into step conical geometry. This solution permits to have filters optimized in dimensions and for high power applications. As shown in this chapter we have demonstrated that by exploiting a step-conical geometries (the helical geometry with modulated radius), the power handling capability of uncoated HRFs can be improved when compared to conventional HRF.

3.2 Presentation of designed prototypes

For the purposes of addressing the trade-off considerations between overall size, helical resonator geometry and inclusion of Rexolite covers, a range of 2-pole filters in

interdigital topology and pseudo-elliptic response has been designed. In particular, these prototypes can be classified according to:

- **The cavity length:** we have selected three values of cavity lengths, in the order to 7 cm , 9 cm and 12 cm respectively.
- **The helix geometry:** we have produced designs with cylindrical and step-conical resonators.
- **The inclusion of Rexolite 1422 TM covers**

Cavity	No Rexolite 1422 TM		With Rexolite 1422 TM	
	Cylindrical	Conical	Cylindrical	Conical
Small	✓	✓	✓	✓
Medium	✓	✓		
Large	✓	✓	✓	✓

Table 3-1:Summary of fabricated prototypes

In total 10 prototypes have been designed as summarised in Table 3-1 above. It is noted that in all designs, and in order to allow for valid comparisons, priority has been given in delivering similar electrical response and therefore the cavity dimensions vary slightly around the values reported above. The exact cavity dimensions for the designed prototypes are reported Table 3-2

Cavity	No Rexolite 1422 TM						With Rexolite 1422 TM					
	Cylindrical			Conical			Cylindrical			Conical		
	x	Y	Z	x	Y	z	x	y	z	x	y	z
Small	65.89	52.71	67.89	50.89	50.71	68.59	65.89	52.71	67.89	49.71	48.89	71.09
Medium	63.89	56.71	86.39	53.89	53.71	91.79						
Large	68.42	54.6	109.2	64.02	55.6	116.0	59.25	58.0	116.0	65.05	58.5	117.0

Table 3-2:Cavity dimensions for fabricated prototypes

The previous Table 3-2 shows the dimensions of the designed HRF with uniform cylindrical and step conical shape with and without Rexolite covers. The terms “Small”, “Medium” and “Large” are related to the length in z direction of the filters (all dimensions are in mm). The filters that were designed at the beginning, are the “Small” cavity; where the approach was to have a good electrical response in a compact geometry. The “Large” cavity where designed in order to maximize the multipactor behaviour maintaining a

good electrical response. All the iterations performed have the purpose to produce more compact filters which have also good multipaction characteristics. The final products of this iterations are the “Medium” size filters; in this design, were not produced a version with dielectric covers.

In the remaining of this section the design and performance characteristics of each set of prototypes are reviewed.

3.2.1 *REXOLITE 1422™ characteristics*

Table 3-3 in the following represents the data sheet of the Rexolite 1422™. Through out these data the most significant and, hence, of corresponding interest are those referring to ϵ_r and $\tan \delta$ values; e.g.

	Unit
ϵ_r	2.53 (from 1KHz to 500GHz)
$\tan \delta$	0.0002 at 1MHz 0.0002 at 30MHz 0.0001 at 10GHz

Table 3-3:Rexolite 1422™ Characteristics

The values that are presented in data sheet ([RD.38]) are used in the simulation of electrical performances of the filters presented in the previous sections. Electromagnetic simulations are performed by means of CST MWS Studio Suite (Finite difference time domain solver).

3.2.2 *The Long Length Cavity Case*

Four different prototype of second order helical filters, have designed in cavities with length of the order of 12 cm:

1. Step conical helical resonator filters with Rexolite 1422™
2. Step conical helical resonator filter without Rexolite 1422™
3. Cylindrical helical resonator filter with Rexolite 1422™.
4. Cylindrical helical resonator filter without Rexolite 1422™.

The geometry of the second order filters are depicted in the following Figure 3-4: e.g.,

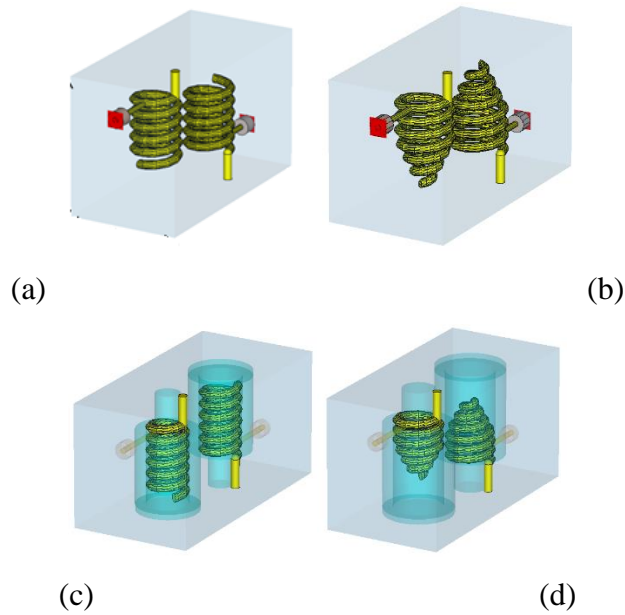


Figure 3-4: Second order filters. (a) Cylindrical Helical resonator without Rexolite 1422 TM ; (b) Step conical helical resonator filter without Rexolite 1422 TM; (c) Cylindrical helical resonator filters with Rexolite 1422 TM [RD.39], (d) Step conical helical resonator filters with Rexolite 1422TM

3.2.2.1 Cylindrical helical resonator filters without REXOLITE 1422TM

The optimized cylindrical helical resonator has the following geometrical characteristics:

- Helix pitch $p= 6.00$ mm
- Helix wire diameter $w=4.13$ mm
- Helix diameter $d=20.25$ mm
- Cavity Height $a=68.42$ mm
- Cavity Width $b=54.6$ mm
- Cavity Length $L= 109.2$ mm

The complete physical characteristics are depicted in the following Figure 3-5; e.g.,

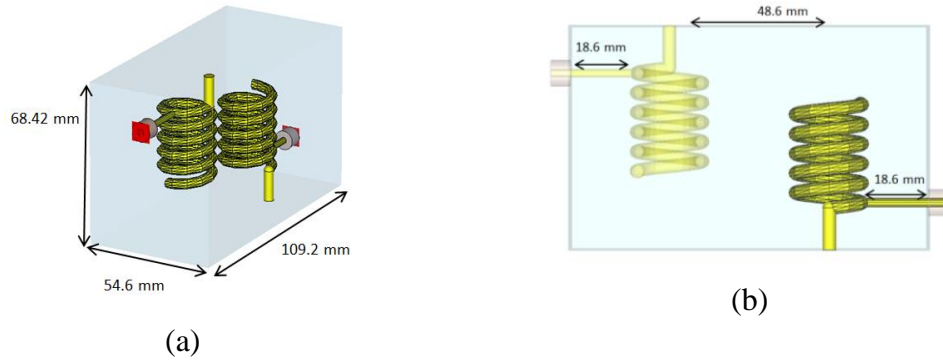


Figure 3-5: Optimized Cylindrical helical resonators filter geometrical characteristics: (a) Perspective view: (b) Side view

3.2.2.2 Step conical helical resonator filters without Rexolite 1422 TM

The optimized step conical helical resonator has the following geometrical characteristics:

- Helix pitch $p= 6.09$ mm
- Helix wire diameter $w=4.13$ mm
- Helix diameter $d=22.00$ mm
- Cavity Height $a=64.02$ mm
- Cavity Width $b=55.6$ mm
- Cavity Length $L= 116$ mm

The complete physical characteristics are depicted in the following Figure 3-6; e.g.,

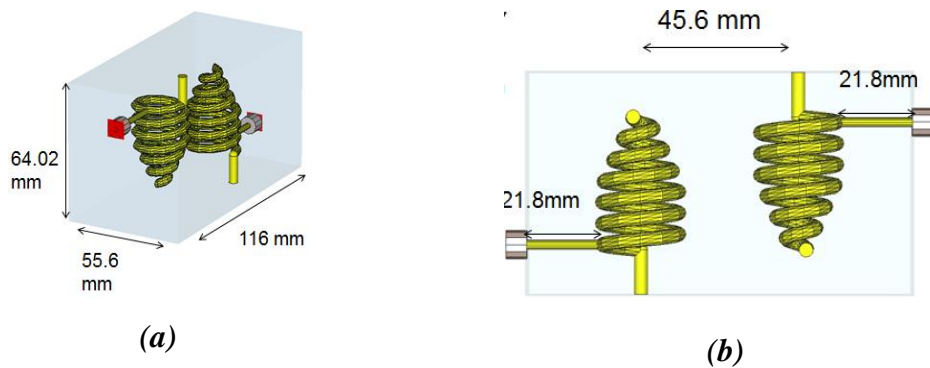


Figure 3-6: Optimized step conical resonators filter geometrical characteristics: (a) Perspective view: (b) Side view

3.2.2.3 Cylindrical helical resonator filters with Rexolite 1422™

The optimized step conical helical resonator has the following geometrical characteristics:

- Helix pitch $p=5.53$ mm
- Helix wire diameter $w=4.13$ mm
- Helix diameter $d=15.8$ mm
- External Rexolite shield diameter $d_{re}=29.92$ mm
- Internal Rexolite support $d_{ri}=11.67$ mm
- Cavity Height $a=59.25$ mm
- Cavity Width $b=58.00$ mm
- Cavity Length $L=116$ mm

The complete physical characteristics are depicted in the following Figure 3-7; e.g.,

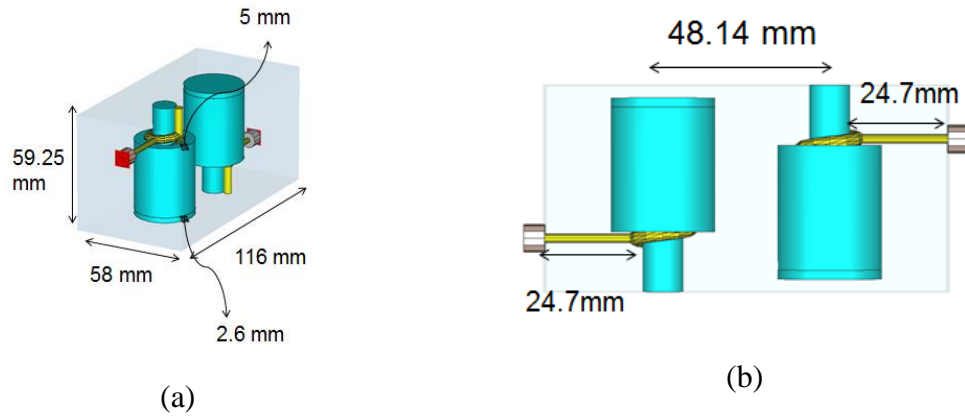


Figure 3-7: Optimized step conical resonators filter geometrical characteristics: (a) Perspective view: (b) Side view

3.2.2.4 Step conical helical resonator filters with Rexolite 1422™

The optimized step-conical helical resonator has the following geometrical characteristics: e.g.,

- Helix pitch $p=4.8$ mm
- Helix wire diameter $w=4.13$ mm
- Helix diameter $d=19.9$ mm
- External Rexolite shield diameter $d_{re}=34.03$ mm
- Internal Rexolite support $d_{ri}=14.00$ mm
- Cavity Height $a=65.05$ mm

- Cavity Width $b=58.5$ mm
- Cavity Length $L=117$ mm

The complete physical characteristics for the step-conical Helical resonator-based 2ND order BPF are depicted in the following Figure 3-8 below; e.g.,

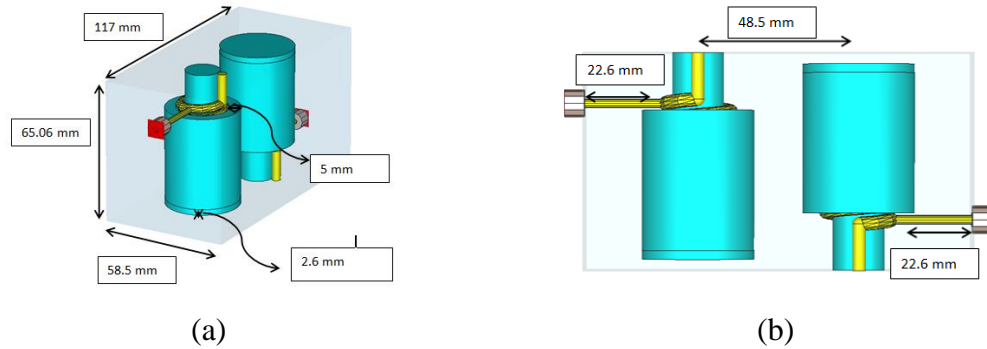


Figure 3-8: Optimized step-conical resonators filter geometrical characteristics: (a) Perspective view; (b) Side view

In the following **Figure 3-9** there are the all the S_{11} parameters superimposed for all the filters of the long cavity case.

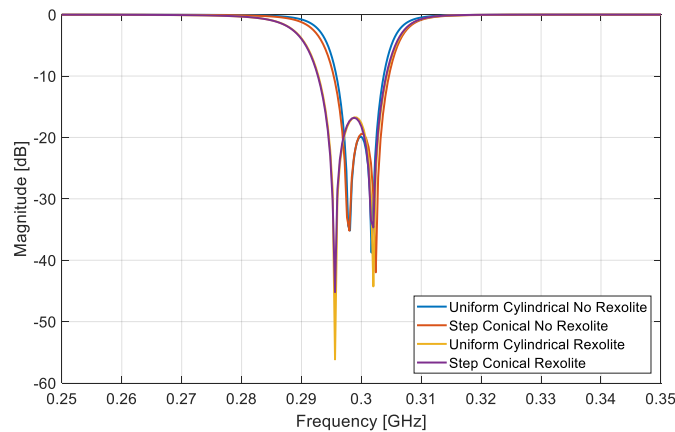


Figure 3-9: Return Loss Comparison of the 4 designed prototypes

In particular the main performances of the filter are:

- Central frequency $f_0=300$ MHz
- Bandwidth $BW=10$ MHz

In the following figure there are the all the S_{21} parameters overlapped for all the filters of the long cavity case.

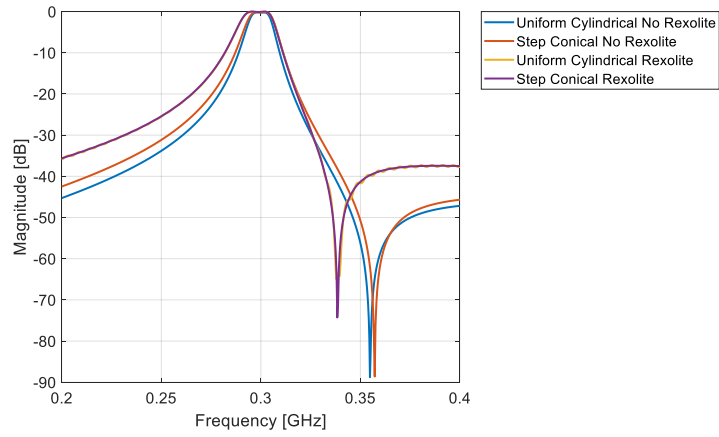


Figure 3-10: Insertion Loss Comparison of the 4 designed prototypes

As shown in previous figures, the return loss of the filters are quite similar and in the order of 18 - 20dB; while the near band rejection has a very sharp profile in higher frequency, as expected for a pseudoelliptic filters. In the presented cases, no optimizers were used, only manual tuning was performed.

3.2.3 The Small Length Cavity Case

Four different prototype of second order helical filters, have designed in cavities with length of the order of 7 cm:

1. Step conical helical resonator filters with Rexolite 1422 TM
2. Step conical helical resonator filter without Rexolite 1422 TM
3. Cylindrical helical resonator filter with Rexolite 1422 TM.
4. Cylindrical helical resonator filter without Rexolite 1422 TM.

The geometry of the second order filters are depicted in the following Figure 3-11

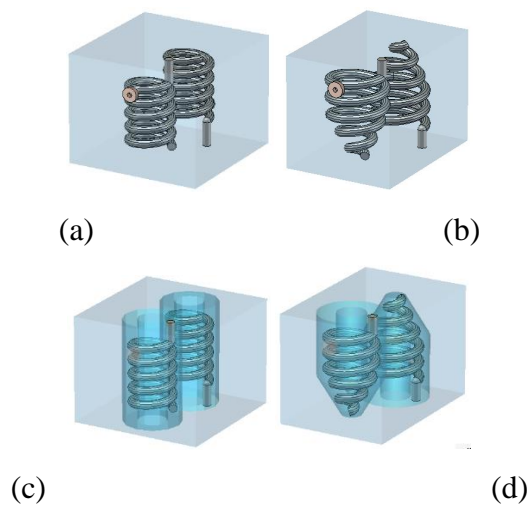


Figure 3-11: Second order filters. (a) Cylindrical without Rexolite 1422TM ; (b) Step conical filter without Rexolite 1422 TM; (c) Cylindrical filter with Rexolite 1422 TM , (d) Step conical filters with Rexolite 1422TM

The difference between the previous presented models (e.g., the Long vs. the Short Length cavity) are:

- The Rexolite™ 1422 completely in-globes the resonators.
- Cavity dimensions are smaller than the presented ones.

Dimensions and electrical performances are depicted in the next following sections.

3.2.3.1 Cylindrical helical resonator filters without Rexolite 1422™

The optimized cylindrical helical resonator has the following geometrical characteristics:

- Helix pitch $p=6.477$ mm
- Helix wire diameter $w=4$ mm
- Helix diameter $d=19.47$ mm
- Cavity Height $a=52.71$ mm
- Cavity Width $b=65.89$ mm
- Cavity Length $L=67.89$ mm

The complete physical characteristics are depicted in the following Figure 3-12

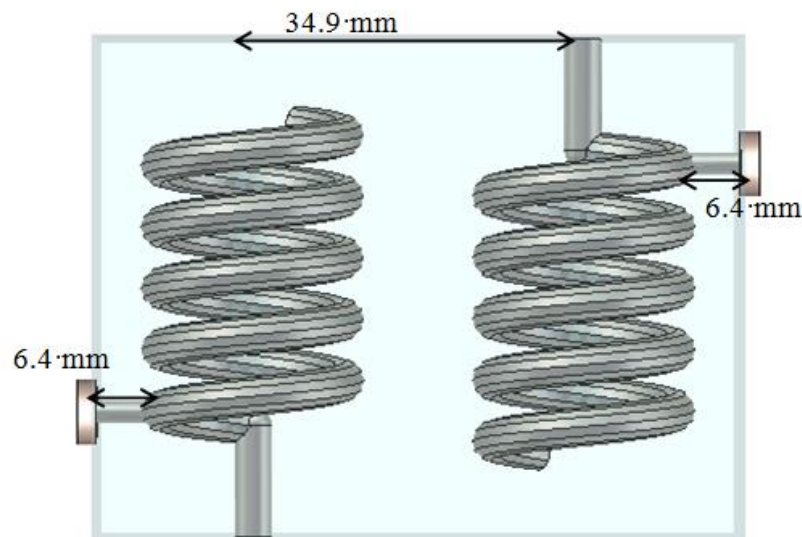


Figure 3-12: Optimized uniform cylindrical resonators filter geometrical characteristics: side view

3.2.3.2 Step conical helical resonator filters without Rexolite 1422™

The optimized step conical helical resonator has the following geometrical characteristics:

- Helix pitch $p=7.577$ mm
- Helix wire diameter $w=4$ mm
- Helix diameter $d=24.17$ mm
- Cavity Height $a=50.71$ mm
- Cavity Width $b=50.89$ mm
- Cavity Length $L=68.59$ mm

The complete physical characteristics are depicted in the following Figure 3-13,

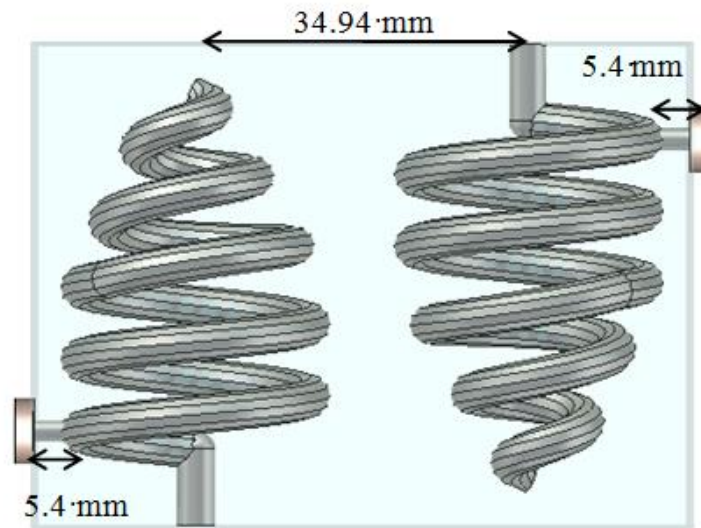


**Figure 3-13: Optimized step conical resonators filter geometrical characteristics:
cut view**

3.2.3.3 Cylindrical helical resonator filters with Rexolite 1422™

The optimized cylindrical helical resonator has the following geometrical characteristics:

- Helix pitch $p=5.877$ mm
- Helix wire diameter $w=4$ mm
- Helix diameter $d=16.37$ mm
- External Rexolite 1422™ shield diameter $d_{re}=25.56$ mm

- Internal Rexolite 1422 TM support dri=11.36 mm
- Cavity Height a=52.71 mm
- Cavity Width b=65.89 mm
- Cavity Length L= 67.89 mm

The complete physical characteristics are depicted in the following Figure 3-14,

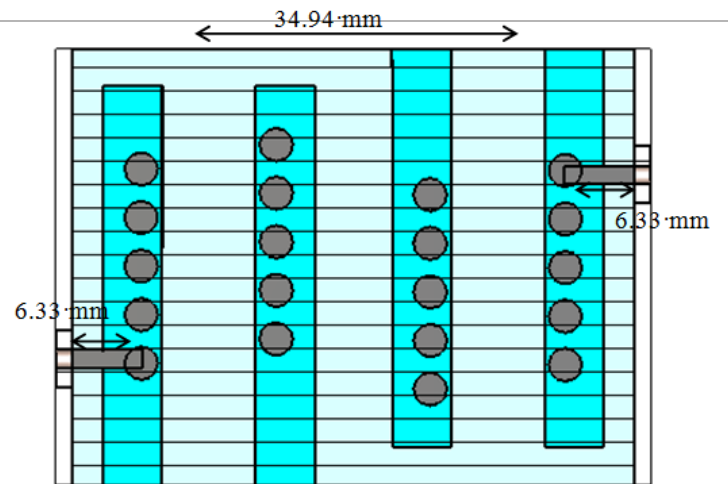


Figure 3-14: Optimized uniform cylindrical resonators filter geometrical characteristics: cut view

3.2.3.4 Step conical helical resonator filters with Rexolite 1422 TM

The optimized step conical helical resonator has the following geometrical characteristics:

- Helix pitch $p= 6.977$ mm
- Helix wire diameter $w=4$ mm
- Helix diameter $d=20.17$ mm
- External Rexolite shield diameter $d_{re}=14.68$ mm
- Internal Rexolite 1422 TM support $d_{ri}=6.59$ mm
- Cavity Height $a=49.71$ mm
- Cavity Width $b=48.89$ mm

- Cavity Length $L = 71.09$ mm

The complete physical characteristics are depicted in the following Figure 3-15,

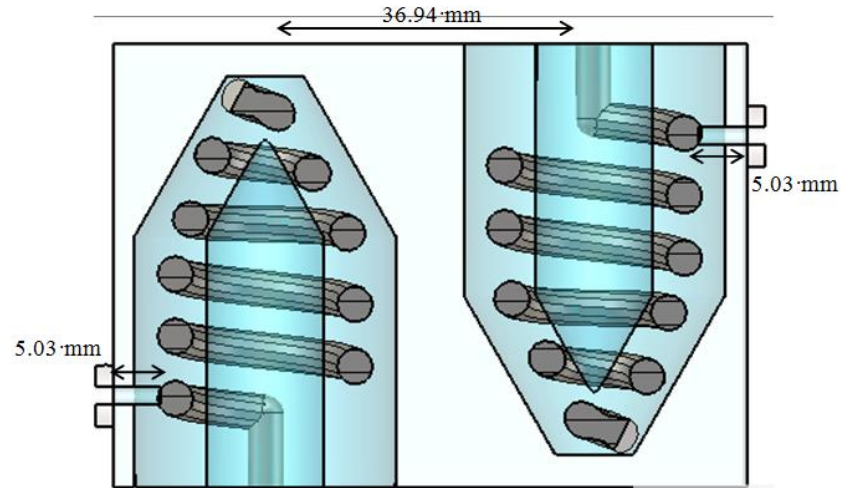


**Figure 3-15: Optimized step conical resonators filter geometrical characteristics:
cut view**

In the following Figure 3-9 there are the all the S_{11} parameters overlapped for all the filters of the small cavity case.

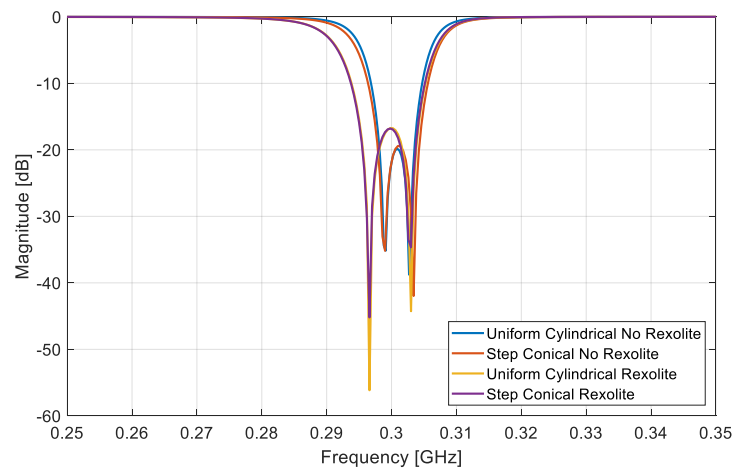


Figure 3-16: Return Loss Comparison of the 4 designed prototypes

In particular the main performances of the filter are:

- Central frequency $f_0 = 300$ MHz
- Bandwidth $BW = 10$ MHz

In the following figure there are the all the S_{21} parameters overlapped for all the filters of the small cavity case.

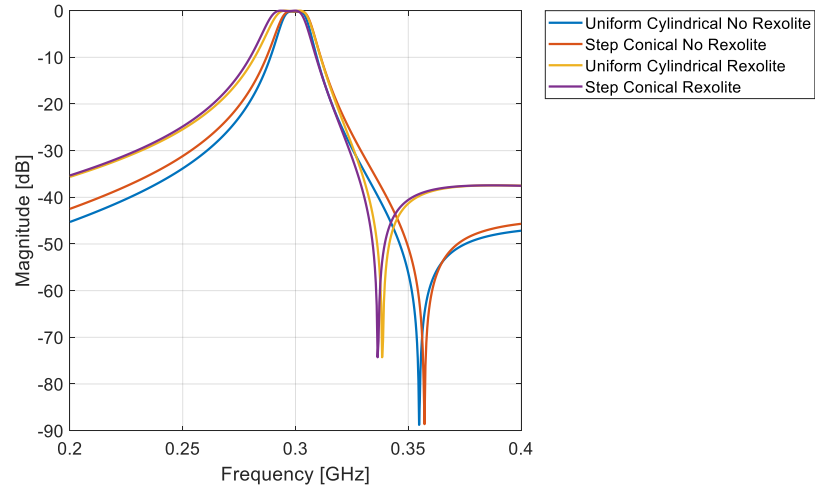


Figure 3-17: Insertion Loss Comparison of the 4 designed prototypes

As shown in previous figures, the return loss of the filters are quite similar and in the order of 18 - 20dB; while the near band rejection has a very sharp profile in higher frequency, as expected for a pseudoelliptic filters. In the presented cases, no optimizers were used, only manual tuning was performed.

3.2.4 The Medium Length Cavity Case

Four different prototype of second order helical filters, have designed in cavities with length of the order of 9 cm:

1. Step conical helical resonator filter without Rexolite 1422 TM
2. Cylindrical helical resonator filter without Rexolite 1422 TM.

The geometry of the second order filters are depicted in the following: e.g.,

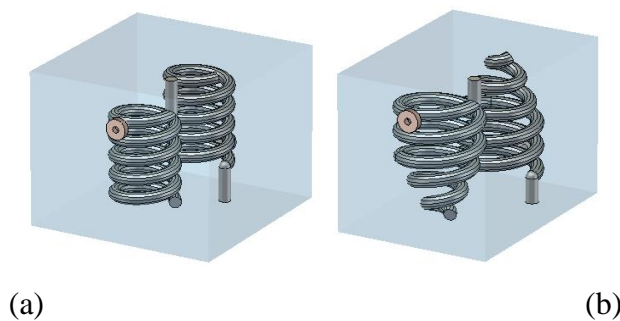


Figure 3-18: Second order filters in a cavity with approximate length 9 cm (medium cavity): (a) Cylindrical resonator without Rexolite 1422 TM ; (b) Step conical resonator filter without Rexolite 1422

3.2.4.1 Cylindrical helical resonator filters without Rexolite 1422 TM

The optimized cylindrical helical resonator has the following geometrical characteristics:

- Helix pitch $p= 6.477$ mm
- Helix wire diameter $w=4$ mm
- Helix diameter $d=20.27$ mm
- Cavity Height $a=56.71$ mm
- Cavity Width $b=63.89$ mm
- Cavity Length $L= 86.39$ mm

The complete physical characteristics are depicted in the following Figure 3-19.,

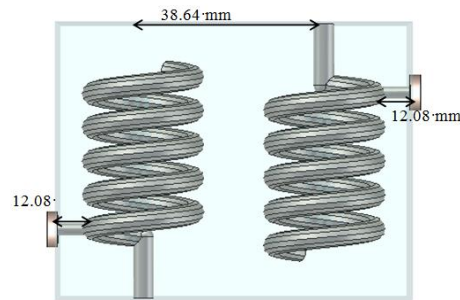


Figure 3-19: Optimized uniform cylindrical resonators filter geometrical characteristics: side view

3.2.4.2 Step conical helical resonator filters without Rexolite 1422 TM

The optimized step conical helical resonator has the following geometrical characteristics:

- Helix pitch $p= 7.577$ mm
- Helix wire diameter $w=4$ mm
- Helix diameter $d=25.47$ mm
- Cavity Height $a=53.71$ mm
- Cavity Width $b=53.89$ mm
- Cavity Length $L= 91.79$ mm

The complete physical characteristics are depicted in the following Figure 3-20,

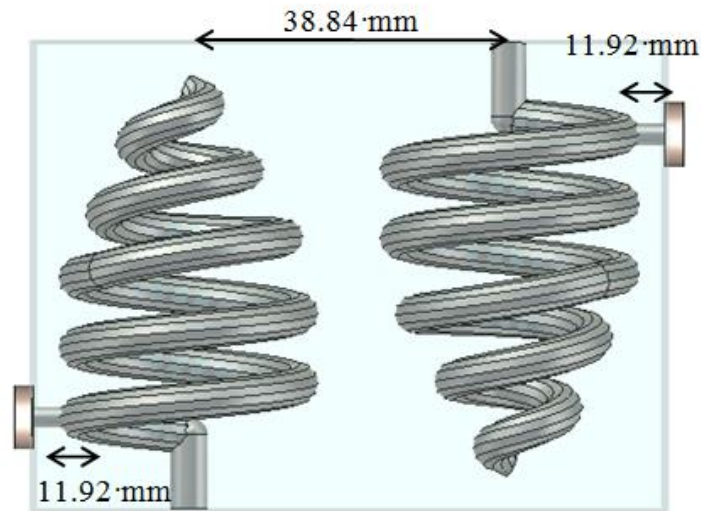


**Figure 3-20: Optimized step conical resonators filter geometrical characteristics:
cut view**

In the following Figure 3-21 there are the all the S_{11} parameters overlapped for all the filters of the medium cavity case.

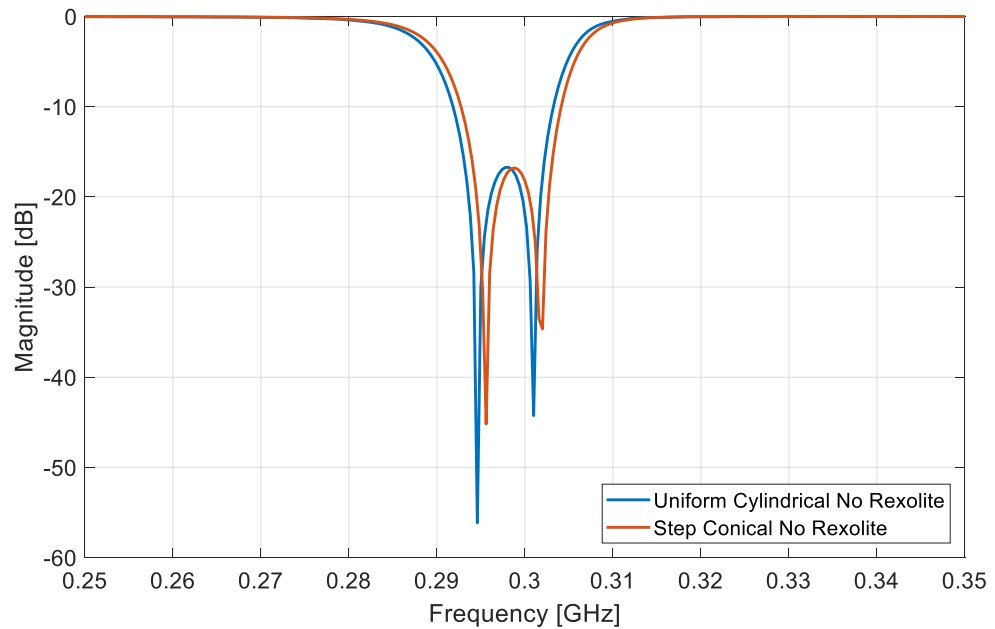


Figure 3-21: Return Loss Comparison of the 2 designed prototypes

In particular the main performances of the filter are:

- Central frequency $f_0=300$ MHz

- Bandwidth BW=10 MHz

In the following figure there are the all the S_{21} parameters overlapped for all the filters of the medium cavity case.

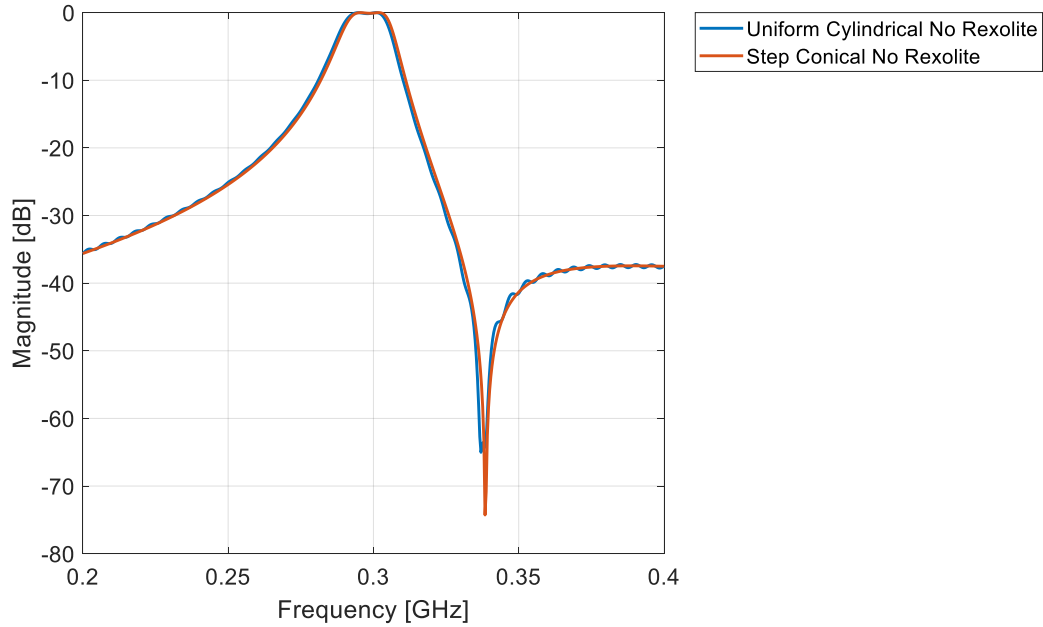


Figure 3-22: Insertion Loss Comparison of the 2 designed prototypes

As shown in previous figures, the return loss of the filters are quite similar and in the order of 18 - 20dB; while the near band rejection has a very sharp profile in higher frequency, as expected for a pseudoelliptic filters. In the presented cases, no optimizers were used, only manual tuning was performed.

3.3 Multipactor analysis

In this section, the multipactor analysis performed on the filters presented above is described. This analysis has been done in order to assess the advantages and disadvantages of the different options in terms of high power handling. It is noted that the high power analysis of these filters is rather complicated and, as a matter of fact, one has to be extraordinary careful when the taking these simulation results as very accurate. There are different factors which have a significant impact into the ability of the numerical techniques employed to determine with accuracy the breakdown power levels in these devices. Indeed, these limitations are mainly originated by uncertainties present which can be hardly controlled. The most important ones are:

1. Geometrical complexity: due to the complexity on the shape of these filters, the electron resonance can become quite complicated, allowing for multipactor areas which one would not expect. The point is that there is not a clear region where a

quasi-parallel plate situation is present, making the interpretation of the results more difficult. This also results in non-trivial multipactor processes which can have a non-clear dependence with the surface parameters.

2. Fringing effects: this is related to the geometry complexity indeed. The fact that the discharge will differ significantly from a typical parallel plate discharge results in a higher degree of difficulty in order to predict the breakdown threshold. This is mainly caused by the fact that the multipactor threshold becomes *extremely* dependent on the surface properties of the device,
3. As mentioned already in the two previous items, the surface properties (SEY) will have an extraordinary impact on the breakdown threshold. This is something completely uncontrolled and, the problem is, that in this type of components, the differences in the breakdown levels when using different SEY parameters can be really huge. This is even more relevant in those cases in which there is not heritage information such as in the Rexolite case.
4. Accuracy on the EM field calculation: this is another possible source of error although it is expected to have much less impact than anything related to the surface properties.

The following Table 3-4 shows the simulation of Breakdown power level in [W] for the all designed filters (i.e. Small, Medium, Large configuration with and without rexolite).

Cavity	No Rexolite		With Rexolite	
	Cylindrical	Conical	Cylindrical	Conical
Small	1.8	3.8	1.5	2.1
Medium	900	205		
Large	360	390	3.6	15.5

Table 3-4: Breakdown power level (in [W]) for all designed filters

The analysis presented in Table 3-4 is performed using copper for the resonators and it seems evident that the worst behaviour comes from the Small cavity configuration with and without Rexolite.

In the following sections, we present the simulations/results in the order that they were done in order to justify the steps we took during the activity.

All simulations have been performed by using SPARK3D. It has been coupled to HFSS or CST depending on the capabilities of each software to export the fields to SPARK3D

(for instance, CST does not export properly the fields to SPARK3D when dielectrics are present).

3.3.1 *The Long Length Cavity Case*

For the initial design was chosen a long length cavity. In this particular case, three main cases were analysed:

- Cylindrical resonator covered by Rexolite 1422 TM
- Step conical resonator NOT covered by Rexolite 1422 TM
- Step conical resonator covered by Rexolite 1422 TM

The multipactor analysis was done at the centre frequency of the filter. This value can slightly change from filter to filter because of some slight frequency shifts in the numerical analysis. In any case, the frequencies used were always close to 300 MHz (designed centre frequency).

Table 3.3.1-1 shows the breakdown power levels found in each of these configurations. We have employed three different SEY values in order to assess the impact of the SEY on the breakdown power level. In particular, for Rexolite 1422 TM we have taken the best possible, so it is expected that breakdown power levels could be even lower in this case.

Structure	Breakdown / W (SEY Copper)	Breakdown / W * (SEY Rexolite)	Breakdown / W (SEY silver)
Cylindrical (w Rexolite)	1.25	3.6	1.18
Conical (w/o Rexolite)	390	--	380
Conical (w Rexolite)	2.4	15.5	2.15

Table 3-5: Breakdown power level for the three configurations considered and using different SEY values.

The results indicate several interesting facts:

1. By far, the best response is obtained with the configuration in which Rexolite 1422 TM is not employed.
2. When using Rexolite 1422 TM there is not a significant difference between the conical and cylindrical configurations.

3. Even using very good SEY properties for Rexolite 1422 TM, the breakdown is just few watts.

In order to explain these results, we can take a look to SPARK3D output data. In particular, the electron emission density on the device surfaces is a very good indicator of the location of the discharge. Figure 3-23, Figure 3-24 show this result in a qualitative way. The red spots indicate the surfaces in which a large emission of electrons took place. These results have been obtained for power levels slightly above the threshold, in order to clearly identify the regions with lower breakdown power level. By inspecting all three images, several conclusions can be extracted:

1. The highest breakdown power level is obtained with the pure metallic filter.
2. Dielectric covers confine electrons in the high field critical zone, decreasing the breakdown because new gaps are indeed present with respect to the case in which no Rexolite 1422 TM is in use.
3. In the design without Rexolite 1422 TM, it seems that the breakdown occurs between the bottom part of the helix and the wall in which the helix stands.

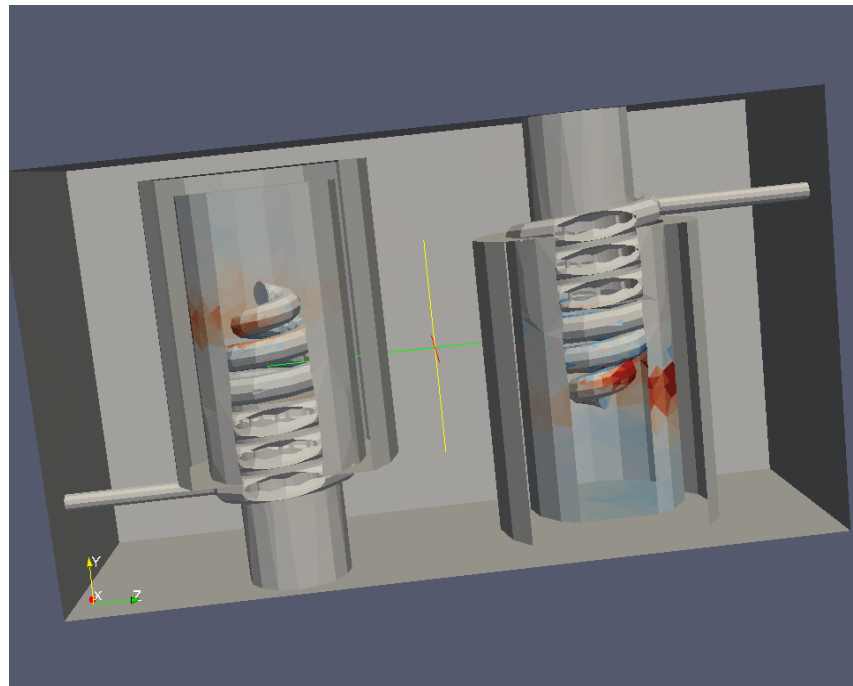


Figure 3-23: Emission density in the case of the conical filter WITH Rexolite 1422TM cover.

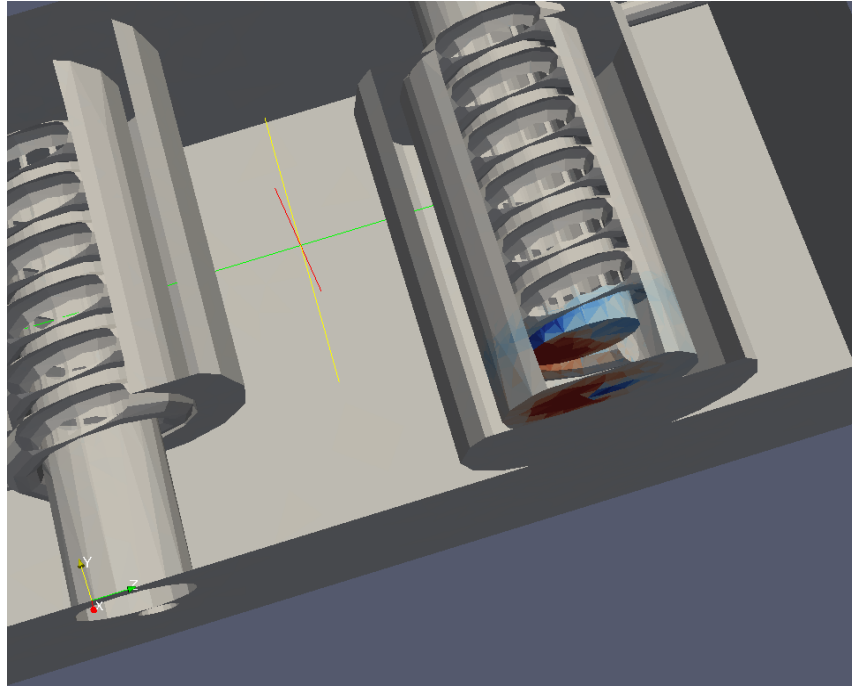


Figure 3-24: Emission density in the case of the conical filter WITHOUT Rexolite 1422™ cover.

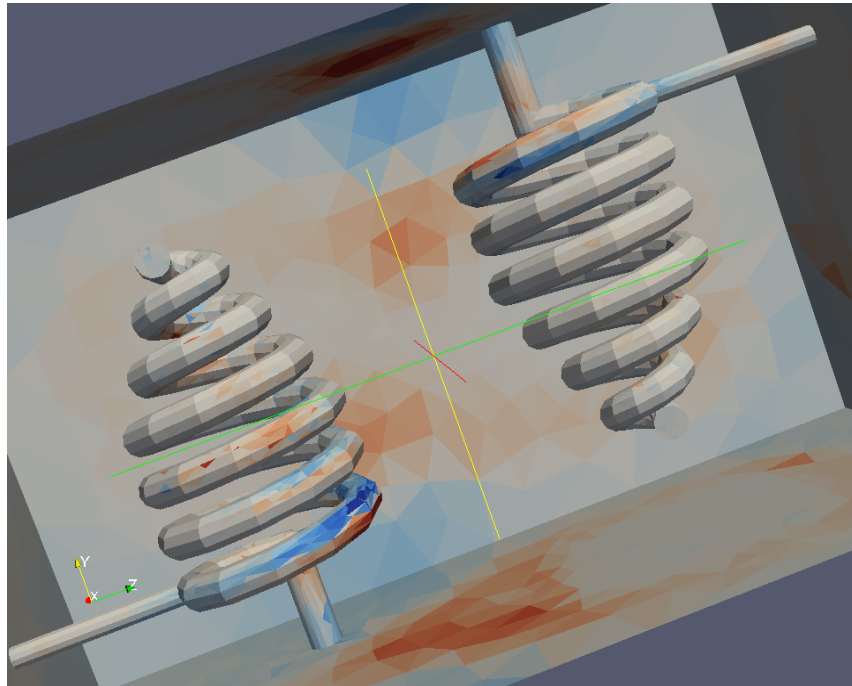


Figure 3-25: Emission density in the case of the conical filter WITHOUT Rexolite 1422™ cover.

3.3.2 The Medium and Short Length Cavity Cases

After these findings, it was decided to abandon the idea of the Rexolite (because of all the complexities added which seem not to help in the multipactor mitigation) and focus on the purely metallic cases. In particular, the idea was to check if we could achieve similar high power behaviours with smaller filter volumes. Indeed, the main idea was to reduce the distance from the ports to the helices to do the design more compact. So, two additional designs were done, with a relatively small distance from the ports to the helices and with an intermediate distance. Both cases were done by using the cylindrical and conical type of resonators. It must be remarked that, due to design constraints, when using a conical or cylindrical resonator, not only the shape of the helix is changing, but also, up to certain point, the cavity dimensions and the distance from the helix to the port. Therefore, a direct comparative between both helix shapes is not as easy as it may seem. **Table 3-6** shows the comparison between the breakdown power levels for the different designs. The first number shown in each cell is the breakdown power level whereas the second one is the estimated multipactor order obtained from SPARK3D. These results have been obtained by using the silver properties according to the ECSS standard.

Cavity	No Rexolite	
	Cylindrical	Conical
Small	1.8 / 10	3.8 / 7
Medium	900 / 5	205 / 5
Large	360 / 5	390 / 5

Table 3-6: Breakdown power level for the three configurations using the SEY of Silver

From the results, several interesting facts have to be remarked:

1. The best design seems to be the "Medium" size design. This is a design in which the distance from the port to the helix is around 12 mm (again, it is important to note that this distance is different for the conical and cylindrical resonators). It is also remarkable the fact that the breakdown in the case of the conical resonator is significantly lower than in the cylindrical one.
2. The "Small" design is clearly the worst case, indicating that probably the distance from the port to the resonator is playing a key role in that case. A significant increase (3 dB) in the breakdown power level in the conical case with respect to the cylindrical one is found in this case.

3. Finally, in the case of the "Large" cavity, the conical and cylindrical resonator results are quite similar. This may be explained by the fact that breakdown in the case of the conical resonator was taken place from the bottom to the helix to the wall in which the helix stands (as seen in Table 3-6) and this is basically the same configuration in both cases.

The items exposed above will be further clarified in the following lines by taking resort to the surface statistics available from SPARK3D.

We start by analysing the small filter case. Figure 3-26 shows the emission density for the small size conical filters obtained in SPARK3D for an input power of 4.125 W, whereas Figure 3-27 shows the emission density for the small size cylindrical filter obtained in SPARK3D for an input power of 1.78 W.

In this case, it is clearly seen that the breakdown occurs in both cases between the port wall and the helix, as expected, because of the small gap involved. Also, it is very interesting to notice how, for the conical filter, the breakdown occurs at a lower section than in the case of the cylindrical resonator. This happens because the gap in the top part of the conical helix is significantly larger than in the bottom part. This also explains why the breakdown threshold is significantly larger in the conical case than in the cylindrical one: the field is higher on the top part of the helix and, therefore, the power needed to develop a discharge in that zone is lower.

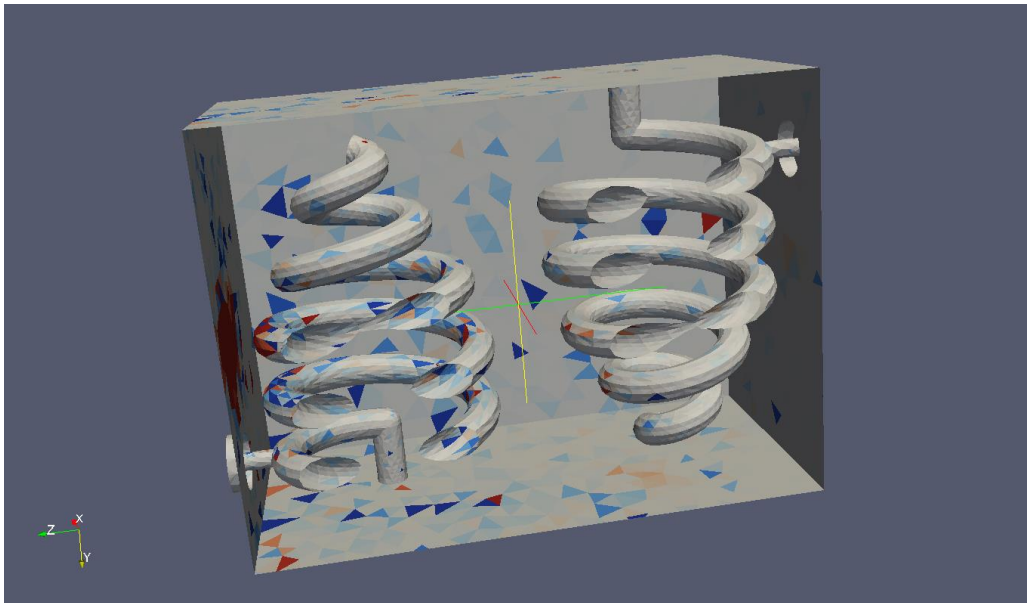


Figure 3-26: Emission density in the case of the small size conical filter.

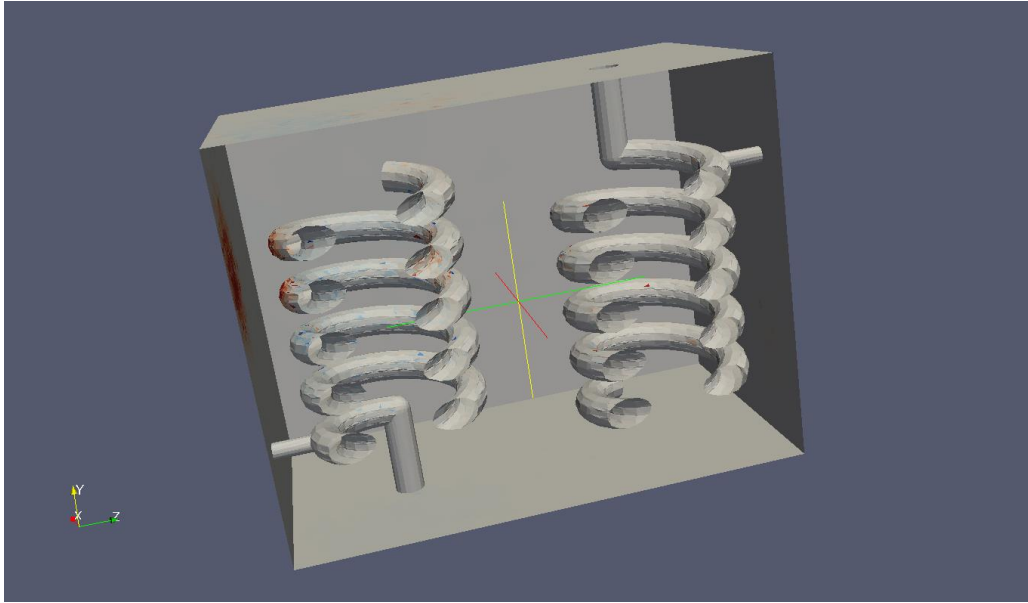


Figure 3-27:Emission density in the case of the small size cylindrical filter.

Next we analyse the "medium size" cavity results. Figure 3-28 shows the emission electron density for a power level of 208 W for the medium size conical filter. It is clearly seen that the discharge occurs between the helix and the wall in which the helix stands (as it happened in the large size filter). However, in the case of the cylindrical filter (Figure 3-29), for an input power of 960 W, it seems that the discharge takes place between the cavity walls. This is a behaviour observed before and it usually happens when the power applied is much higher than the typical range of operating of the cavity component.

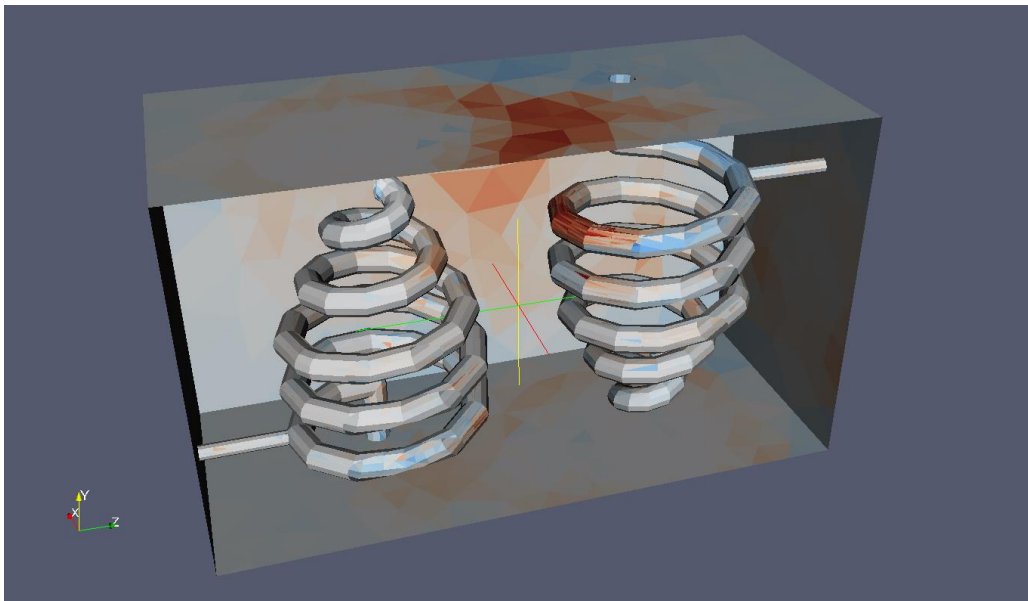


Figure 3-28:Emission density in the case of the medium size conical filter.

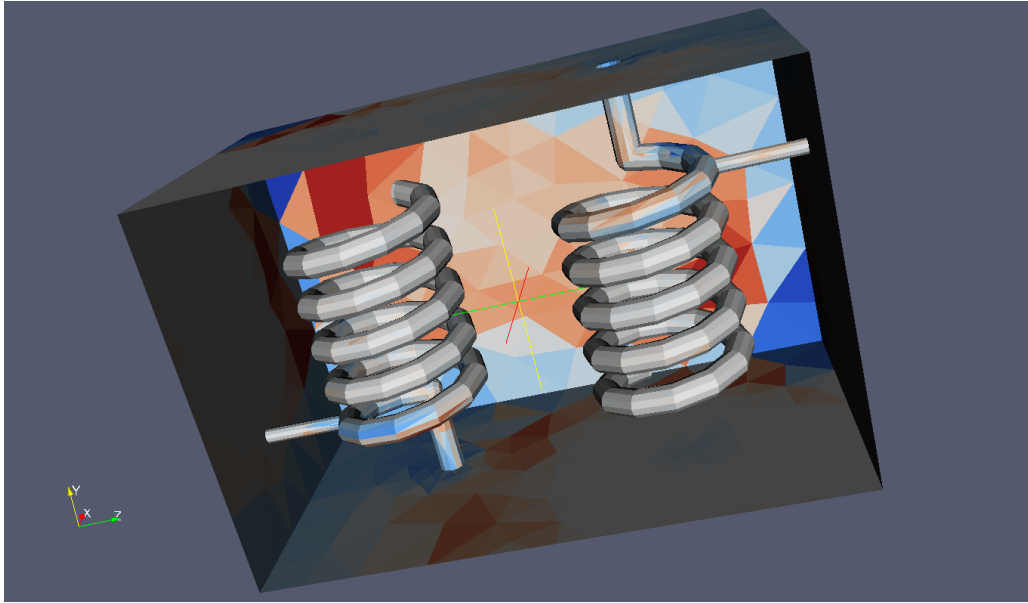


Figure 3-29: Emission density in the case of the medium size cylindrical filter.

After analysing these results, it was decided to perform high power simulations with different surface materials. This was done in order to assess the possible impact of the Surface Electron Yield variation on the threshold and to analyse what can happen when the prototypes are manufactured and tested. Table 3-7 shows the breakdown thresholds for the case of Aluminium, whereas Table 3-8 shows the same for Alodine. It is seen that there can be a drastic reduction on the breakdown threshold. The reason for this is associated to the fringing effect in which the discharge strongly depends on the surface properties. This dependence can be so strong that one can pass from a situation in which breakdown is not possible to a situation in which the breakdown is just few watts (see, for instance, the comparison between Alodine and aluminium for the medium size cylindrical case).

It is interesting to see, how, as the material becomes better, the multipactor order goes down. This is caused by the fact that, in order to compensate the electron loss, the production rate has to increase which can be only achieved by releasing more electrons per impact (increasing the input power) and by increasing the number of impacts with time (lower multipactor order, which is also achieved by increasing the power level).

Cavity	No Rexolite	
	Cylindrical	Conical
Small	1 / 9	0.55 / 7
Medium	7.3 / 11	3.8 / 11

Large	100 / 8	32 / 8
-------	---------	--------

Table 3-7: Breakdown power level for the three configurations using the SEY of Aluminum

Cavity	No Rexolite	
	Cylindrical	Conical
Small	31 / 5	900 / 2
Medium	No Break.	2150 / 2
Large	2500 / 3	No Break.

Table 3-8: Breakdown power level for the three configurations using the SEY of Alodine

In Figure 3-30, the emission density is shown for the medium size filter (cylindrical configuration) in the aluminium case at an input power of 7.375 W. It can be seen that breakdown in this case can occur between the top part of the helix and the wall above it, but also, there seems to be the possibility to have discharge between the wires of the helix. In other words, the worsening of the SEY properties used in the simulation allows for different discharge zones which are, otherwise, not possible.

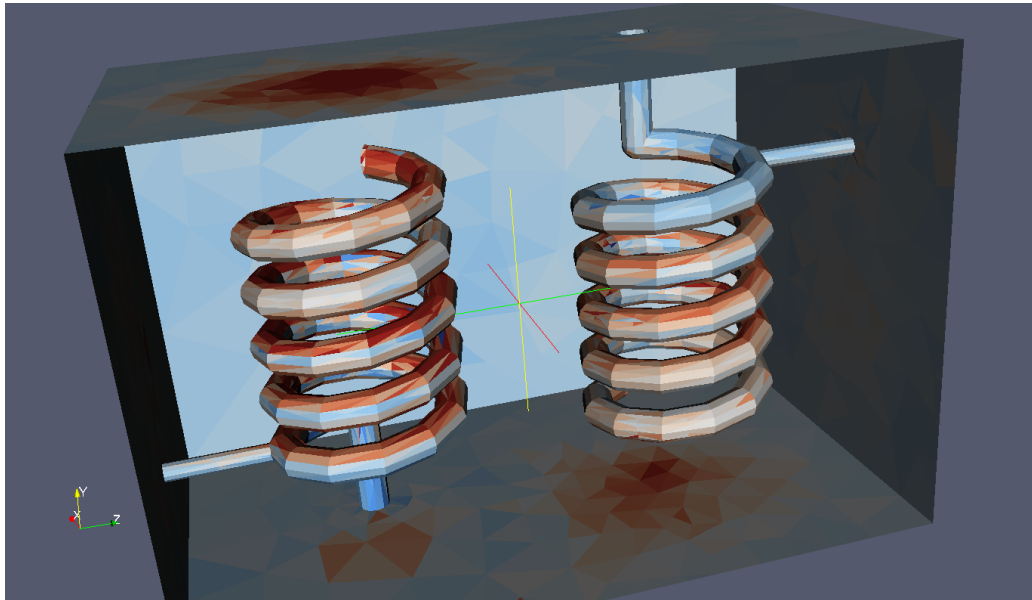


Figure 3-30: Emission density in the case of the medium size cylindrical filter for Aluminum SEY

In Figure 3-31, the emission density is shown for the medium size filter (conical configuration) in the aluminium case at an input power of 3.875 W. It can be seen that breakdown in this case occurs between the top part of the helix and the wall above it. In this case, this must be the worst area because of the small gap present. To point out again what is occurring, one could argue that this discharge location should be also present in case of using other SEY parameters. However, due to the shape of the top part of the helix, fringing effects are here noticeable which leads to the possibility that breakdown could only occur when the SEY properties are such that the electron loss can be compensated by increasing the field in the zone (i.e. increasing the input power).

3.3.3 *Small length cavity with rexolite*

Just to finalize the analysis of the results and due to the fact that the small length cavity with rexolite was analysed in the past, we provide here some understanding of what happens in this case. Figure 3-31 shows the emission density in this case. The discharge occurs between the port walls and the lateral part of the rexolite and also between the top/bottom part of the rexolite and the top/bottom cavity walls.

It is interesting to notice that the discharge between the lateral side of the rexolite and the port cavity walls does not take place at the minimum distance but on the sides of the rexolite cylinder. This is probably caused by the fact that, indeed, the fd product at the minimum gap is at the left side of the multipactor mode order one so breakdown is not possible unless the gap becomes larger, which is the reason why the resonance is displaced.

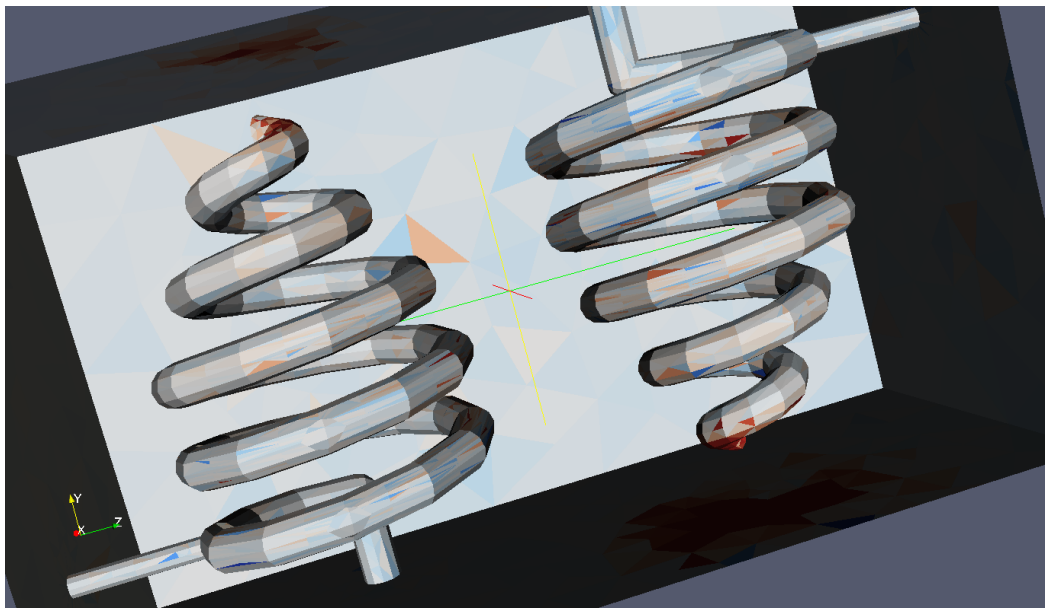


Figure 3-31: Emission density in the case of the medium size conical filter for Aluminum SEY

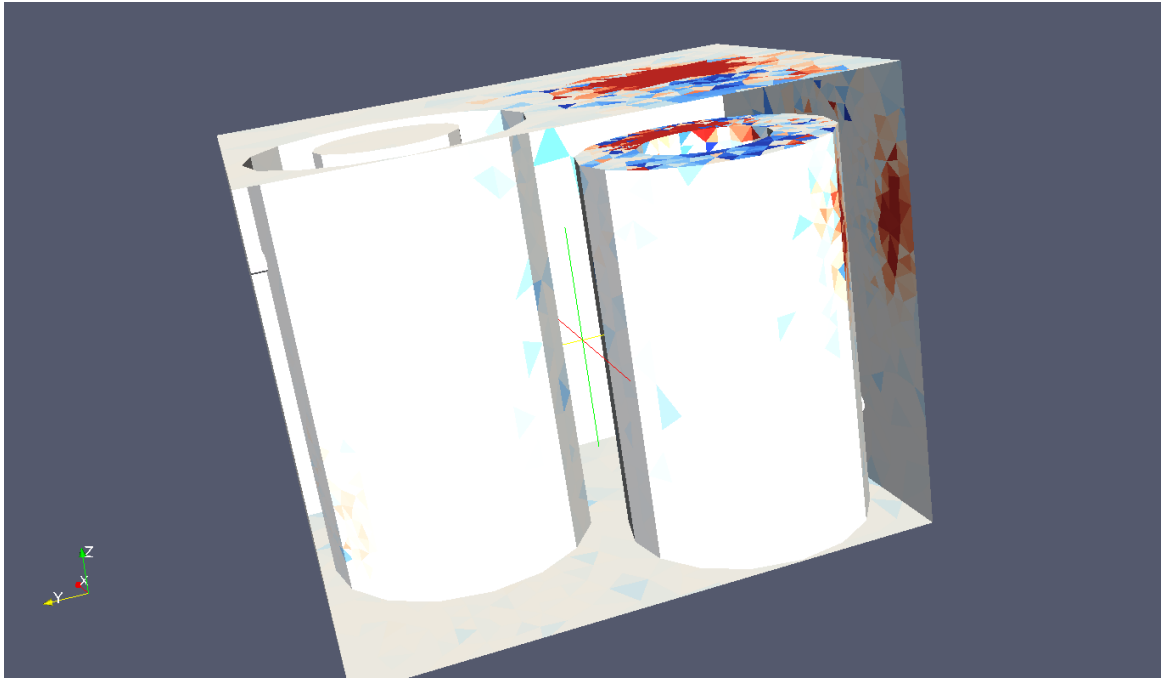


Figure 3-32: Emission density in the case of the small size cylindrical filter for silver SEY

3.3.4 *Designed prototypes and multipaction analysis results*

The design process that is used during this project, has brought at the analysis of ten different types of second order helical resonator filters as shown in the following Figure 3-33

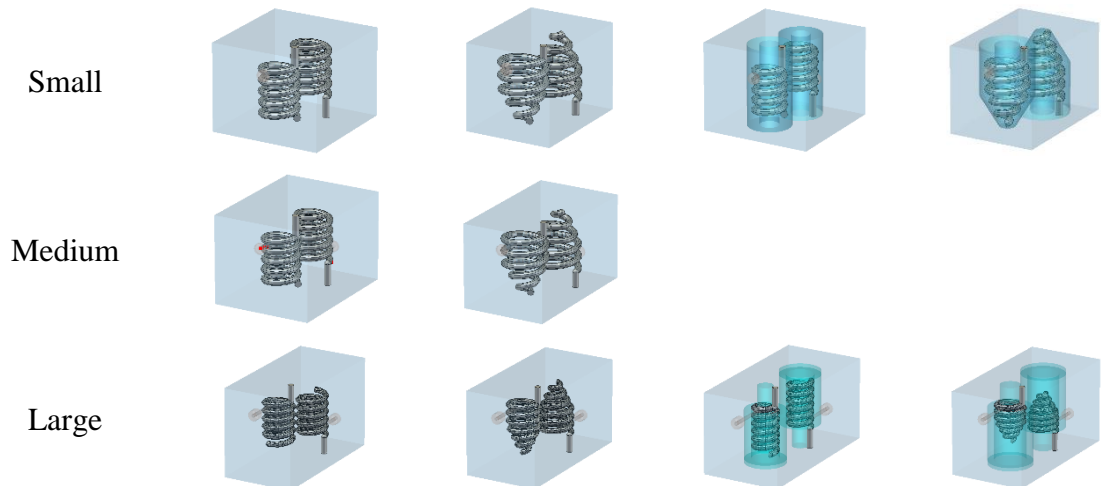


Figure 3-33: Overall pictures of the analyzed structures

With regards to the investigation on prototypes with improved power handling, a series of ten 2nd order filter prototypes have been designed and assessed in terms of their electrical performance and power handling. The key differentiators between the prototypes are:

- The size of the hosting cavity (small, medium, large)
- The use of cylindrical or step-conical helices
- The use of Rexolite covers

The power handling performance of the prototypes is summarised in the tables below from Table 3-9 to Table 3-11.

Power handling (W): **Aluminium**

Cavity	No Rexolite	
	Cylindrical	Conical
Small	1 / 9	0.55 / 7
Medium	7.3 / 11	3.8 / 11
Large	100 / 8	32 / 8

Table 3-9: Multipactor analysis with Aluminium

Power handling (W): **Silver**

Cavity	No Rexolite	
	Cylindrical	Conical
Small	1.8 / 10	3.8 / 7
Medium	900 / 5	205 / 5
Large	360 / 5	390 / 5

Table 3-10: Multipactor analysis with Silver

Power handling (W): **Alodine**

Cavity	No Rexolite	
	Cylindrical	Conical
Small	31 / 5	900 / 2
Medium	No Break.	2150 / 2
Large	2500 / 3	No Break.

Table 3-11: Multipactor analysis with Alodine

Based on these results, these observations could be done

Observation 1: In order to achieve the same electrical response, the dimensions of the filters have to be tuned and this seems to affect the power handling significantly. **The trends defined by macro scale dimensions are not always visible due to micro-scale differences**

Observation 2: Different materials seem to affect power handling significantly. From this observations, the following conclusions could be formulated.

Conclusion 1: The use of conical geometries give a significant improvement only for small cavities.

Conclusion 2: It appears that significant gains can be obtained by increasing the cavity dimensions.

In order to meet these conclusions, 4 different prototypes are chosen:

1. The Medium Cavity Uniform Cylindrical helical resonator + 17 micron for silver plating (**M.U.S**)
2. The Long Cavity Uniform Cylindrical helical resonator + 17 micron for silver plating (**L.U.S.**)
3. The Long Cavity Step Conical helical resonator + 17 micron for silver plating (**L.SC.S.**)
4. The Medium Cavity Uniform Cylindrical helical resonator with Alodine (**M.U.A**)

In the Table 3-12 is also presented the ratio between the filters multipaction power level compared to the power level of small cylindrical helix filter covered with Rexolite dielectric cap.

Cavity	No Rexolite		With Rexolite	
	Cylindrical	Conical	Cylindrical	Conical
Small	1.2	2.53	1	1.4
Medium	600	136.66		
Large	240	260	2.4	10.33

Table 3-12: ratio between multipaction power level and power level of small cylindrical filters with rexolite for all prototypes

The previous table shows the history for the development of the filters prototypes. In fact, the first approach was to meet the electric response and try to obtain filters with small foot print; and the process brought to the design of classical cylindrical helices filter (the

Small one in the table). The designed prototype was simulated for multipaction and it results in a very poor performance. For this reason the first way that was attempted was to use a classical technique that consists in covering the helices with dielectric rexolite caps [RD.35]. This solution was used to make comparison between the other filters. Also this solution was simulated for multipaction and the results is in line with the no rexolite case. In this case also a solution using a stepped conical was tried and an improvement seems to appear. Following the approach proposed in [RD.36] a large gap approach was tried and the results are reported in Table 3-12. (Large) The improvement, without rexolite, seems to be evident. In order to obtain a reduced footprint and maintain the good power handling characteristics, another step in the design is implemented moving to Medium length filters. So the final point of the design results in the medium length uniform cylindrical filter that conjugates the positive characteristics for multipaction and a relative small dimensions.

As anticipated in the Chapter introduction, at the end of the design presented in this chapter, it seems evident that the helical resonator filters seems to be a promising candidate for high power filters. In fact the classical alternative of filters in UHF band for high power applications is combline filters. The following Table 3-13 compares the length of the medium length cavity filters with combline filters [RD 31]

Medium Cylindrical helices filter	86.39mm
Comblin filter	127mm
Ratio	1.47

Table 3-13: Comparison between combline and helical filters

As presented in table the combline is much longer than the helical resonator. The other possibility is to use lumped element filters, but The quality factor results very low: the helical resonator filter has a $Q = 2000$ while the lumped elements are in the order of 10. All these considerations are used in order to justify the choice of the prototypes that have been manufactured and presented in the next chapter.

CHAPTER 4 – TEST CAMPAIGN OF OMUX STUDY

4.1 Manufacturing of the prototypes

4.1.1 *Prototype manufacturing*

During the design phase, different types of resonators were designed as shown in Figure 3-33

All the prototypes that were designed have taken into account the issue of the multipaction effect; So in this perspective a series of 10 pseudoelliptic second order filters have been designed and optimized considering their electrical and power handling characteristics.

The key differences between prototypes are as follows:

- Dimensions of the cavity (small, medium and large)
- Use of cylindrical or tapered helices
- Using rexolite covers

Power handling performances are summarized in the previous chapter 3

Concerning these results, the following conclusions can be drawn:

- 1) To achieve the same electrical responses, filter sizes must be tuned and appear to have a significant impact on power handling. This means that macroscopic scales are not always visible due to microscopic differences.
- 2) Different materials seem to have a significant impact on power handling.

For these reasons we can conclude:

- A) The use of conical geometry for the helices yields remarkable results only for small cavities.
- B) It seems that really worthwhile effects in limiting multipaction can be obtained by increasing the size of the cavities.

For these reasons, it has been chosen to produce 4 different prototypes:

- 1) Medium Cavity Uniform Cylindrical helical resonator + 17 micron for silver plating (M.U.S)
- 2) Long Cavity Uniform Cylindrical helical resonator + 17 micron for silver plating (L.U.S)

- 3) Long Cavity Step Conical helical resonator + 17 micron for silver plating (L.SC.S.)
- 4) Medium Cavity Uniform Cylindrical helical resonator with Alodine (M.U.A)

The following paragraphs, divided into cavities and resonators, report the prototype production process; A further paragraph explains how the tuning process was achieved.

4.1.1.1 Cavity

The cavities that house the helices inside have been produced in the Heriot Watt University's Mechanical Workshop. Cavities were obtained for drilling machining from brass blocks. The manufacturing process has followed various phases ranging from mechanical drawing to real mechanical machining and checking the mechanical dimensions of the single cavity.

First of all, the mechanical drawing was made from the RF electrical design; With this process, it transfers what has been achieved in the RF project in the model that is physically feasible. In fact, what is possible in a theoretical model may actually be unworkable for the limits of the constructive technology chosen. The following figure shows how the mechanical model of the filter was made.

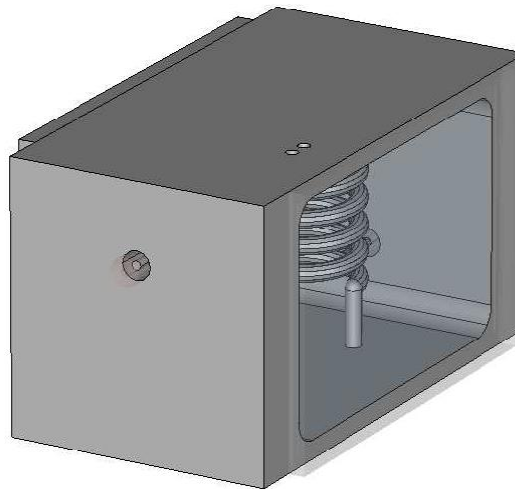


Figure 4-1: Mechanical drawing of the filter

In the figure it can be seen that, for realization purposes, the edges of the cavity were made curved. In addition, the side walls, where the connectors are housed, have been thickened to easily accommodate the connectors. Lastly, it is noticed that the lids that

close the cavity have been designed so that only the inner part of the cavity can be closed, thus saving in weight.

The cavities were made by digging with a brass block cutter. Discharged, for each type of filter, the dimensions of the cavities and lids and their pictures are reported.

- **M.U.S. prototype 3D model**

The following figure shows the dimensions of the M.U.S. cavity. As already mentioned, the edges of the rounded cavities can be noticed because of the tolerances of the manufacturing process. Also, you can observe the venting holes, needed for multipaction tests.

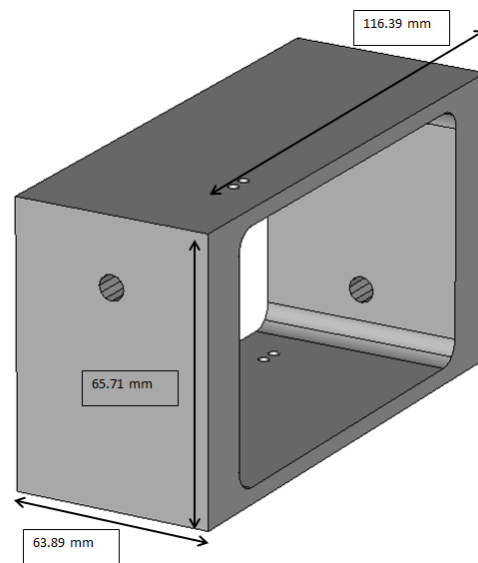


Figure 4-2: 3D model of the M.U.S. cavity

The venting holes, as anticipated, are necessary to bring the air out into the cavity, which would be trapped when the filters are brought under vacuum. The size and number of venting holes are set using the ESA multipactor calculator tool. In fact, the atmospheric pressure requirement for the multipaction test should be conducted at a pressure of 1.5×10^{-3} Pa, so it has been established that the filter should reach this condition in less than 1000 minutes. The following figure shows de-venting analysis. This analysis is necessary for the correct de-venting of the components. In fact, if the ambient background pressure in an RF component is sufficiently high (typically above 10^{-2} Pa), then the multipaction discharge is replaced by a low-pressure gas discharge, where both electrons and ions contribute to free space charge. Low-pressure gas discharges can occur over a wider range of RF voltages than multipaction. To avoid such problems, component venting is designed using the proper suite in the ESA Multipactor Tool.

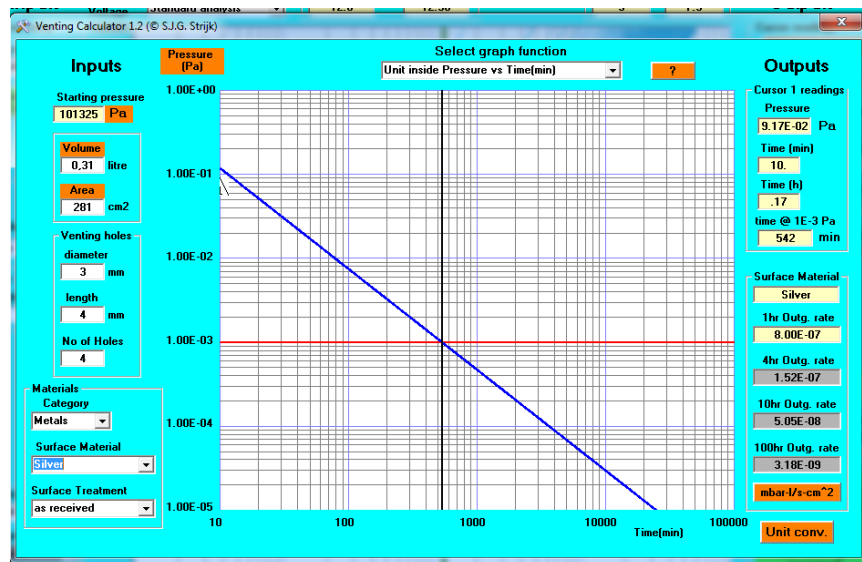


Figure 4-3: Venting analysis for M.U.S. [RD.32]

The following figure instead shows the filter cover, in particular a 2.5mm wide groove was created to facilitate mounting.

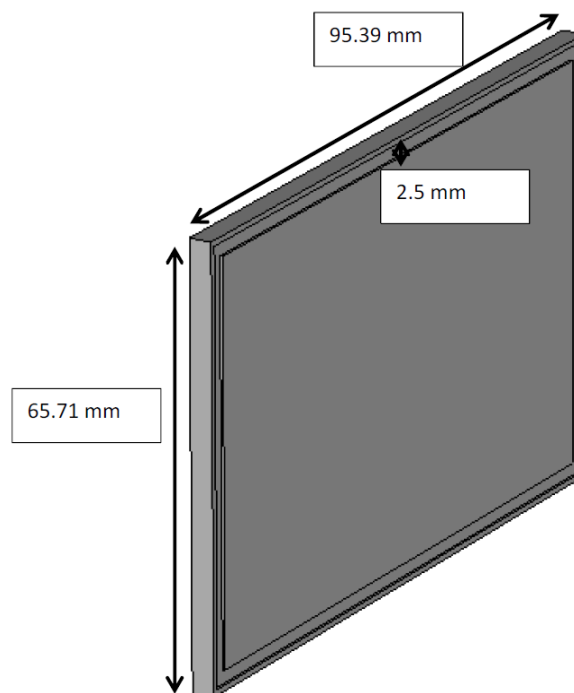


Figure 4-4: 3D model for Covers of the M.U.S.

The picture below shows the cavity and lid as well as the mechanical workshop.

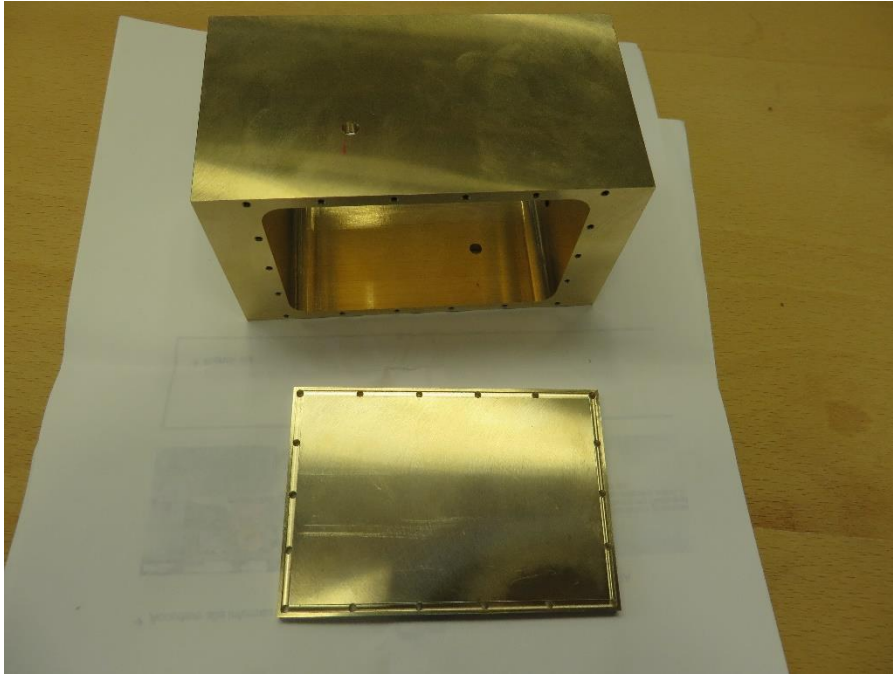


Figure 4-5: Cavity and Covers of the M.U.S.

- **L.U.S. prototype 3D model and results**

The following figure shows the dimensions of the cavity L.U.S. As already mentioned, the edges of the rounded cavities can be noticed because of the tolerances of the manufacturing process. In addition, you can observe the venting holes required for multipaction tests.

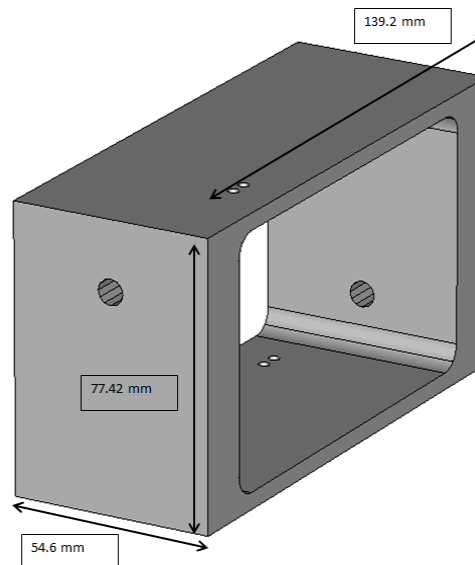


Figure 4-6: 3D model of the L.U.S. cavity

The venting holes, as anticipated, are necessary to bring the air out into the cavity, which would be trapped when the filters are brought under vacuum. The size and number of venting holes are set using the ESA multipactor calculator tool. In fact, the atmospheric pressure requirement for the multipaction test should be conducted at a pressure of

$1.5 \times 10^{-3} \text{ Pa}$, so it has been established that the filter should reach this condition in less than 1000 minutes. The following figure shows de-venting analysis.

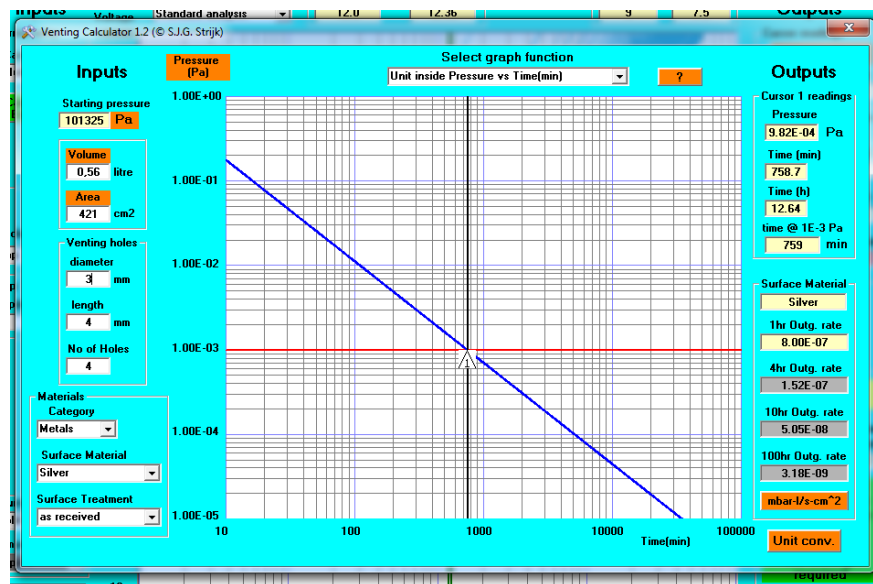


Figure 4-7: Venting analysis for L.U.S. [RD.32]

The following figure instead shows the filter cover, in particular a 2.5mm wide groove was created to facilitate mounting.

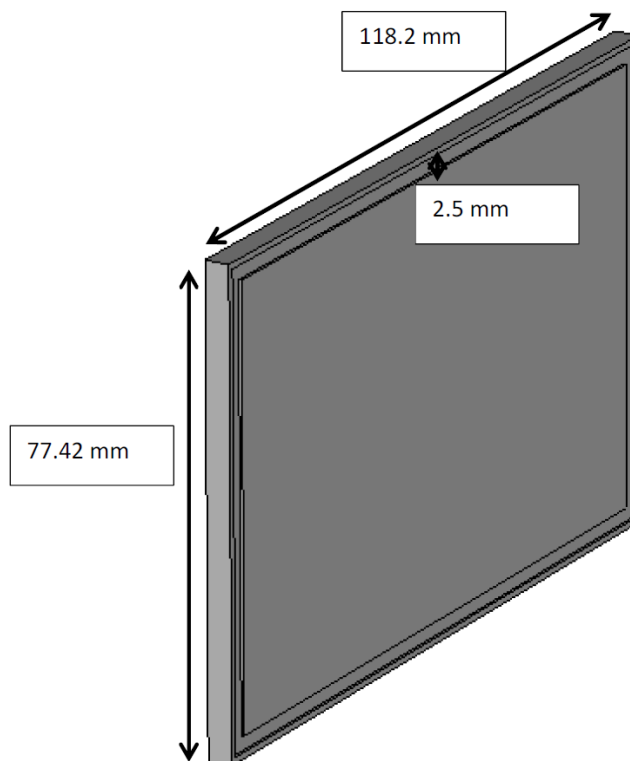


Figure 4-8: 3D model for Covers of the L.U.S.

The following photo shows the cavity realized from mechanical workshop.

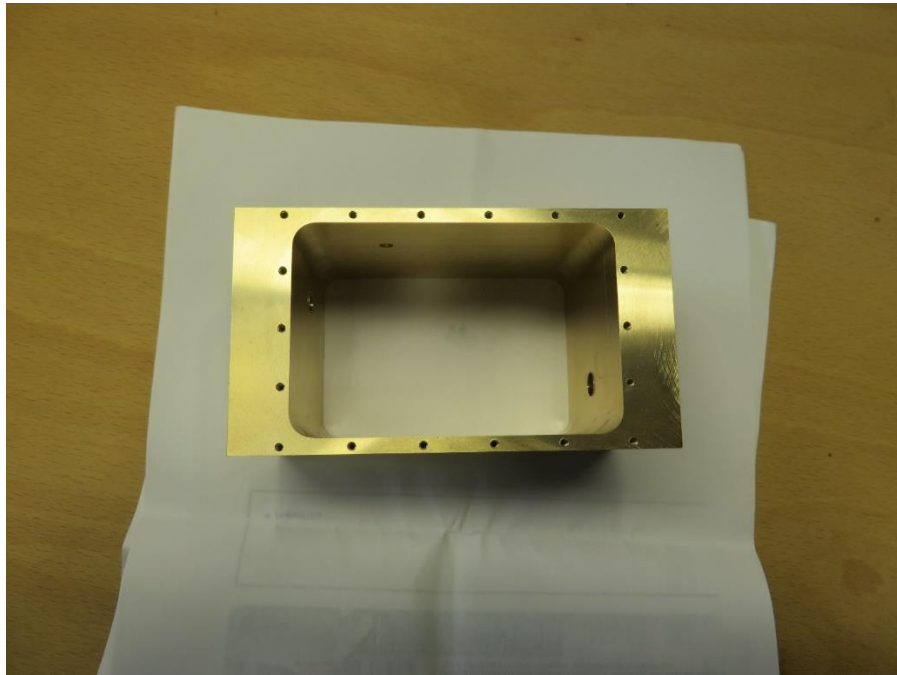


Figure 4-9: Cavity of the L.U.S.

- **L.SC.S. prototype 3D model and results**

The following figure shows the dimensions of the cavity L.SC.S. As already mentioned, the edges of the rounded cavities can be noticed because of the tolerances of the manufacturing process. In addition, you can observe the venting holes required for multipaction tests.

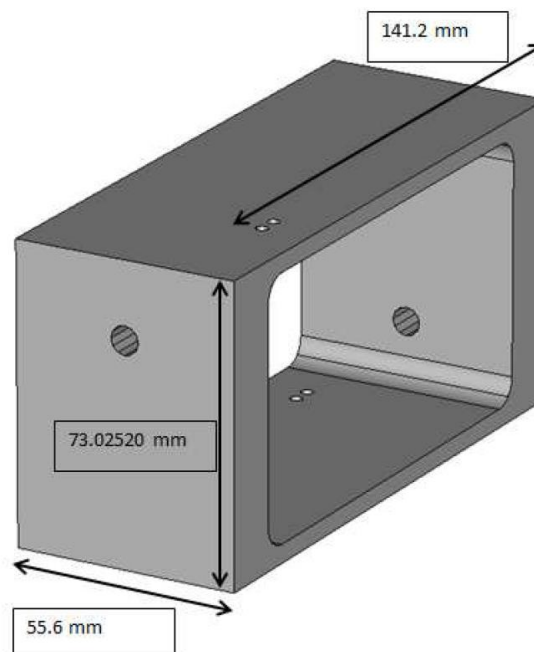


Figure 4-10: 3D model of the L.SC.S. cavity

The venting holes, as anticipated, are necessary to bring the air out into the cavity, which would be trapped when the filters are brought under vacuum. The size and number of venting holes are set using the ESA multipactor calculator tool. In fact, the atmospheric pressure requirement for the multipaction test should be conducted at a pressure of $1.5 \times 10^{-3} \text{ Pa}$, so it has been established that the filter should reach this condition in less than 1000 minutes. The following figure shows de-venting analysis.

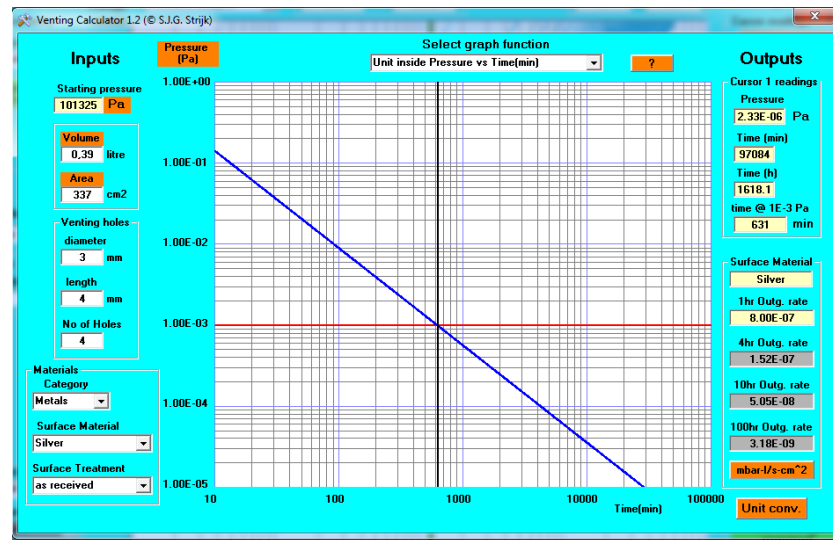


Figure 4-11: Venting analysis for L.SC.S. [RD.32]

The following figure instead shows the filter cover, in particular a 2.5mm wide groove was created to facilitate mounting.

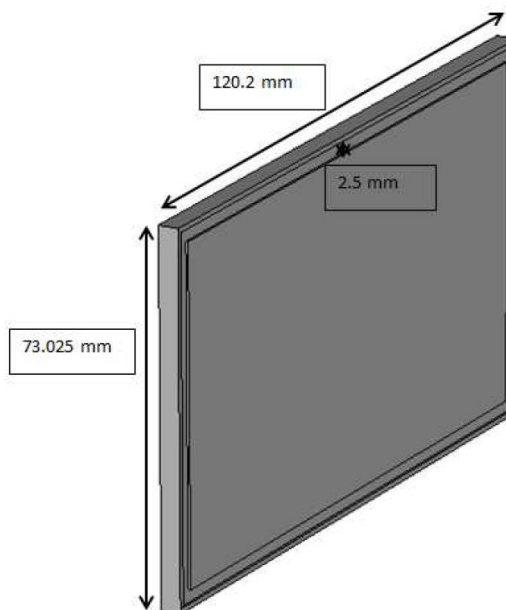


Figure 4-12: 3D model for Covers of the L.SC.S.

The photo below shows the cavity as well as the mechanical workshop.

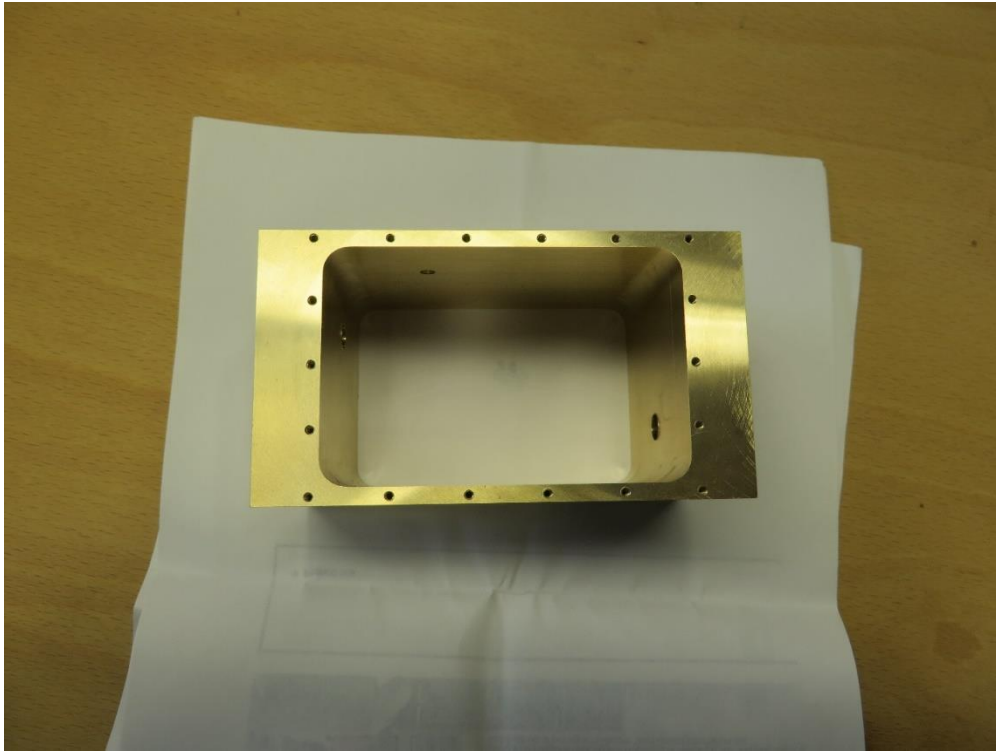


Figure 4-13:Cavity of the L.SC.S.

4.1.1.2 Helix

The helices are the resonators that are housed in the cavity. They were made of enamelled copper wire AWG 6 (4.11mm diameter). In order to realize them, the mechanical workshop wound copper wire on special preformed cylindrical supports to achieve cylindrical and step-shaped helices (see figure).



Figure 4-14:support for the helix realization

The results is reported in the following figure.

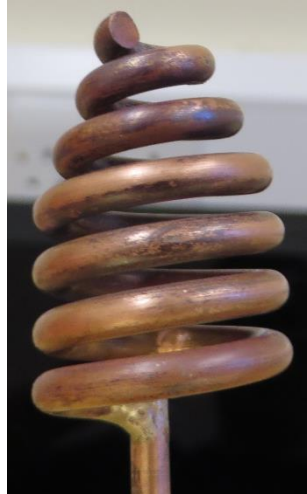


Figure 4-15:Step conical helix

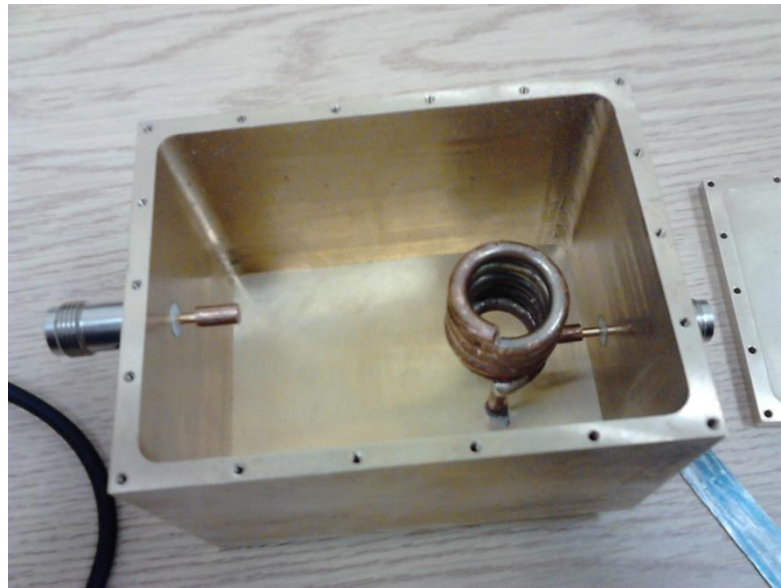


Figure 4-16:Cylindrical helix

4.1.1.3 Tuning

Filter tuning was performed starting directly from the filter in its final configuration without surface treatments. The filters are tested using a VNA to evaluate the response in terms of their s-parameters. The connectors are not welded to the helices; the helices are trimmed and cut until they reach the desired result (central frequency, bandwidth, and zero transmission). This is the most delicate part because, due to the mechanical stresses given on the helix, there is a deformation on the turns, which must be retrieved by resetting the deformations that have arisen. In addition, the contact point of the connector on the helix is a point to be taken into consideration. In fact, in order to obtain a well-matched filter, the contact point must be in a precise position on a helix loop. This was accomplished by connecting a copper cylinder directly to the connector and looking for

the contact point by rotating the helix around the ground pin. Once the point has been found, this has been marked so as to accurately establish the point of contact (see figures).



**Figure 4.1-17:Realization of the cylindrical copper for the connector position
(cylindrical helix)**



**Figure 4.1-18:Realization of the cylindrical copper for the connector position (step-
conical helix)**

Lastly, the cavities used for tuning are not those for the multipaction test, but the dummy pieces made exclusively for tuning purposes.

4.1.1.4 Assembly and plating

At the end of the tuning process, the helices are assembled into their cavities and silver plated or chromated. The following photos report the assemblies

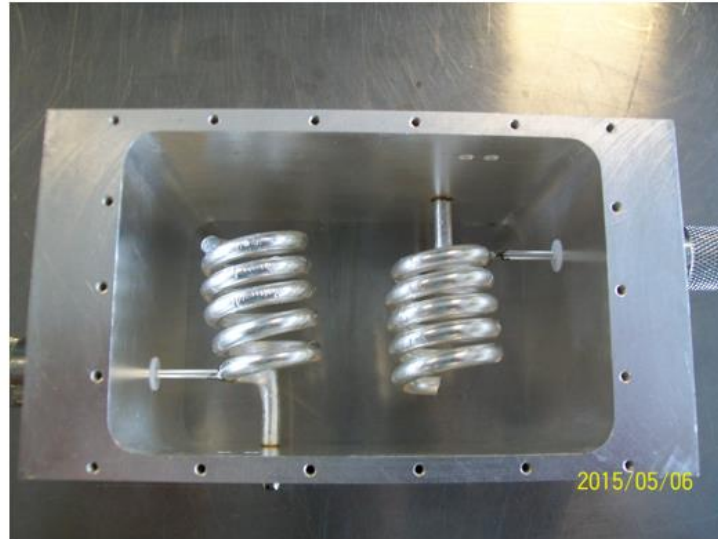


Figure 4-19:Assembled Silver Plated M.U.S.

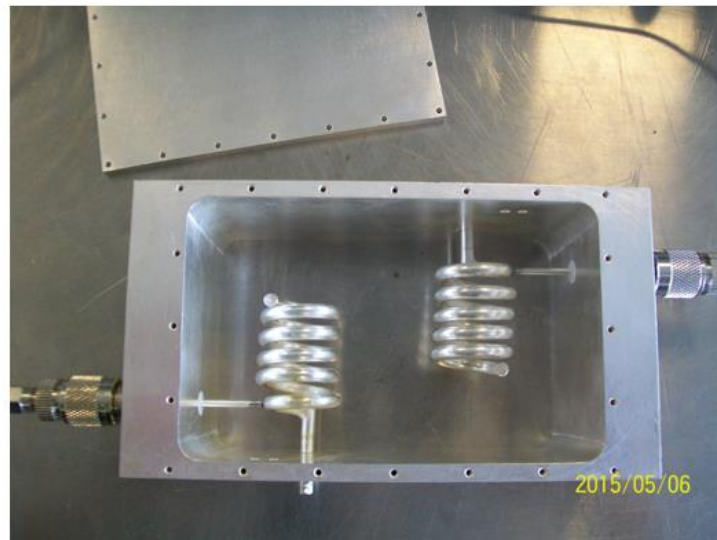


Figure 4-20:Assembled Silver Plated L.U.S.

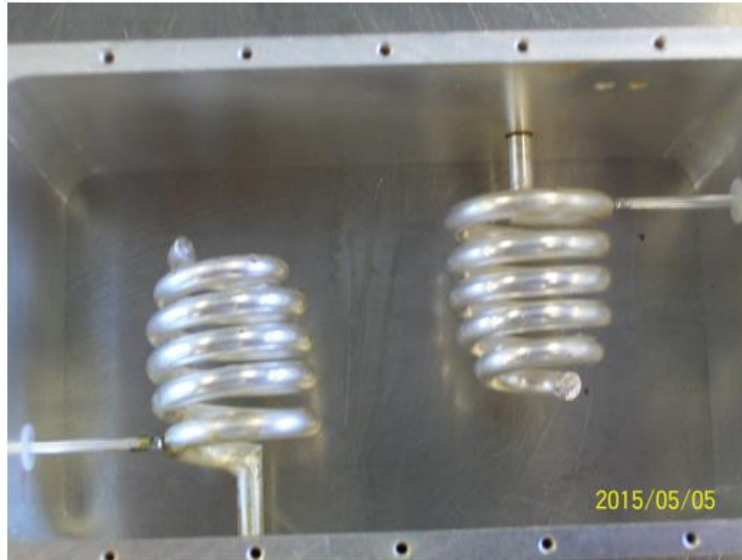


Figure 4-21:Assembled Silver Plated L.S.C.S.

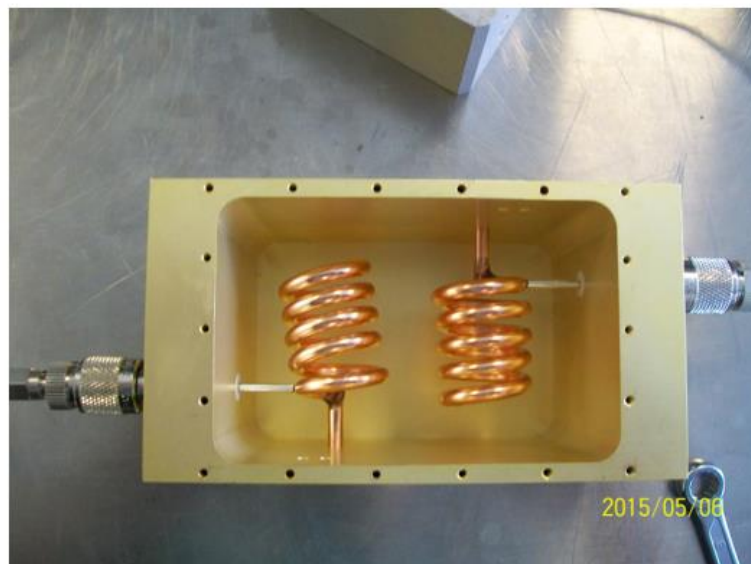


Figure 4-22:Assembled M.U.A.

4.1.2 Low Power test

4.1.2.1 RF test campaign

There were two types of test campaigns: low power and high power RF campaigns.

The low power campaign was performed to verify that the filters were performing satisfactorily with regard to the S near band parameters. In fact the return loss of the all filters are in the order of 18-20dB and the insertion loss is always better than 0.3dB in

band. This verification has also proved to be necessary to demonstrate that the tuning process has been carried out appropriately.

The test campaign was conducted in the RF laboratory of Space Engineering in Rome and below there are the measured values of the filters in question, compared to the simulated values. The good results of the filters behaviour in terms of electric performances are evident in the next figures, where all the prototypes response are depicted overlapped.

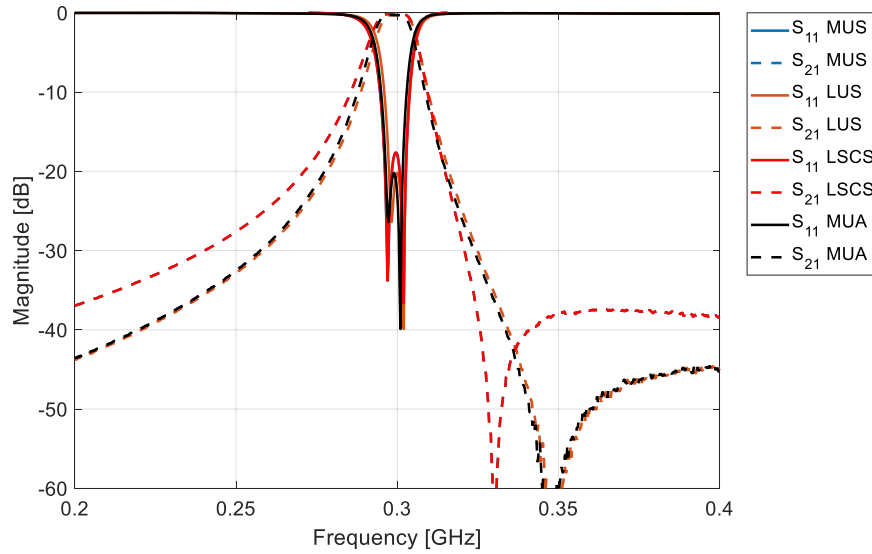


Figure 4-23: Overall measurements of the measured filter prototypes

What it is possible to see from the previous figure is that the response of the filter results in line with the desired near band rejection and return loss for all the measured prototypes.

In detail the following figure shows the Return loss of all manufactured filters

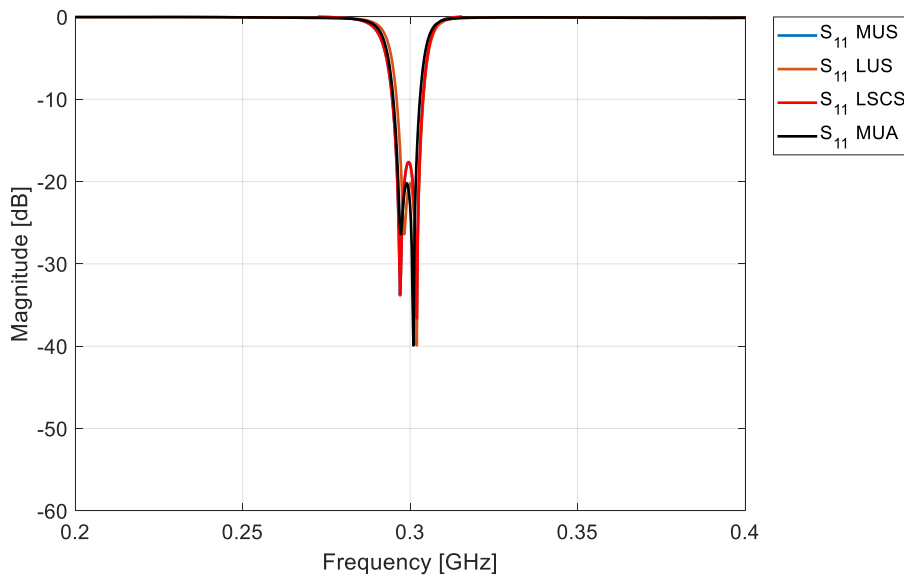


Figure 4-24: Return Loss of the measured filter prototypes

As evident the filter response results in a very good behaviour giving a return loss in the order of 18-20dB. The next figure shows the measured Insertion loss.

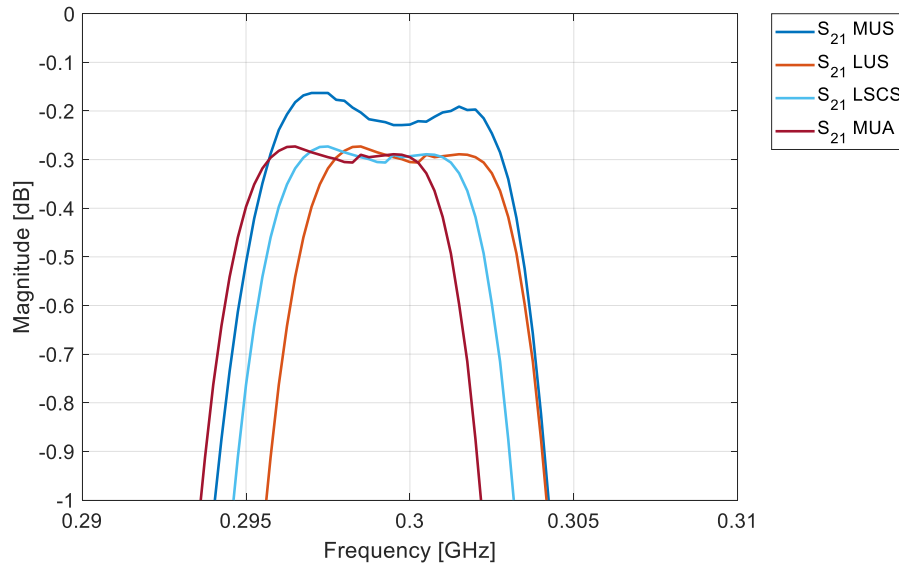


Figure 4-25: Insertion Loss of the measured filter prototypes

The last figures states that the realized filters have very low loss. In any case the best behaviour is found for the MUS filter that combines the benefits of a small length of the waveguide housing (smaller than LUS) and silver plating surface treatment.

Generally, Slight Mismatching is due to the tuning process that, being the most delicate part, does not allow for greater precision. As regards the insertion loss, it was seen to be better than 0.3dB for each filter, while the simulations were performed with the ideal material, since no final conductivity due to surface treatment processes (chromatic conversion and silvering). The theoretical mismatch with the theoretical results are mainly related to extreme difficulties in the manufacturing process; in fact a very precise machine tools, can remove problems and no corrective actions during the tuning needs to be performed. Moreover, a precise manufacturing permits to have the correct soldering process between the helices and the connectors, that is the most sensible point. All the manufacturing uncertainties makes the tuning process much difficult and impacts on the RF performances and Multipaction, as it is visible in the next section dedicated to the power handling analysis.

4.1.3 High Power test

4.1.3.1 High power test premises

A block diagram of the test apparatus and how the test was conducted is shown in the following Figure 4-26

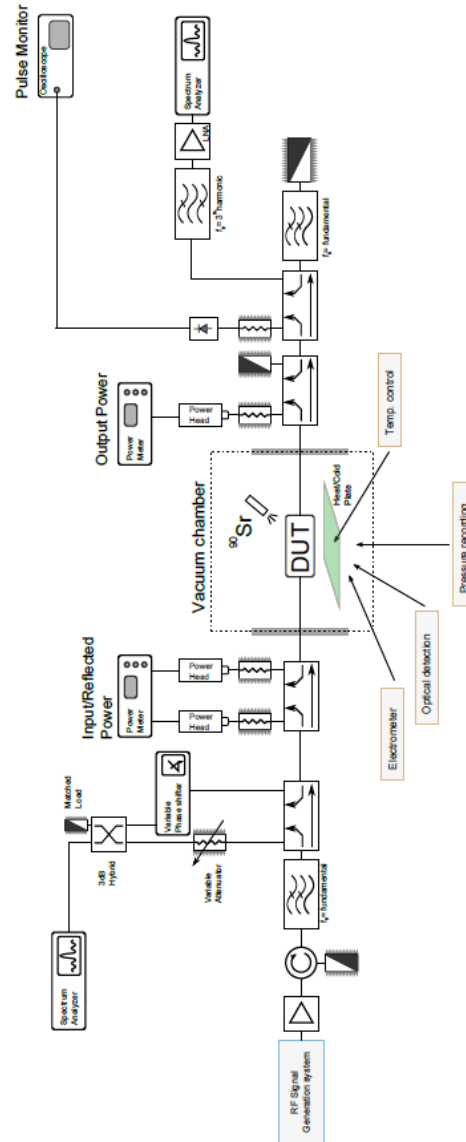


Figure 4-26: Basic RF Breakdown Test Bed.

To measure the presence of multipaction, the following systems were used:

1. Nulling of Forward/Reverse Power Detection Method

In this detection system a proportion of transmitted and reflected power is coupled into a phase and amplitude-matching network. Once the system is balanced, the two signals produce a null, which is very sensitive to amplitude and phase variations

within the system. An RF discharge creates an imbalance and a loss of the null. One disadvantage is that it is difficult to achieve and hold a good null.

2. Third Harmonic Detection

This detection method is one of the most reliable detection methods in use and works because a discharge spreads energy over the spectrum, resulting in increased power in harmonics. For optimum operation, the harmonics generated by the HPA need to be filtered out, good coupling of the generated harmonic components is also required.

3. Electron Avalanche Detector

This method relies on the ability of a small positively charged probe to attract free electrons generated as a result of a discharge. A high impedance amplifier connected to the probe provides impedance transformation of 50 Ohm. An oscilloscope or voltmeter may then be used to monitor the probe current.

4. Optical Detection

A very effective detection method is to detect photons that are released during the RF Breakdown, either from the surface of the material or by ionising the residual gas molecules present within the vacuum system. An optical fibre is placed through a small hole in RF component as near as possible to the photo-multiplier outside the chamber. Any output from the photo-multiplier is displayed on an oscilloscope and also triggers a RF breakdown occurrence detector.

In the following **Table 4-1** there are described the Multipaction test parameters

Multipaction Test	
Frequency	300 MHz
Pressure	$< 1.5 \cdot 10^{-5}$ mbar
Temperature	ambient
PRF	1000 Hz
Pulse width	40 μ s
Duty Cycle	4%
Max. RF power (Peak)	850 W

Table 4-1: Multipaction test parameters

A thermal bake-out was performed under high vacuum during 20 hours at +70 °C ($\pm 5^\circ$ C) with no RF Applied.

The results of the test are depicted in the following **Table 4-2**.

D.U.T.	MEASUREMENTS	MEASUREMENTS	SIMULATION	SIMULATION
	Power @ 1st Discharge	Power @ 2nd Discharge	SEY-1 (Aluminium)	SEY-2 (Silver)
M.U.S.	11.7 W	11 W	7.3 W	900 W
L.U.S.	74.4 W	74.6 W	100 W	360 W
L.S.C.S.	36.6 W	33.7 W	32 W	390 W

Table 4-2: Summary of Multipaction test results

In order to compare the analysis with SPARK 3D and ESA/ESTEC Multipactor calculator, the CAD model of the M.U.S. is simulated into CST™ and the fields are extracted, as presented in the following **Figure 4-27**. The simulation in CST is set with 1W of input power and 300 MHz of centre frequency.

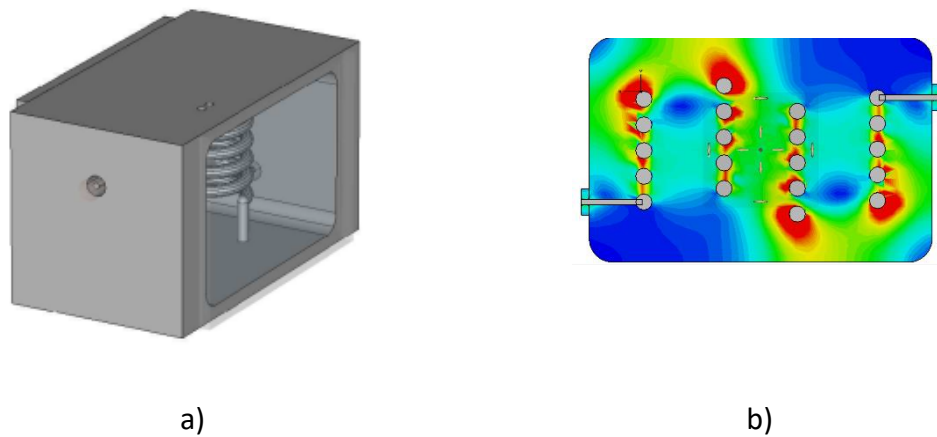


Figure 4-27: a) M.U.S. 3D CAD Model b) Electric field distribution of the simulated model

after the calculation of the electric fields, 4 different path, as described in Figure 4-28, are chosen to perform the integration of the electric field to obtain the Voltages. In particular the 4 gap are:

1. Distance between top of the helix and side wall (Figure 4-28 a)).
2. Distance between the top of the helix and lateral wall (Figure 4-28 b)).
3. Distance between the pitch of the helix (Figure 4-28 c)).
4. Distance between the top of the helix and top wall (Figure 4-28 d)).

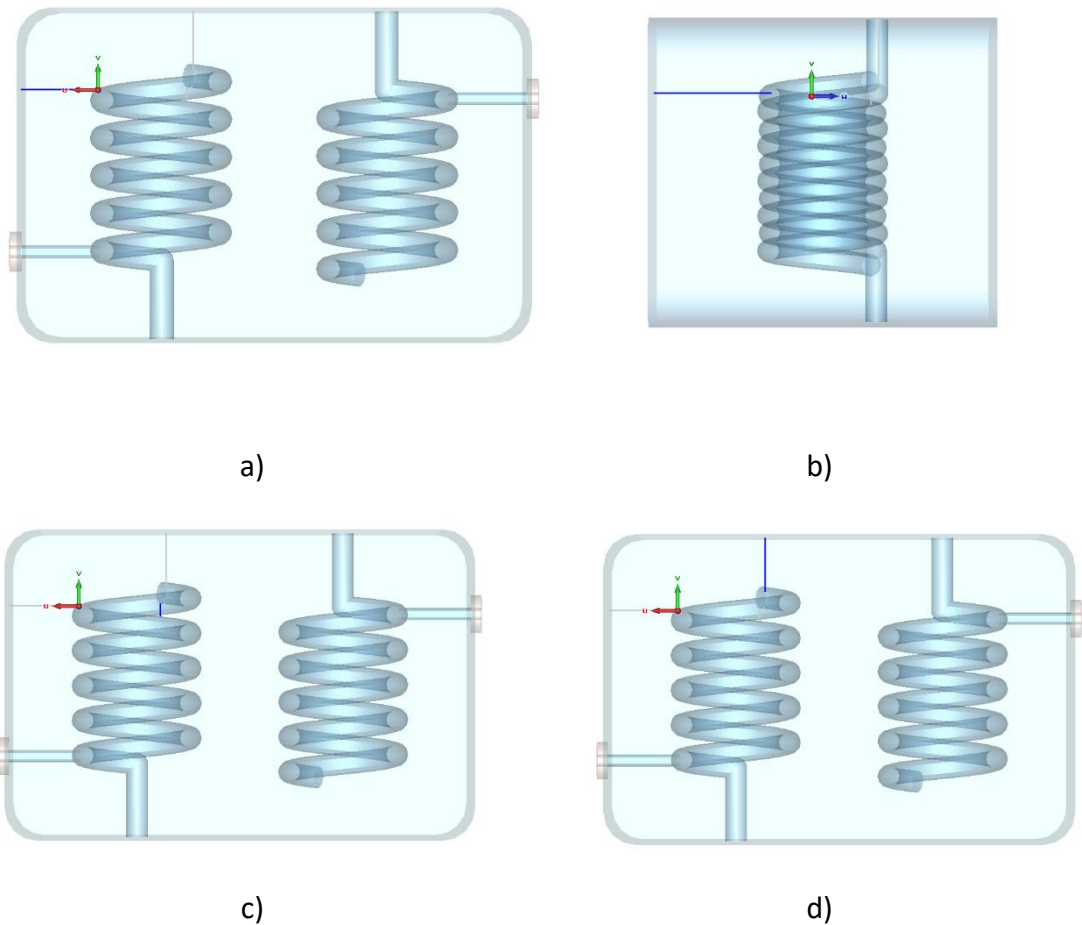


Figure 4-28: 4 different integration path scenarios

A parallel analysis of the same model, is performed by ESA/ESTEC Multipactor calculator, as depicted in the following Figure 4-29. In particular the analysis is set in the following way:

1. **Center Frequency:** 300 MHz (the same imposed in CST)
2. **Input Power:** 1 W (the same imposed in CST)
3. **Gap:** this is the numerical value of the path for the integration of the electric field, described in **Figure 4-28**.
4. **Surface Material:** Aluminum.
5. **ECSS Voltage Breakdown Threshold:** Is the limit where the Multipaction phenomenon appears and it is the output of the analysis.

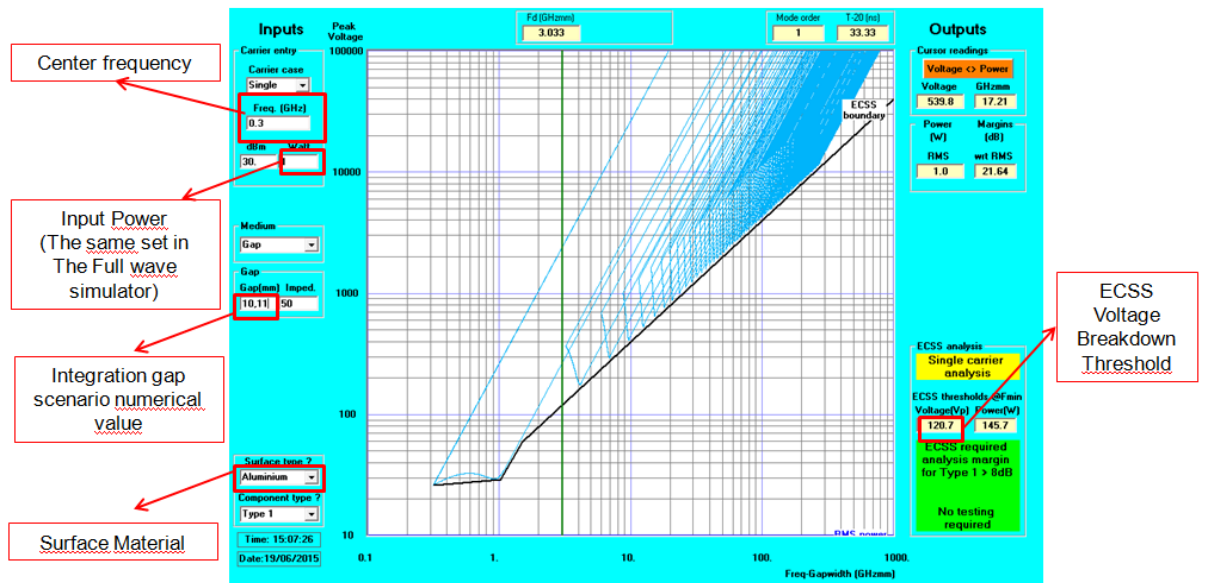


Figure 4-29: ESA/ESTEC Multipactor Calculator Analysis [RD.32]

The final results of this analysis is depicted into the following Table 4-3.

	Gap [mm]	Voltage calculated via CST [V]	ECSS Voltage Breakdown Threshold [V]	Input Power [W]	Input Power for breakdown [W]
Integration Path 1	13.091	107.765	156.300	1	2.103
Integration Path 2	22.268	97.544	265.900	1	7.431
Integration Path 3	2.417	11.531	28.100	1	5.938
Integration Path 4	10.113	113.231	120.700	1	1.136

Table 4-3: ECSS Analysis

In the previous Table 4-3 Input Power for Breakdown is input power to set in CST to have the corresponding ECSS Voltage Breakdown Threshold. The relation used for the calculation is the following

$$P_{Input\ Breakdown} = \left(\frac{V_{ECSS}}{V}\right)^2 P_{input} \quad (4-1)$$

The following Table 4-4 shows the final comparison between the ECSS analysis tool (ESA/ESTEC Multipactor Calculator) and SPARK3D analysis

D.U.T.	MEASUREMENTS Power @ 1st Discharge [W]	MEASUREMENTS Power @ 2nd Discharge [W]	SIMULATION SPARK3D SEY-1 (Aluminium) [W]	SIMULATION ECSS SEY-1 (Aluminium) [W]
M.U.S.	11.7	11	7.3	1.136

Table 4-4: Comparison Between ECSS analysis tool and SPARK3D

4.2 Discussion

4.2.1 Conclusion

In conclusion this work has demonstrated several aspects of using the helical resonator filter for high power operations.

First of all, the improvement with respect to multipaction of helix filters without dielectric filling has been studied and experimentally verified. In fact, it is noted that there is a drastic improvement (from 10 W to 75 W) in multipaction behaviour passing from small cavities to large cavities. This aspects is of fundamental importance considering the complex helix resonators filter geometry.

On the other hand, also the step-conical structure of the helix is developed and studied, but there are no significant improvement using this kind of configuration, as confirmed by simulation and tests results.

It is demonstrated (through simulation and measurements) that is possible to achieve a breakdown voltage values similar to those obtained by means of introducing Rexolite within the filters. In fact, this additionally leads to improvements in terms of mass, costs and Q factor with a small sacrifice of volume.

Finally, the simulated and measured multipaction results are presented in Table 4-2; it is evident that the measured multipaction results of the silver plated filters are very close to the SPARK3D results obtained considering aluminium SEY. The SEY values for

practical silver-plated components is in the order of aluminium mainly due to the criticality of the process of silver plating.

Considering the classical solution used to avoid multipaction, the comparison is not immediate; in fact the other classical solutions for low frequencies and high power, are helices with rexolite dielectric cap, and combline. These solutions are often customized for the multipaction characteristics, so it is not easy to find correct information. Following [RD.31] and [RD.33], the following table could be derived

Filter Topology	Theoretic Power Handling[W]
Comblin	100W
Helices with rexolite dielectric cap	90W
Medium uniform silver plating helical resonator filters	900W
Long uniform silver plating helical resonator filters	360W
Step conical silver plating helical resonator filters	390W

Table 4-5: Comparison Between classical solution for multipaction and medium/long uniform/step conical silver plating filter

As evident from Table 4-5 the theoretical characteristics of the helical resonator filters, permits to have a good increment for the multipaction.

Moreover, the table shows the theoretical value that are the only parameters that could be compared. In fact, as conclusion of the work, it is possible to summarize the results in order to have a clear point of view regarding the advantages and disadvantages of the helical resonator geometry. Using Table 3-13 that compares the length of the medium helical filter and combline filter, with Table 4-5 (focused on the medium cavity), the multipaction values vs the dimensions make the medium uniform helical resonator filters the best candidates for the power handling applications. The most evident and critical disadvantage is related to the fabrication issue: in fact, the combline filters could be manufactured by direct drilling the cavity and pins, making the machining process very robust. The realization of the helical filter is divided into two phases: the cavity realization with classical manufacturing and the helical realization. All this process introduces uncertainties on the production that make the process not robust. The high uncertainties in production, impacts in the tuning of the filter. In this sense, the tuning process modifies the filter geometry and it has a dramatic impact on the multipaction performances as

described in Table 4-2. So, in conclusion, the positive characteristic of the helical resonator, could be efficiently used if the manufacturing process will become more robust.

As last remarks, a comparison analysis between SPARK3D and ESA/ESTEC Multipactor Calculator was performed and Measured vs. SPARK3D obtained results indicate significant improvements compared to ECSS corresponding results; this indicates that ECSS implementation is quite conservative as compared to SPARK3D analysis.

5.1 Introduction

5.1.1 *Potential applications of the dual mode concentric helices*

The term Search and Rescue (SAR) is a set of rescue operations conducted by the use of trained people with the use of specific air or land vessels aimed at the safeguarding of human life in particular danger; in order to have a situation of Search and Rescue, it is necessary that there has been an event that has put at risk human lives. This event can mainly be e.g. due to:

- subjective Carelessness: e.g. face without proper preparation and equipment environments are particularly hostile to humans.
- Disaster: such as that which occurs following a disastrous event may be as fires, earthquakes and other atmospheric phenomena and not.

Once the event has occurred, the research and recovery of victims, takes place through various stages. First of all, there is the necessity to locate the geographical region where there was a risk; the greater the accuracy with which it determines the danger zone, the best and most effective are interventions. In this case one can speak of a transaction prior to the actual procedure of search and retrieval. this is a crucial stage that concentrate all coordination tasks and for this there is the need to be able to rely on technology with very fast response times. So, in this phase, the most important thing to do is to establish (or re-establish) communications with the areas in which it occurred the danger. Normally, in case of danger, the classical communication infrastructure could be destroyed or unusable, then, it is necessary to have a replacement communication system. This system should be:

- Dedicated exclusively to the research and recovery mission
- Stable in order to avoid disturbances
- Robust so you have no interruptions in communications.

So, in the design of a communication system for search and rescue operations, it is extremely important to keep in mind this type of aspects.

Among the various communication systems, the system considered in this work, is the satellite telecommunications system. This type of system is chosen for several reasons; First of all, the communication link does not require bulky terrestrial infrastructure: Satellite service is available virtually anywhere on earth using small portable ground

terminals. This feature is essential if there is the necessity to replace or restore telecommunications services that are no longer functional, or to catch up with telecommunications remote or inaccessible services (typical example is remote mountainous areas). A further reason for choosing satellite communications is due to the fact that can be dedicated for sectors: for example, it is possible to think a satellite phone service exclusively dedicated to military communications or secure communications, without using telephone networks for civil use.

As already said, Satellites for the Search and Rescue are designed to provide a way to communicate to remote areas. Historically the first satellite service Search and Rescue was in September 1982 when the Russian satellite Cosmos-1383 received a distress signal from the two planes had crashed. The satellite was able to give the exact location to the airport and within rescuers. The Figure 5-1 below shows a typical configuration of a satellite mission for Search and Rescue.

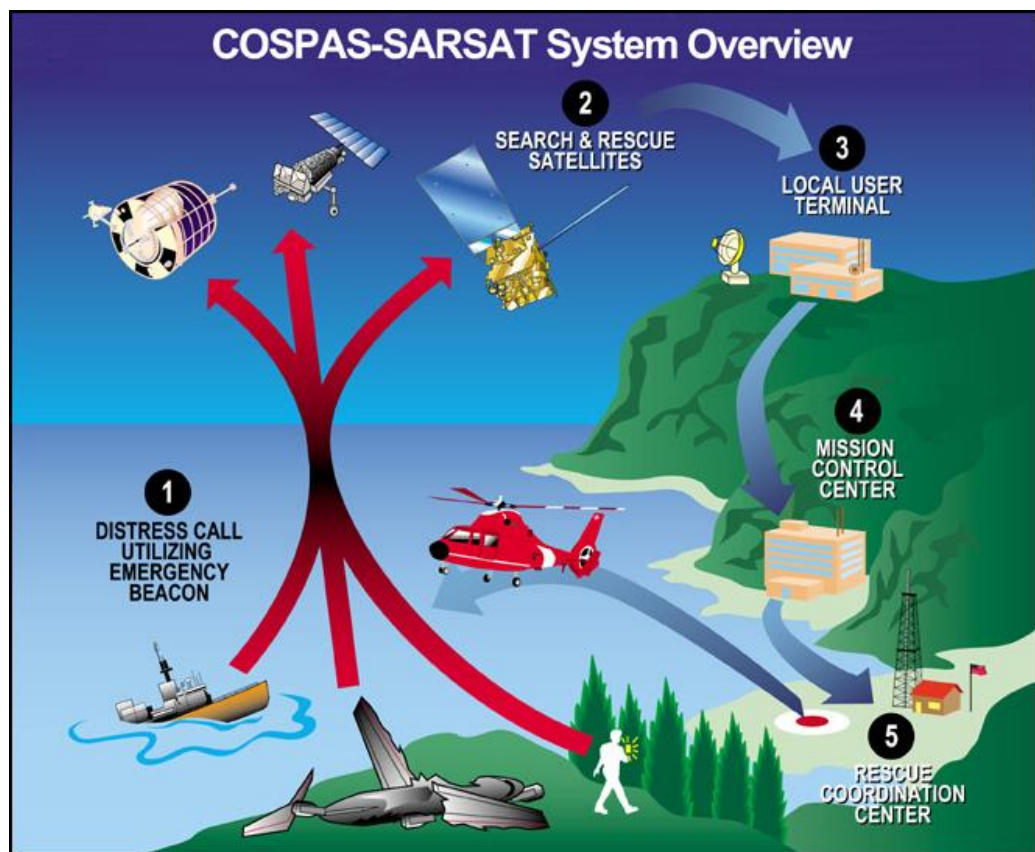


Figure 5-1: Typical mission Search and Rescue (COSPAS-SARSAT)

Because of stringent requirements, mainly regarding weather phenomena, the frequencies of the Tx and Rx are limited mainly to the UHF (300 MHz to 3 GHz). In this range of frequencies, the wavelengths characteristics ranging from meter to ten centimeters thus leading to the filters to have characteristic dimensions of a few tens of centimeters (see

Figure 5-2 below that comes from the analysis and tests presented in the previous chapter).

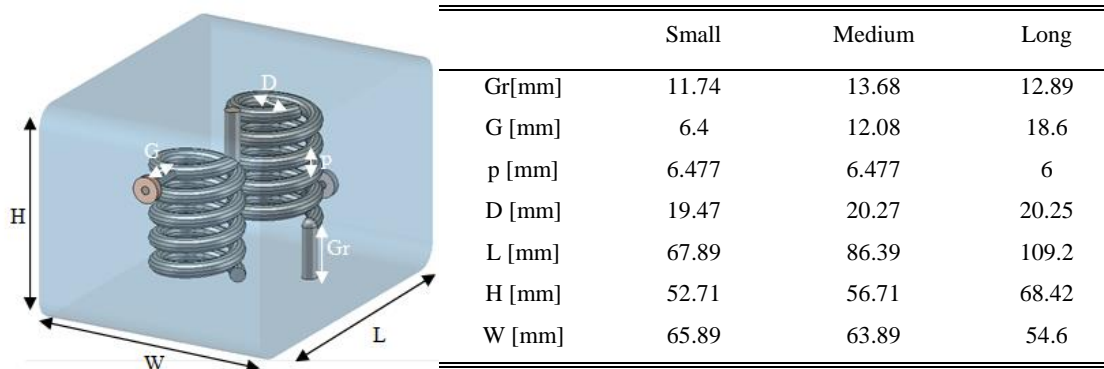


Figure 5-2: helical resonator filter at 300 MHz

Although this type of size are tolerable for terrestrial applications, they are limiting in satellite field.

A further example of satellite applications in which it is possible to use in helical filters can be found in Cubesat



Figure 5-3: Typical Cubesat (Cubesat 3U of IMT Srl)

The Cubesat are very small size satellites in terms of volume and mass which are primarily used for study and research purposes. In the last decade, a growing interest has been directed towards this type of satellite applications, because the small size and simple design makes the masses of important impact on construction costs. In addition, using low-cost components, allows access to space also to universities and research institutions. The low production cost allows to obtain different experimental payload type. For example, focusing on satellites for amateur radio communications, operating frequencies are in the field of UHF. Due to the fact that a cubesat presents characteristics of small dimensions and masses, it is necessary to think of a very compact configuration if there is the will to use the excellent characteristics of the helical filters.

For what concerns the passive filters, resonators in the case of RF, a technique used to save space and make a much more compact configuration, is to have dual mode resonators. Dual mode resonators using two degenerate resonant modes in the same structure can achieve higher order response since a physical cavity corresponds to two electromagnetic resonant cavities. In order to achieve this effect in resonators with helix, it is possible to use the fact that the electric and magnetic fields in the helices are radial and therefore the integrals that define the pair, depend exclusively on the helix radius; so suitably sizing the helix radius and height, it is possible to get a pair of degenerate modes in the same cavity. A further system to have a dual-mode effect is to insert two helices, one inside the other in a concentric manner. In this case, the resonator becomes a double helix, whose fields are still radial. The advantage of this configuration is that, it can be shown that the integrals of coupling depend on the radii of the helices and their heights. The first approach to single helix was originally presented in the work of Ray Kwok [RD.19], while the second approach, followed in this thesis, originates from the work of R. Hayes [RD.20]. These two approaches are presented in the following paragraphs.

5.1.2 Dual mode helical resonator filters

As shown in previous chapters, the helix filters have been used in RF when the filters with lumped elements have too high losses and coaxial resonators $\lambda / 4$ are too bulky. Normally the helices are designed to operate in the fundamental mode. The size may still be excessive, so often embedded helices dielectric material are used. This choice means that it is possible to have a reduction of the space, but the losses increase. In the past, a solution which involves the use of higher order modes into a helix has been proposed in the work by R. Kwok [RD.19].

Starting from the sheath helix model, the eigenvalue equation shown below is obtained:

$$\frac{K'_n(ha)I'_n(ha)}{K_n(ha)I_n(ha)} = -\frac{(h^2 a^2 + n\beta a \cot \alpha)^2}{K_0^2 a^4 h^2 \cot^2 \alpha} \quad (5-1)$$

where:

- k is the free space propagation constant
- $\beta = \sqrt{h^2 + k^2}$ is the axial propagation constant
- h is the radial propagation constant
- I_n, K_n Are modified Bessel functions. The apices are the first derivatives in ha

The solution of this equation that presents a degenerate behavior of the electrical and magnetic fields, is that for the mode $n = 1$ as shown in Figure 5-4

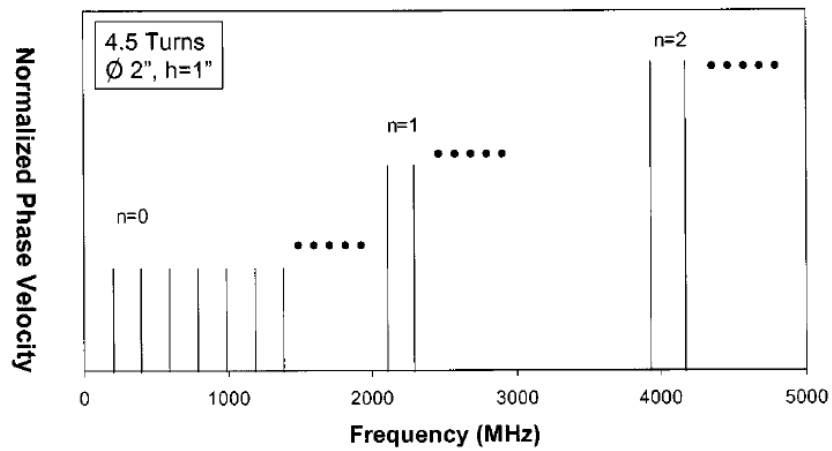


Figure 5-4: modes N=0,1,2 of sheath helix model [RD.19]

With this background, a dual mode filter helix is designed as shown in Figure 5-5

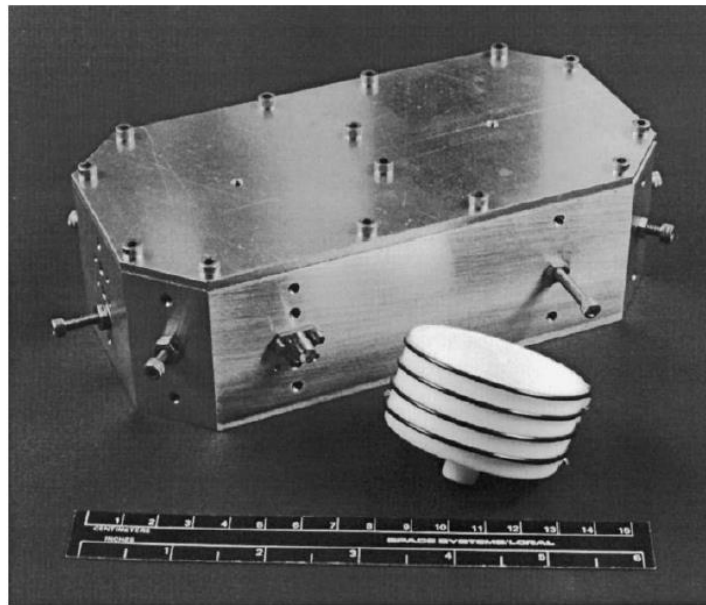


Figure 5-5: helical dual mode filter [RD.19]

While the answer is given in the Figure 5-6:

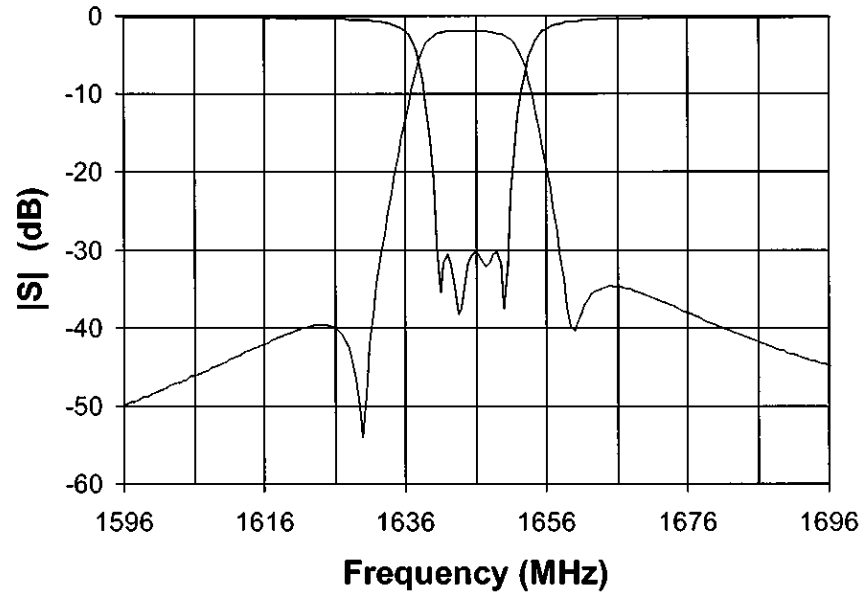


Figure 5-6: Response of dual mode filter [RD.19]

Although the Kwok work has introduced, for the first time, the concept of a dual mode filter in the helix, this configuration has some limitations:

- The helices are wrapped around a dielectric block which impacts the total losses of the filter
- The filter needs tuning screws that have an impact on the total performance of the filter

All these features have led to investigate new solutions that would provide an optimal design regarding size and performance.

5.1.3 The evolution of the helical structures: Higher order modes of the concentric helices

As indicated previously, one of the problems that have occurred in the use of helices dual mode in the Kwok approach, is to have still quite important structures as regards weight and sizes.

In this context, it is necessary to move on to new configurations, and the ideal solution is found in the work of R.E.Hayes ([RD.20]). The concept that is exploited in this work is to have two concentric helices and the expression of the electric and magnetic fields in this configuration. The analysis of a structure of this type, leads to interesting consequences, which can be exploited for the realization of filters.

5.1.4 The concentric helix structure

The problem of electromagnetic waves that propagate in a system consisting of two infinitely long concentric helices in the free space (see Figure 5-7), can be addressed as a problem with boundary conditions. The expression for the field components can be written in terms of cylindrical wave functions.

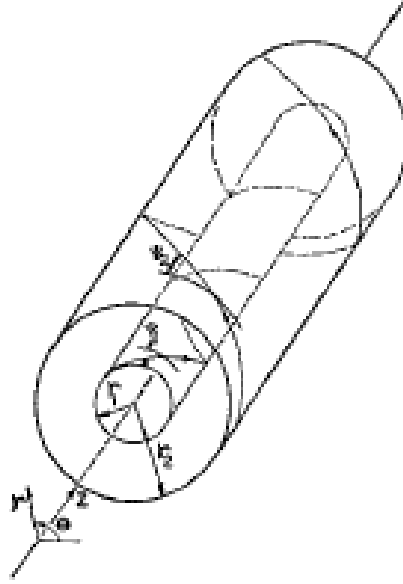


Figure 5-7: schematic representation of concentric helices

With the reference to the previous figure, the concentric helices are divided into three regions:

- Region 1 with $r < r_1$
- Region 2 with $r_1 < r < r_2$
- Region 3 with $r > r_2$

The geometrical parameters for the concentric helices definitions are the following:

- Internal radius r_1
- External radius r_2
- Internal pitch angle ψ_1
- External pitch angle ψ_2

After defining these parameters, you can switch to write the fields components. The expressions and calculations are reported in APPENDIX (from pag. 122 to pag. 131).

From the calculation performed in APPENDIX (from pag. 122 to pag. 125), the equation of the dispersion as shown below is obtained

$$\begin{aligned}
& \left[(1 + \xi)^2 P_{n1} + \frac{y^2}{x^2} P'_{n1} \right] \left[\left(1 + \frac{r_1 \cot \psi_2}{r_2 \cot \psi_1} \xi \right)^2 P_{n2} + \left(\frac{\cot \psi_2}{\cot \psi_1} \right)^2 \frac{y^2}{x^2} P'_{n2} \right] \\
& - \left[\left(1 + \frac{r_1 \cot \psi_2}{r_2 \cot \psi_1} \xi \right)^2 R_n + \frac{\cot \psi_2}{\cot \psi_1} \frac{y^2}{x^2} R'_n \right] \left[(1 + \xi) \left(1 + \frac{r_1 \cot \psi_2}{r_2 \cot \psi_1} \xi \right) R_n \right. \\
& \left. + \frac{\cot \psi_2}{\cot \psi_1} \frac{y^2}{x^2} R'_n \right] = 0
\end{aligned}
\tag{5-2}$$

Where

$$\bullet \quad P_{n1} = I_{n1} K_{n1}, P_{n1} = I'_{n1} K'_{n1} \tag{5-3}$$

$$\bullet \quad P_{n2} = I_{n2} K_{n2}, P_{n2} = I'_{n2} K'_{n2} \tag{5-4}$$

$$\bullet \quad R_n = I_{n1} K_{n2}, R'_n = I'_{n1} K'_{n2} \tag{5-5}$$

$$\bullet \quad x = \tau r_1, y = k r_1 \cot \psi_1 \tag{5-6}$$

$$\bullet \quad \xi = n \frac{\sqrt{\cot^2 \psi_1 x^2 + y^2}}{x^2} \frac{\cot \psi_1}{|\cot \psi_1|} \tag{5-7}$$

The τ values satisfy the equation of the dispersion providing the propagation constants of the various modes that propagate. So, depending on the frequency, one can determine the β for each considered mode. The calculation is very complex and a set of routines for determining it was produced and verified by means of a full wave simulator.

First it established the geometry to simulate commercial software (CST) as shown in Figure 5-8

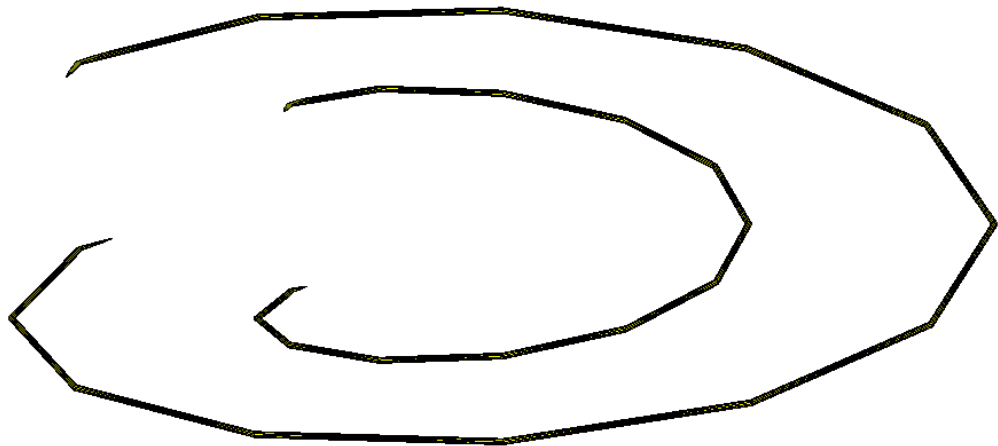


Figure 5-8: Geometrical model concentric helices

This model was then simulated with eigenmode solver with the boundary conditions presented in Chapter 2.

The geometric parameters that were used in the analysis are reported in the Table 5-1 below

Parameter	Value	Description
d	16 [mm]	Internal Helix diameter
d1	32 [mm]	External Helix diameter
p	6.53 [mm]	Internal Helix pitch
p1	6.53 [mm]	External Helix pitch

Table 5-1 : geometrical parameter of concentric helices

The theoretical analysis results were verified with those obtained by electromagnetic simulation and are shown in Figure 5-9

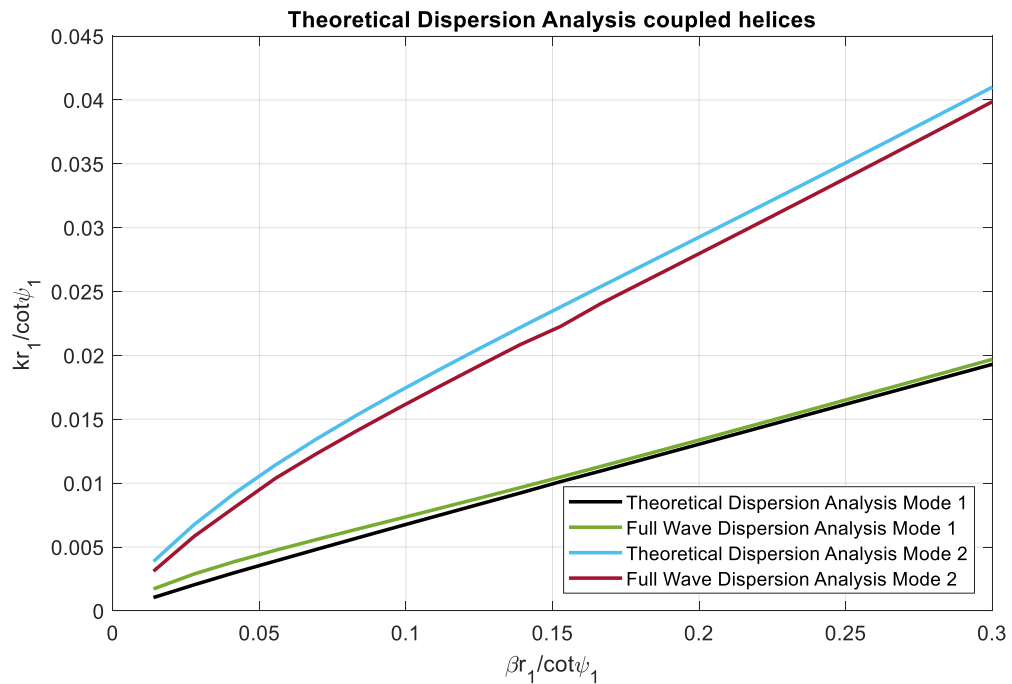


Figure 5-9: Comparison between the simulation and theoretical model

As can be seen, the adherence between the two techniques are sufficiently similar, and it is the confirmation that:

- The theoretical model helices sheath is sufficiently accurate to describe the behavior of concentric helices.
- The theoretical model is used to determine the propagation constant for each frequency, for each mode in a very short time.

- As soon as the β is fixed, the costants $a_n^{(1)}$, $b_n^{(1)}$, $a_n^{(2)}$, $b_n^{(2)}$, $c_n^{(2)}$, $d_n^{(2)}$, $a_n^{(3)}$, $b_n^{(3)}$ that regulate the fields are calculated.
- From the determination of electric and magnetic fields, it is possible to evaluate the coupling coefficients between the two helices which is crucial for the proper evaluation of the performance of the filters.

As anticipated, once the constant β is determined, it is possible to calculate coefficients which determine the electric and magnetic fields. For the first time we have calculated them and they are shown in APPENDIX (from pag. 129 to pag. 131).

In the Figure 5-10 we have been reported for the r component of the electric field as example.

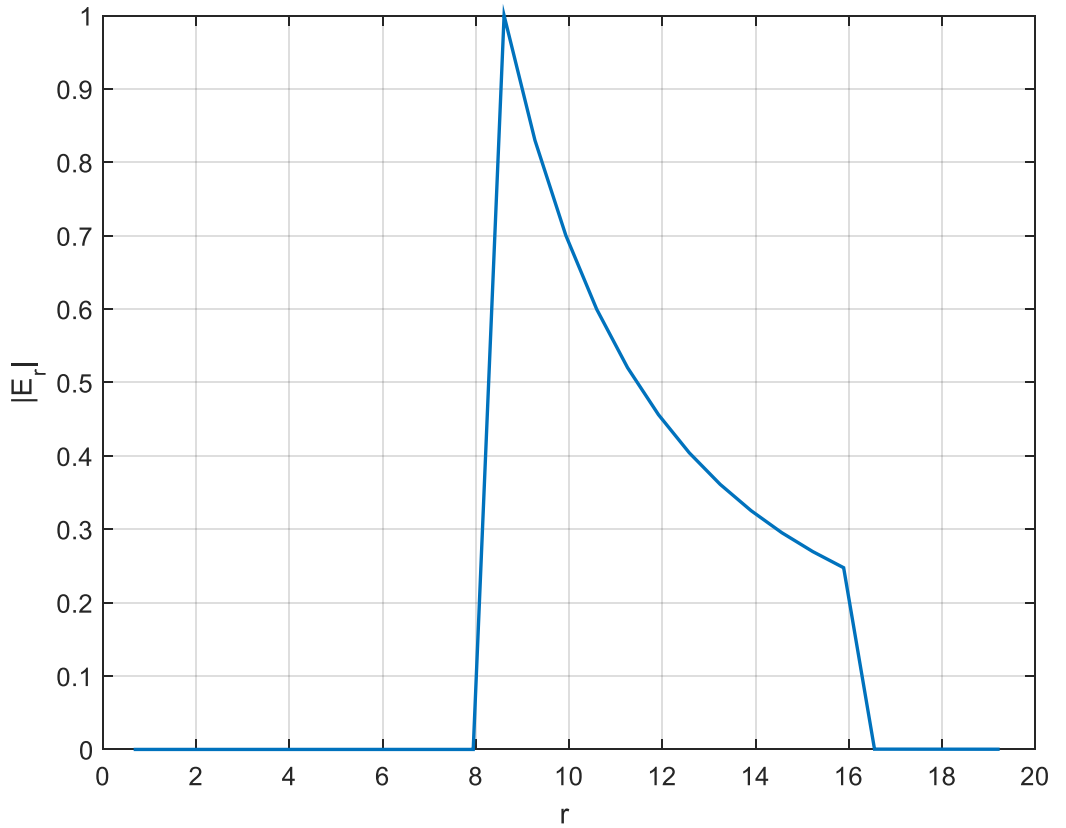


Figure 5-10: Electric field radial component

A test was also conducted using the model of full wave electromagnetic simulator. It is possible to notice that representations tend to coincide with the theoretical ones at the decreasing of the diameter of the wire (see Figure 5-11 below)

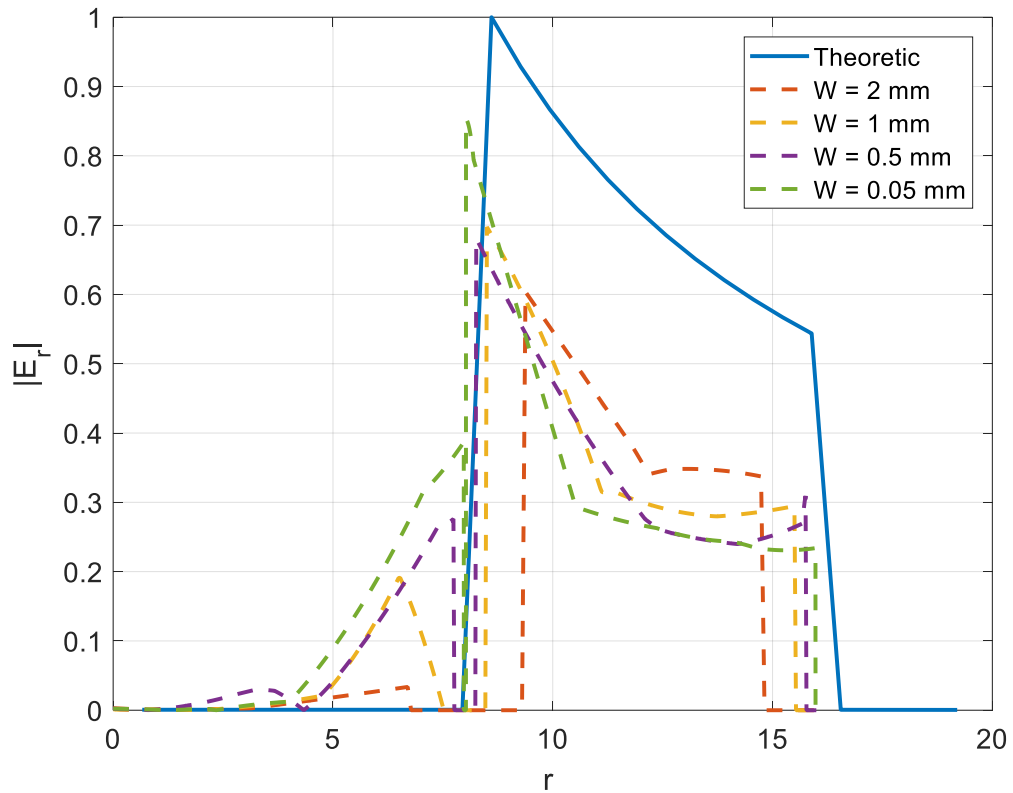


Figure 5-11: Comparison by varying the W wire diameter

These characteristics are strictly valid for the infinite length helices, but are extremely useful for a first sizing of the structures to be used for the realization of a filter.

5.2 Filter design

5.2.1 Synthesis and Analysis of dual mode filter

The filter design was conducted using the classical techniques for the synthesis of the filters. First it started with the design of the second order filter, and then move on to a fourth order filter. The filter specifications are as follows:

- Central Frequency: 745 MHz
- Bandwidth: 10 MHz
- RL: 16 dB

Using a program designed for the purpose, the filter response is obtained as described in Figure 5-12

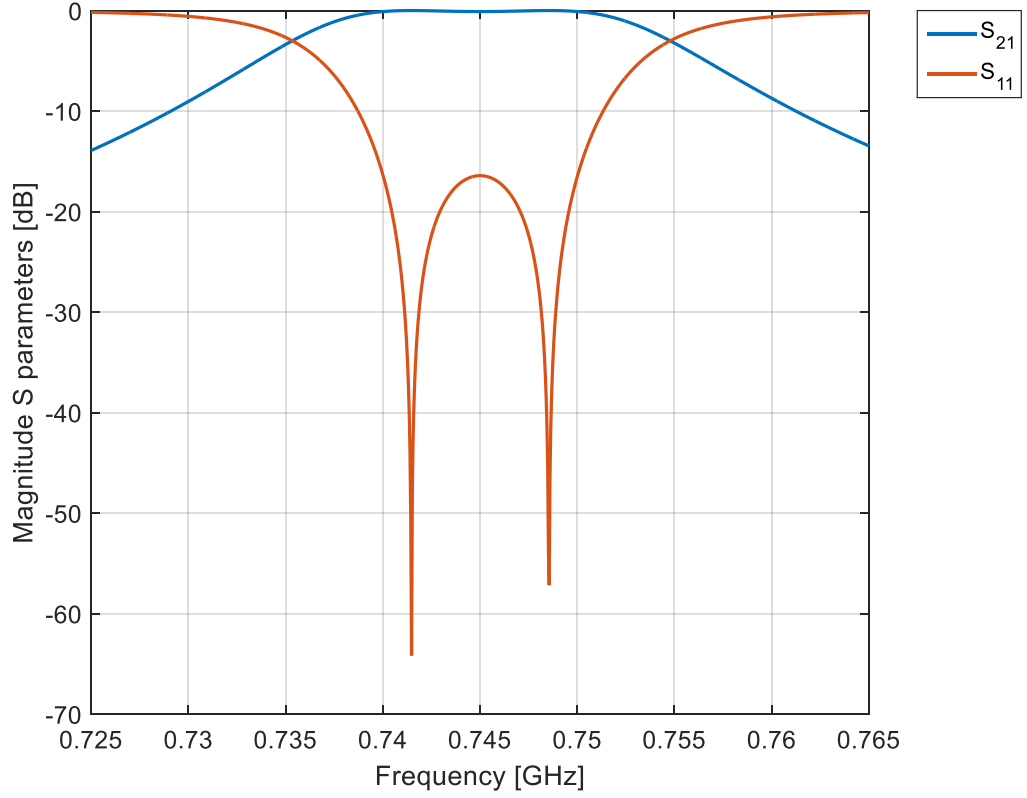


Figure 5-12: S parameters ideal filter

The parameters from the synthesis are:

- Coupling factor $K_{12} = 0.022$
- External quality factor $Q_e = 55$

In order to have a first dimensioning, we used the theoretical values calculated with the procedures described above. In particular, in order to calculate the geometric parameters of the first attempt of the helices, it is used the well known formula that describes the coupling coefficients:

$$K_{12} = \frac{1}{2} \left(\frac{f_{02}}{f_{01}} + \frac{f_{01}}{f_{02}} \right) \sqrt{\left(\frac{f_{p2}^2 - f_{p1}^2}{f_{p2}^2 + f_{p1}^2} \right)^2 - \left(\frac{f_{02}^2 - f_{01}^2}{f_{02}^2 + f_{01}^2} \right)^2}$$

The coupling could be determinate via optimization using closed formulas from previous chapter (single helix dispersion analysis) and the results presented in this chapter (double helix dispersion analysis). In fact, the procedure for the coupling coefficient is the following:

- 1) Using first attempt dimensions (radius and pitch) two helices are dimensioned
- 2) The resonant frequencies f_{01} and f_{02} are calculated for the two helices

- 3) The two separated helices are assembled in the concentric configuration
- 4) The resonant frequencies f_{p1} and f_{p2} corresponding at two different modes are calculated
- 5) The coupling coefficient is calculated

The presented procedure is an iterative algorithm that stops when the desired coupling coefficient is reached.

Then using this information in an unconstrained optimization routines in matlab™ , we have the following situation

- Internal helix diameter: 12.96 mm
- External helix diameter: 21.6 mm
- Internal helix pitch: 1.24 mm
- External helix pitch: 2 mm

The geometric parameters thus obtained were used to construct a model in CST. Also other characteristics of a real physical structure are taken into account:

- The dimensions of the cavity that hosts the helices
- The wire dimensions.
- The mass pin

The first attempt structure was built and optimized in CST (see Figure 5-13), giving the following results

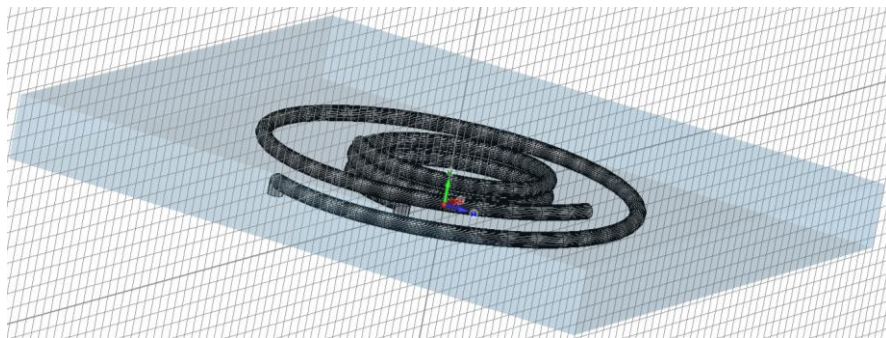


Figure 5-13: first approach structure

- Internal helix diameter: 11.9664 mm
- External helix diameter: 23.921 mm

- Internal helix pitch: 1.07677 mm
- External helix pitch: 1.7983 mm

The values obtained by using the technique developed with closed formulas give the first attempt dimensions of the filter. The analysis and optimization of the filter is obtained by means of a full wave simulator.

As regards the external quality factor, the procedure used was to place two inductive pin connected to a coaxial connector at the base of the two helices as shown in Figure 5-14

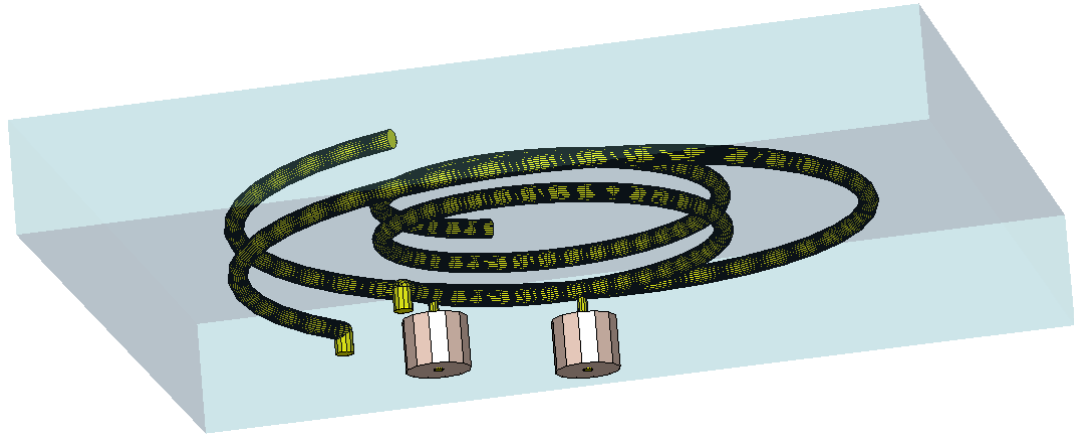


Figure 5-14: I/O pin position

The position of the inductive pin connected to the coaxial connectors has been chosen and optimized. After a first analysis, a simulation with the following results are obtained.

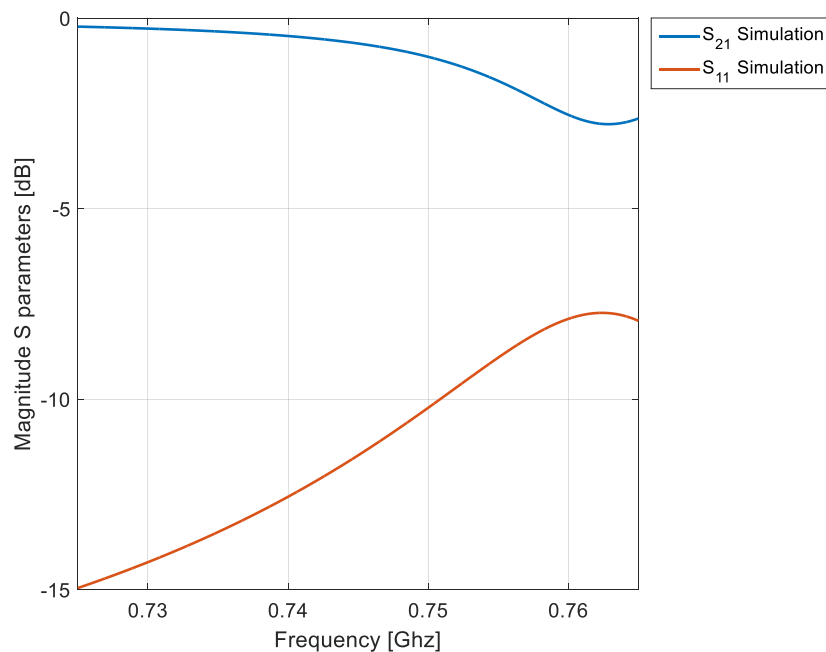


Figure 5-15: initial situation

As can be seen from the figure, the initial situation is quite far from the desired. In particular, in this case a relation between the two helices diameter was imposed (the external helices is imposed to be two times larger than the internal one). This first result does not seems to be the correct approach; so a new relation between the diameter of two helices is imposed: using the propagation constant calculated with the proposed technique, λ_g are calculated and the length of the helices are $\frac{\lambda_g}{4}$ of the first mode. This relation fixes the height and the number of pitches : trying to maintain the height of the helices equal and fixing the diameter of the internal one, the outer helix is automatically obtained. This empirical relation constitutes the best first approximation for the calculation for the optimization. At this point, the helices characteristic parameters such as the two pitches, the two diameters and pin positions with coaxial connectors are optimized. The result of the optimization is shown in Figure 5-16

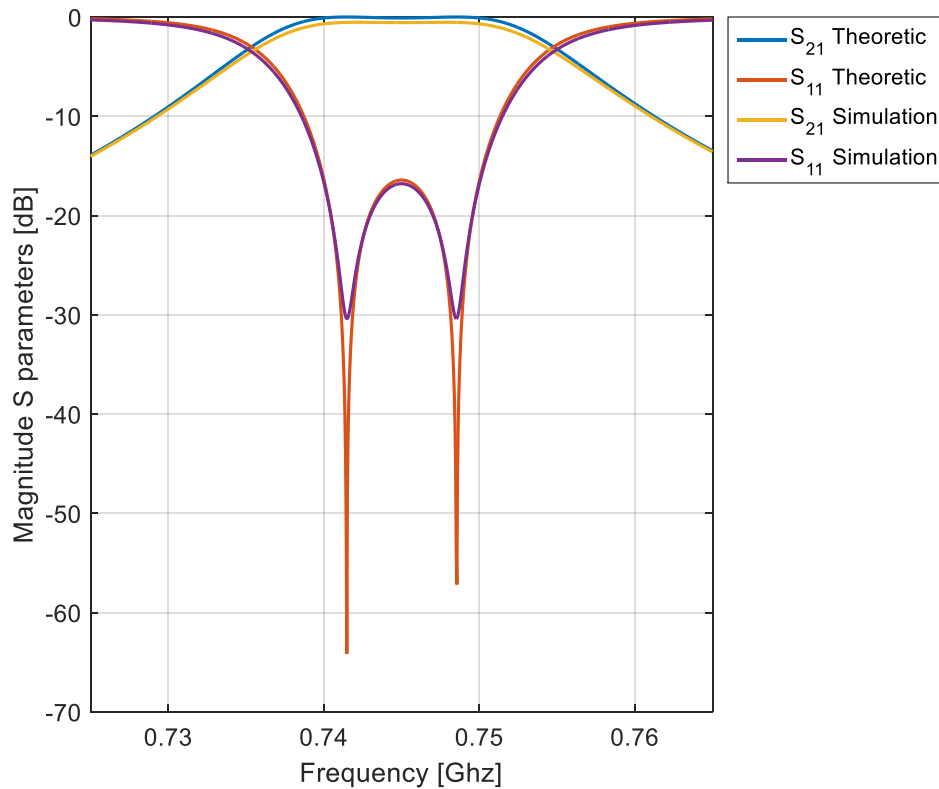


Figure 5-16: simulation results compared with the theoretical one

The following table shows the total time for the tuning and optimization of the filter. The technique used is the following:

- Matlab calculation of decoupled helices resonances f_{01} and f_{02}
- Matlab calculation of coupled helices resonances f_{p1} and f_{p2}
- Matlab coupling calculation

- Matlab coupling optimization
- Updating CST model using Matlab output
- CST optimization of the filters

All the procedure is automatized using Matlab that directly communicate with CST by updating the Electromagnetic model.

Operation	Time
Calculation of decoupled helices resonances f_{01}	5.2 sec
Calculation of decoupled helices resonances f_{02}	5.2 sec
Calculation of decoupled helices resonances f_{p1}	8.4 sec
Calculation of decoupled helices resonances f_{p2}	8.4 sec
Coupling optimization	2.33 min
CST optimization of the filters	3.45 hours
TOTAL	3.48 hours

Table 5-2 : Calculation time for second order dual mode filters using the proposed technique

The data in the table are extracted from the log files of CST and Matlab.

To enforce the concept, a table with the time for the synthesis without the previous described technique is proposed. The technique used is the following:

- 1) Calculation of the f_{01} and f_{02} for two separate helices using full wave simulation.
The resonant frequency is calculate as the value where the $|S_{11}|$ present a peak
- 2) Calculation of the f_{p1} and f_{p2} for two coupled helices using full wave simulation.
The resonant frequency is calculate as the value where the $|S_{21}|$ present two peaks
- 3) Calculation of the coupling

The process is iterative and it will bring to results that need for a final optimization. The following table shows the result time duration for the all calculation as in the prescribed procedure and the final optimization. 5 iterations were necessary to reach a preliminary result. In the table there are not included the time for 3D modelling in full wave electromagnetic simulator. The data in the table are extracted from the log files of CST

Operation	Time
Calculation of decoupled helices resonances f_{01}	22 min

Calculation of decoupled helices resonances f_{02}	22 min
Calculation of decoupled helices resonances f_{p1}	53 min
Calculation of decoupled helices resonances f_{p2}	53 min
CST optimization of the filters	3.45 hours
TOTAL (considering 5 iterations before CST final optimization)	16 hours

Table 5-3 : Calculation time for second order dual mode filters using only electromagnetic model

Comparing Table 5-5 and Table 5-6, it seems evident the advantages of the proposed optimization and tuning technique: The optimization of a closed form model is less time consuming of full electromagnetic model, so the optimization and tuning is divided in two part:

- 1) The closed form models are numerically solved and optimized and the results constitutes the input for the full electromagnetic model
- 2) The electromagnetic model is optimized with classical optimization routine

This technique permits to reduce the calculation times that it is usually of several hours using only full electromagnetic model optimization.

5.3 Design examples 4th order filter

5.3.1 4th order

Following the realization of the second order filter, it has been thought to realize the design of a 4th order filter using the configuration with concentric helices.

The characteristics of the filter to be implemented are:

- Central Frequency: 750 MHz
- Bandwidth: 30 MHz
- RL: 20 dB

Furthermore, to test the characteristics of this type of filter and increase the out of band rejection, it was thought to give a zero in transmission at the frequency of 790 MHz. The filter thus produced was simulated in CST and is reported in the figure from Figure 5-17 to Figure 5-19 below.

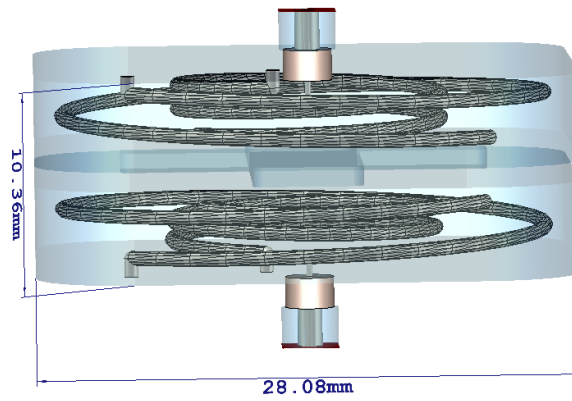


Figure 5-17: 4th order filter layout

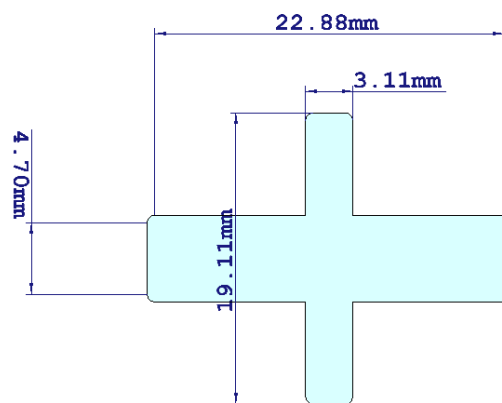


Figure 5-18: cross iris connecting the two resonators

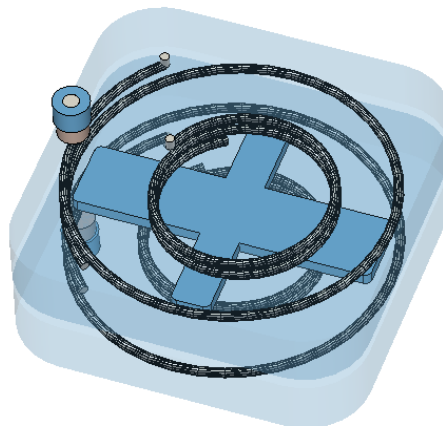


Figure 5-19: filter structures

The characteristics are depicted in the following Table 5-4

Parameters	Description	Value

p_1	Pitch of the internal helix	1.17 mm
p_2	Pitch of external helix	1.89 mm
n_1	Number of turns of internal helix	2.15
n_2	Number of turns of external helix	1.27
d_1	Diameter of internal helix	12.61 mm
d_2	Diameter of external helix	21.02 mm
W	Wire diameter	0.723 mm
W_{in}	Internal pin diameter	0.15 mm
U_{lin}	Length of one branch of the cruciform Iris	24.68 mm
U_{lin2}	Length of other branch of the cruciform Iris	3.03 mm
W_{lin}	Width of one branch of the cruciform Iris	18.16 mm
W_{lin2}	Width of other branch of the cruciform Iris	5.54 mm

Table 5-4 : 4th order geometrical characteristics

The filter was simulated considering:

- Connector real dimensions
- Conductivity of $\sigma = 6.2 \cdot 10^7$

These considerations are due to the choice of being able to fabricate the filter only with COTS materials. In this sense, the diameter of the wire of the helices is based on a diameter of a wire WG19 standard wire.

The connector is a K type connector whose specifications are shown in [RD.28]

The conductivity is $\sigma = 6.2 \cdot 10^7$ equal to that of silver; Indeed, to ensure good performance, it was thought to silver plate the filter. The following figures from Figure 5.3.1-20 to Figure 5-22 show the calculated performance of the filter.

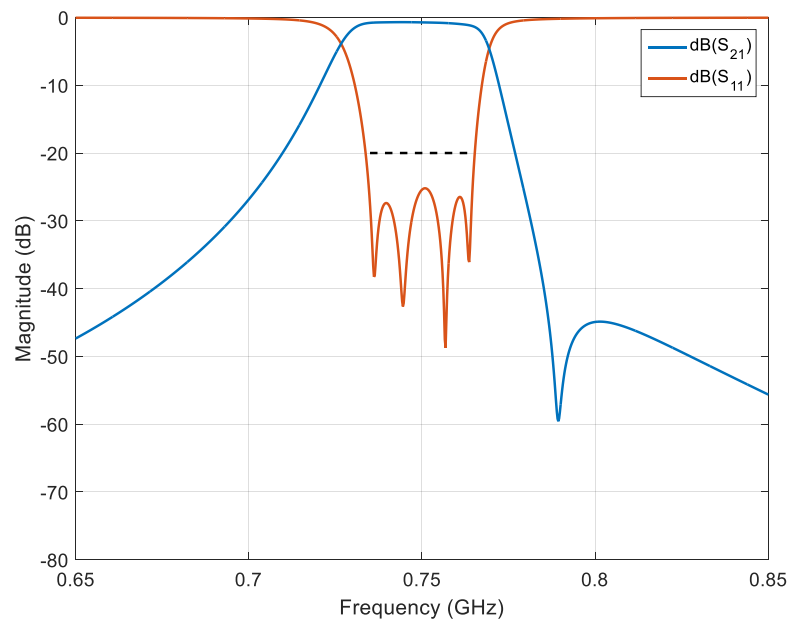


Figure 5.3.1-20: In Band RF performances

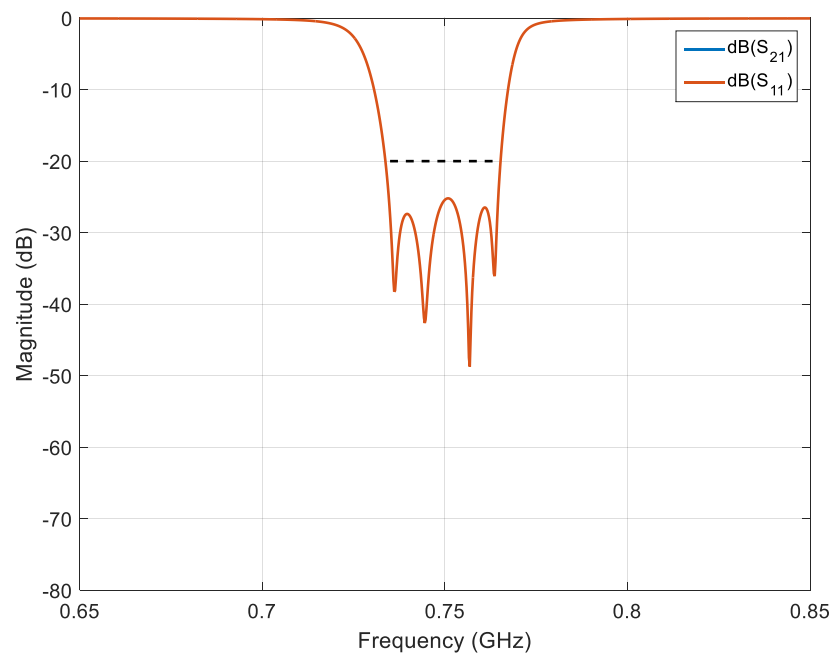


Figure 5-21: In Band Return Loss

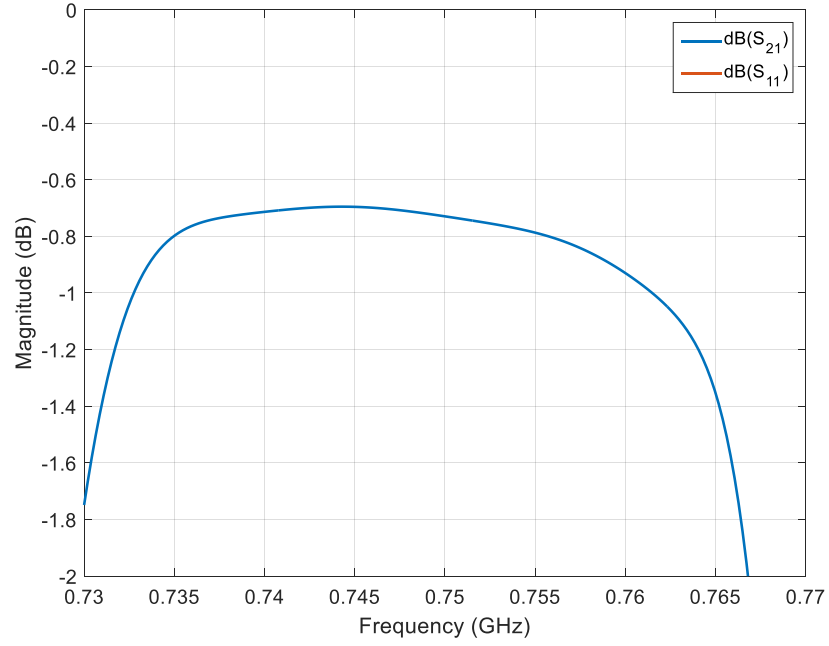


Figure 5-22: In Band Insertion Loss

5.4 Discussion

In this chapter we have explored, for the first time, the characteristics of the dual mode filters in circular helices. This type of configuration allows for the extremely compact structures because uses two resonant modes per cavity. Compared to the previous works, this new configuration has very obvious advantages. In the first place, the helices being rather compact, there is no need to have a block of material that must support; in fact, previous configurations of filters in dual mode helix, needed to wrap the helices in blocks of dielectric. This type of choice has an impact on total losses of the filter and relative performances. The fact of not having then dielectric media, from a clear benefit on the insertion loss of the filter.

In addition, this new type of configuration presents no tuning elements making the structure tuning less. This type of choice in addition to having impacts on performance, also leads to other advantages: in fact, for the embodiments to be carried out with machine tools, save the drilling (threaded hole of the tuning screws) corresponds to a remarkable advantage for the realization simplification. Furthermore, the tuning screws introduce an uncertainty in the measurement of performance that, in such a complicated filter, may be unacceptable.

The last undoubted advantage of this configuration is that, the entire structure is extremely compact; as shown in the Figure 5-23 below.

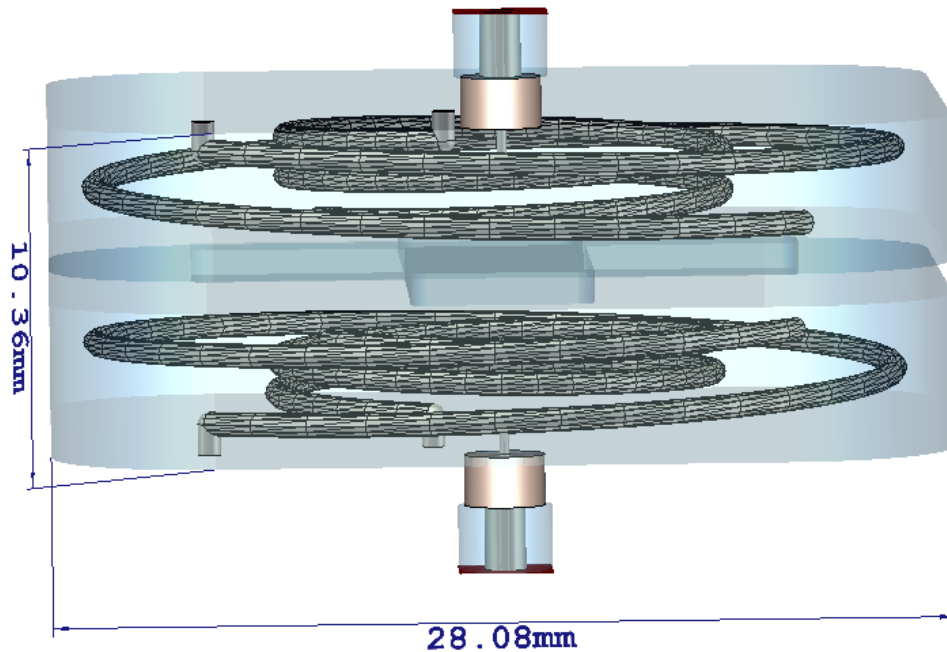


Figure 5-23: 4th order filter layout

This size has never been realized and would make the extremely compact filter and usable within a IMUX.

Moreover, the innovative design technique gives the filter dimensioning in very short time and this is excellent in terms of mass production design. In order to demonstrate that, a classical 4th order in line filter using helices was realized. The following Table 5-5 shows the comparison between dimensions of the cavity housing the dual mode filter and the classical 4th order in line filter.

	Length	Width	Height
Dual mode	28.08	28.08	10.36
Classical in line 4 th order filter	80.63	29.81	26.46
Ratio between dimensions	2.87	1.06	2.55

Table 5-5: Comparison between dual mode and classical in line 4th order filter

Table 5-5 shows also the ratio between the classical filter and dual mode; it seems evident that the concentric helices results in a more compact solution. The following Figure 5-24 shows the model of classical 4th order filter

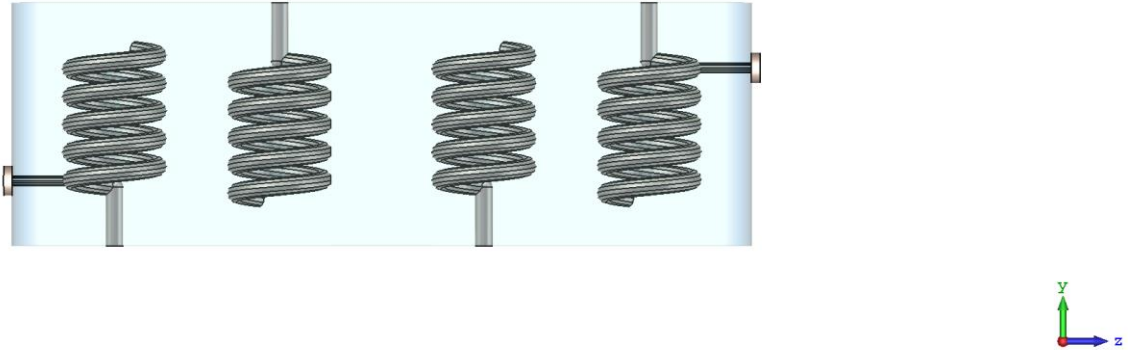


Figure 5-24: Classical 4th order filter

The filter layout in Figure 5-24 is realized in order to have a response that is similar to dual mode configuration as shown in

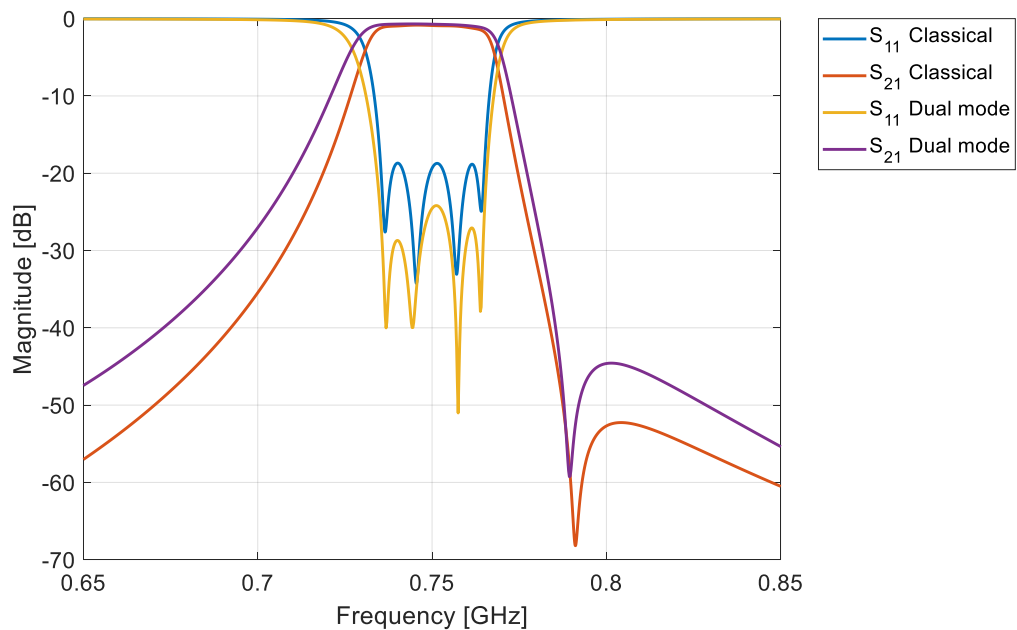


Figure 5-25: Comparison between classical and dual mode 4th order filter

Focusing on the dimensions and masses , the following table shows the typical dimensions and mass of the classical filter solution in the same frequency range. The data coming from state of the art commercial off the shelf as reported in [RD.47] and [RD.48].

Filter Topology	Width [mm]	Length [mm]	Height [mm]	Mass [grams]
Ceramic dielectric	75	37	52.8	288.2
Interdigital	72.83	19.02	108.93	212
Dual mode concentric helices	28.08	28.08	10.36	8.41

Table 5-6: Comparison between dual mode and classical prior art commercial filter

As it is evident from Table 5-6, the dimension reduction is evident: compared to the ceramic dielectric the ratio between the dimensions is in the order 2 for the width and in order 5 for height; considering the Interdigital solution, the ratio between dimensions is in order of 2 for the width and in order of 10 for the length. Regarding the mass, the ceramic dielectric filter is composed by aluminium (density of $2.81[\text{g}/\text{cm}^3]$) and (ceramic (density of $3.22[\text{g}/\text{cm}^3]$), the interdigital is made by aluminium while the dual mode concentric helices is completely composed by plastic polymer (density of $1.03[\text{g}/\text{cm}^3]$). On the other hand, these advantages are associated with disadvantages. The first and most important is surely the realization difficulties; In fact, the extreme compactness of the filter makes the manufacture definitely problematic. Furthermore, the spiral structure of the helices, makes it difficult for the positioning of the pin connectors that come into contact with the resonators in the helix. Finally, since the helices are concentric, the relative positions have to be determined with very high precision.

Considering above discussion, it is very complicated to make a prototype that has all the features required within driven tolerances. In this regard, future work that may be expected for this type of filter is the possibility to realize it with the usual manufacturing techniques. Another road that is possible, is the use of 3D manufacturing techniques. In fact this type of 3D printing technique could be used for these prototypes, since there is no need to produce the individual pieces (cavity helices and pin) but, everything would be produced as a single piece by breaking down any the alignment problems.

CHAPTER 6 – CONCLUSIONS AND FINAL CONSIDERATION

6.1 Generals

This work presents the design of the filters for UHF satellite payloads trying to give a different point of view related to payload communication system. In this way, different kind of filters are necessary: channel filters, that has to drive a very little amount of power, are used in the receivers (uplink); while the output filters, that drive a very large amount of power, are in the transmitters (downlink).

For satellite payloads, the dimensions and the mass of the components are very important and needs to be reduced. Typically, the dimensions of waveguide passive microwave components decreases with the frequency increasing. For the UHF frequencies (from 300MHz to 3GHz) the wavelength is in the range of 1m to 100mm. Considering that the wavelength is proportional to the dimensions of a hollow waveguide, a filter in waveguide operating in this frequencies has a dimensions that is not suitable for satellites payload. The solution adopted in this work is to use cavities loaded with spiral helices.

The entire work is focused on the possibility to extend the helical filter technologies for output filters and channel filters.

6.2 Output filters – The OMUX

Considering the fact that in the transmitters the power involved is typically in the order of hundreds of watts, the components of a transmitter has to survive those levels of power. Moreover, the components has to be of low mass and dimensions.

Various filters technologies are available for high power applications, such combines, lumped elements and helical resonators. The combine technology is quite mature as far as the RF performances such as low insertion loss, high return losses and high near band rejection are concerned, but it has the disadvantages of the high mass and dimensions. On the other side, the lumped element technology permits to have filters with reduced dimensions and low weight but the high losses and low Quality factor are not desirable for RF performances.

Helical resonator filters combine the good RF characteristics of the combine with the reduced mass and dimensions of lumped element technologies. These characteristics makes the helical resonator filters good candidates for UHF output filters; but there are issues on the power handling. In fact, for space satellite environment the high power driving into a passive components could ingenerates multipaction effects as described in Chapter 3

The design of the filters, performed in this work, has the aim to minimize the appearance of multipaction inside the filter, considering three design choice such as loading the helices with dielectrics or increasing the internal distance between helices and cavity walls or modulating the spiral helices (from cylindrical to Step-Conical). For power handling purposes, the particular geometry of this kind of filters, needs to be studied with particular and dedicated software tools. The actual tools that are used are based on parallel plate concept and they are not reliable for particular geometry such helices; so it is necessary to use a complete different routines that implements a more accurate physical model of the phenomenon. This software tool (SPARK3D™) permits to have a very accurate analysis and supports the RF design. Moreover, using this kind of approach permitted to reduce the number of possible filters produced during all the design phases. Four different prototypes of second order pseudo-elliptical helical resonator filters were manufactured in Heriot Watt University Workshop. The prototypes were assembled and tuned in Rome (Space Engineering SPA) and Edinburgh, and they were tested for RF performances in Rome; while the multipaction test was performed in Valencia ESA-VSC High Power RF Laboratory.

The multipaction test results show that the helical resonator filters could be good candidates for high power applications for future UHF payloads.

In order to increase the multipaction margin, the future activities in this frame, is to implement new technique for the design integrating the possibility to load helices with Rexolite™ dielectrics cover and/or modulating the shapes of the helices in order to obtain an optimized configuration.

6.3 Input filters – The IMUX

From the receiver point of view, the signal has to be divided into channels in order to be processed in the transponder. This separation operation is implemented by IMUX filters. For the UHF Payloads, considering what is described in previous sections, the filters of the OMUX have the scope to separate correctly the signal in the channels bandwidth.

In this way, the RF characteristics of channel filters are:

- High near band Rejection
- High Return Loss
- Low insertion Loss

From the mechanical point of view the low weight and low mass are much more stringent than the output filters. In order to maintain the dimensions and weight small, very often

the filters are designed in dual mode topology. This technique uses the properties of the resonant frequencies of the filters structures: in fact, using two degenerating modes of a resonator, it is possible to have the effect of two electromagnetic cavities inside a mechanical single one. The immediate effect of this technique is evident: the filter dimensions are reduced if compared to the single mode case. The other consequence is also the reduction of the weight of the single resonators. For the UHF applications, it is not possible to use classical dual mode waveguide resonator technologies, so the dual mode concept has to be implemented in different kind of resonator.

Dual mode helical resonator filters were implemented in the past but, the theoretical substrate was not well consolidated and the results remains not completely understood. Moreover, the previous experience in dual mode helices, did not give filters that have small dimensions and weight.

In this work, the dual mode helical resonator filter is used but implementing a radically new concept. In particular, for the dual mode implementation, two concentric helices mounted one inside the other are used for the purpose. This method is chosen because it permits to have a theoretical substrate that is developed in this work, and because the fact that, mounting helices in concentric way, permits to save space, gaining in dimension reduction.

With the technique explained into the thesis a pseudo-elliptic dual mode concentric helices fourth order filter is designed and the RF performances are very high in terms of near band rejection, return loss and insertion loss.

6.4 Conclusive remarks

In conclusion, the work done for the single mode helices for high power applications was very useful to understand the multipaction effects on structures that are not planar. Moreover, the multipaction tests was a perfect occasion to validate the physical model of the multipaction discharge. The helical technology seems to be promising for high power applications ([RD.34]).

The future of this activity could take two different way: enforce the design of the helical resonator filters loading it with dielectric caps over the helices in order to enforce the multipaction margin; or shaping the helices in optimized geometry ([RD.35]).

For the dual mode helices, the future of the activity is the production of what is designed and , in case of success it is possible to study the multipaction discharge in this kind of structure.

From personal experience of the author, the most critical part of the project, is the manufacturing. In fact, for the single mode helices, the manufacturing rose up a lot of difficulties that had to be solved and had an impact on the RF performances. Moreover, a classical manufacturing process could be very expensive for this particular realization. In order to improve this aspects it is possible to realize all the filter using innovative 3D printing. In fact this kind of process give the possibility to realize complex geometries with very stringent accuracy. For the future it is possible to realize the single mode helices using metal 3D printing and realize particular shaping for the helix.

A similar approach is used for the production of the dual mode helices filter. In fact, in order to produce a prototype, a low cost 3D printing using polymers was preliminary assessed. The filters realized in this way is also silver plated in order to limit losses. The following figures shows the realized filters



Figure 6-1: cavity with concentric helix

In Figure 6-1 it is possible to see the concentric helices directly integrated into the cavity it is possible to see the extremely small dimensions of the filter: the cavity is compared to the dimension of one coin.

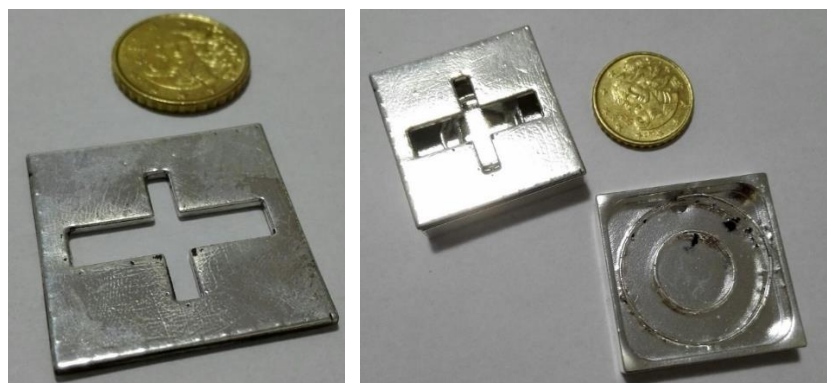


Figure 6-2: coupling iris and the second half of the concentric helical resonator

The previous Figure 6-2 shows the coupling iris and the second half that constitutes the complete filter. On the iris, it is possible to see the accurate surface finishing of the silver plating process.

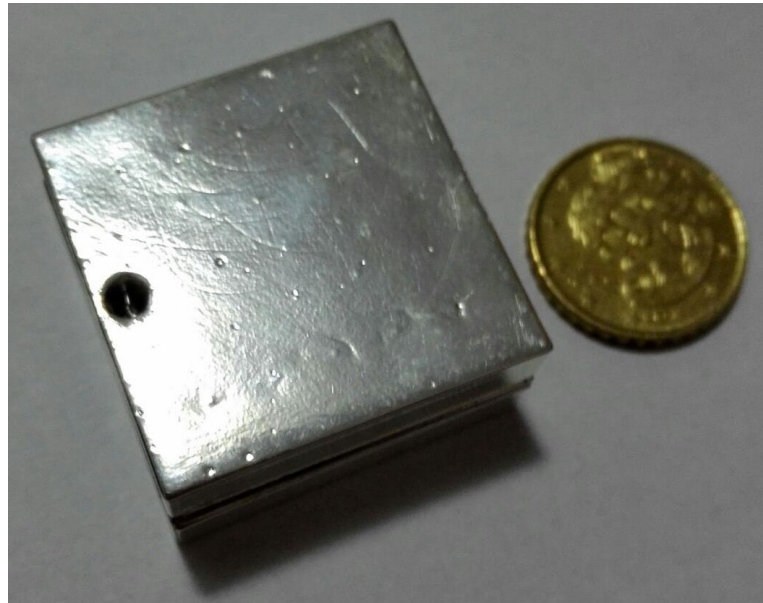


Figure 6-3: Assembled filter without connectors

The Figure 6-3 shows the filter completely assembled without connectors. The dimensions of the complete assembly are very compact and this aspect is very interesting for an UHF payload application.

The final step is the RF test of the dual mode helical resonator filter that is finalizing the assembly with the mounting of the connectors that are the most critical part. The test campaign will end with the RF performance test.

APPENDIX

Formulas in CHAPTER 2

Field Inside Helix

$$r < a$$

$$E_z = A I_0(\gamma r) e^{j(\omega t - \beta z)} \quad (\text{A } 1)$$

$$E_r = \frac{jA\beta}{\gamma} I_1(\gamma r) e^{j(\omega t - \beta z)} \quad (\text{A } 2)$$

$$E_\theta = \frac{jA\beta}{\gamma} I_1(\gamma r) \tan \psi I_1(\gamma r) e^{j(\omega t - \beta z)} \quad (\text{A } 3)$$

$$H_z = -jA \frac{\gamma}{\omega \mu} \frac{I_0(\gamma a)}{I_1(\gamma a)} \tan \psi I_0(\gamma r) e^{j(\omega t - \beta z)} \quad (\text{A } 4)$$

$$H_r = A \frac{\beta}{\omega \mu} \frac{I_0(\gamma a)}{I_1(\gamma a)} \tan \psi I_1(\gamma r) e^{j(\omega t - \beta z)} \quad (\text{A } 5)$$

$$H_\theta = jA \frac{\omega \epsilon}{\gamma} I_1(\gamma r) e^{j(\omega t - \beta z)} \quad (\text{A } 6)$$

$$r > a$$

$$E_z = A \Delta_0 \left[K_0(\gamma r) - \frac{K_0(\gamma \beta)}{I_0(\gamma b)} I_0(\gamma r) \right] e^{j(\omega t - \beta z)} \quad (\text{A } 7)$$

$$E_r = -jA \frac{\beta}{\gamma} \Delta_0 \left[K_1(\gamma r) + \frac{K_0(\gamma \beta)}{I_0(\gamma b)} I_1(\gamma r) \right] e^{j(\omega t - \beta z)} \quad (\text{A } 8)$$

$$E_\theta = A \tan \psi \Delta_1 \left[K_1(\gamma r) - \frac{K_1(\gamma \beta)}{I_1(\gamma b)} I_1(\gamma r) \right] e^{j(\omega t - \beta z)} \quad (\text{A } 9)$$

$$H_z = jA \frac{\gamma}{\omega \mu} \tan \psi \Delta_1 \left[K_0(\gamma r) + \frac{K_1(\gamma \beta)}{I_1(\gamma b)} I_0(\gamma r) \right] e^{j(\omega t - \beta z)} \quad (\text{A } 10)$$

$$H_r = A \frac{\beta}{\omega \mu} \tan \psi \Delta_1 \left[K_1(\gamma r) - \frac{K_1(\gamma \beta)}{I_1(\gamma b)} I_1(\gamma r) \right] e^{j(\omega t - \beta z)} \quad (\text{A } 11)$$

$$H_\theta = jA \frac{\omega \epsilon}{\gamma} \Delta_0 \left[K_1(\gamma r) + \frac{K_0(\gamma \beta)}{I_0(\gamma b)} I_1(\gamma r) \right] e^{j(\omega t - \beta z)} \quad (\text{A } 12)$$

Where the quantities are defined as follows

- A Arbitrary constant
- I_0 Modified Bessel funtion of the first type and zero order
- I_1 Modified Bessel funtion of the first type and first order
- K_0 Modified Bessel funtion of the second type and zero order
- K_1 Modified Bessel funtion of the second type and first order
- $\gamma^2 = \beta^2 - \beta_0^2$ radial propagation constant
- $\beta_0 = \frac{\omega}{c}$ free space propagation constant
- $\beta = \frac{\omega}{v_p}$ propagation constant
- $\omega = 2\pi f$
- c lighth velocity

- v_p phase velocity
- r, θ, z cylindrical coordinate
- a helix radius
- ψ helix pitch angle (direction of conduction)
- b cylindrical sheath radius.
- $\Delta_0 = \frac{I_0(\gamma a)I_0(\gamma b)}{I_0(\gamma b)K_0(\gamma b) - I_0(\gamma a)K_0(\gamma b)}$
- $\Delta_1 = \frac{I_0(\gamma a)I_1(\gamma b)}{I_1(\gamma b)K_1(\gamma b) - I_1(\gamma a)K_1(\gamma b)}$

Formulas in CHAPTER 5

Fields inside concentric helix

Region 1

$$E_r^{(1)} = \left[\frac{i\beta}{\tau} I'_n(\tau r) a_n^{(1)} - \frac{\mu\omega n}{\tau^2 r} I_n(\tau r) b_n^{(1)} \right] F_n \quad (\text{A } 13)$$

$$E_\theta^{(1)} = \left[\frac{-n\beta}{\tau^2 r} I_n(\tau r) a_n^{(1)} - \frac{i\mu\omega}{\tau} I'_n(\tau r) b_n^{(1)} \right] F_n \quad (\text{A } 14)$$

$$E_z^{(1)} = [-I_n(\tau r) a_n^{(1)}] F_n \quad (\text{A } 15)$$

$$H_r^{(1)} = \left[\frac{n\omega\epsilon}{\tau^2 r} I_n(\tau r) a_n^{(1)} + \frac{i\beta}{\tau} I'_n(\tau r) b_n^{(1)} \right] F_n \quad (\text{A } 16)$$

$$H_\theta^{(1)} = \left[\frac{i\omega\epsilon}{\tau} I'_n(\tau r) a_n^{(1)} - \frac{n\beta}{\tau^2 r} I_n(\tau r) b_n^{(1)} \right] F_n \quad (\text{A } 17)$$

$$H_z^{(1)} = [-I_n(\tau r) b_n^{(1)}] F_n \quad (\text{A } 18)$$

Region 2

$$E_r^{(2)} = \left[\frac{i\beta}{\tau} I'_n(\tau r) a_n^{(2)} - \frac{\mu\omega n}{\tau^2 r} I_n(\tau r) b_n^{(2)} + \frac{i\beta}{\tau} K'_n(\tau r) c_n^{(2)} - \frac{\mu\omega n}{\tau^2 r} K_n(\tau r) d_n^{(2)} \right] F_n \quad (\text{A } 19)$$

$$E_\theta^{(2)} = \left[\frac{-n\beta}{\tau^2 r} I_n(\tau r) a_n^{(2)} - \frac{i\mu\omega}{\tau} I'_n(\tau r) b_n^{(2)} - \frac{n\beta}{\tau^2 r} K_n(\tau r) c_n^{(2)} - \frac{i\mu\omega}{\tau} K'_n(\tau r) d_n^{(2)} \right] F_n \quad (\text{A } 20)$$

$$E_z^{(2)} = [-I_n(\tau r) a_n^{(2)} - K_n(\tau r) c_n^{(2)}] F_n \quad (\text{A } 21)$$

$$H_r^{(2)} = \left[\frac{n\omega\epsilon}{\tau^2 r} I_n(\tau r) a_n^{(2)} + \frac{i\beta}{\tau} I'_n(\tau r) b_n^{(2)} + \frac{n\omega\epsilon}{\tau^2 r} K_n(\tau r) c_n^{(2)} + \frac{i\beta}{\tau} K'_n(\tau r) d_n^{(2)} \right] F_n \quad (\text{A } 22)$$

$$H_\theta^{(2)} = \left[\frac{i\omega\epsilon}{\tau} I'_n(\tau r) a_n^{(2)} - \frac{n\beta}{\tau^2 r} I_n(\tau r) b_n^{(2)} + \frac{i\omega\epsilon}{\tau} K'_n(\tau r) c_n^{(2)} - \frac{n\beta}{\tau^2 r} K_n(\tau r) d_n^{(2)} \right] F_n \quad (\text{A } 23)$$

$$H_z^{(2)} = [-I_n(\tau r) b_n^{(2)} - K_n(\tau r) d_n^{(2)}] F_n \quad (\text{A } 24)$$

Region 3

$$E_r^{(3)} = \left[\frac{i\beta}{\tau} K'_n(\tau r) a_n^{(3)} - \frac{\mu\omega n}{\tau^2 r} K_n(\tau r) b_n^{(3)} \right] F_n \quad (\text{A } 25)$$

$$E_\theta^{(3)} = \left[\frac{-n\beta}{\tau^2 r} K_n(\tau r) a_n^{(3)} - \frac{i\mu\omega}{\tau} K'_n(\tau r) b_n^{(3)} \right] F_n \quad (\text{A } 26)$$

$$E_z^{(3)} = [-K_n(\tau r) a_n^{(3)}] F_n \quad (\text{A } 27)$$

$$H_r^{(3)} = \left[\frac{n\omega\epsilon}{\tau^2 r} K_n(\tau r) a_n^{(3)} + \frac{i\beta}{\tau} K'_n(\tau r) b_n^{(3)} \right] F_n \quad (\text{A } 28)$$

$$H_{\theta}^{(3)} = \left[\frac{i\omega\varepsilon}{\tau} K_n'(\tau r) a_n^{(3)} - \frac{n\beta}{\tau^2 r} K_n(\tau r) b_n^{(3)} \right] F_n \quad (\text{A } 29)$$

$$H_z^{(3)} = [-K_n(\tau r) b_n^{(3)}] F_n \quad (\text{A } 30)$$

where

$$\bullet \quad F_n = \exp[in\theta + i\beta z] \quad (\text{A } 31)$$

$$\bullet \quad \tau = \sqrt{\beta^2 - k^2} \quad (\text{A } 32)$$

In the next section will be explained the coefficients of the fields, using the boundary conditions, also it will be presented with the equation of the dispersion

Analysis and numerical techniques of concentric helix

As previously seen, the expression of the fields, for the various regions, is the following

Region 1

$$E_r^{(1)} = \left[\frac{i\beta}{\tau} I_n'(\tau r) a_n^{(1)} - \frac{\mu\omega n}{\tau^2 r} I_n(\tau r) b_n^{(1)} \right] F_n \quad (\text{A } 33)$$

$$E_{\theta}^{(1)} = \left[\frac{-n\beta}{\tau^2 r} I_n(\tau r) a_n^{(1)} - \frac{i\mu\omega}{\tau} I_n'(\tau r) b_n^{(1)} \right] F_n \quad (\text{A } 34)$$

$$E_z^{(1)} = [-I_n(\tau r) a_n^{(1)}] F_n \quad (\text{A } 35)$$

$$H_r^{(1)} = \left[\frac{n\omega\varepsilon}{\tau^2 r} I_n(\tau r) a_n^{(1)} + \frac{i\beta}{\tau} I_n'(\tau r) b_n^{(1)} \right] F_n \quad (\text{A } 36)$$

$$H_{\theta}^{(1)} = \left[\frac{i\omega\varepsilon}{\tau} I_n'(\tau r) a_n^{(1)} - \frac{n\beta}{\tau^2 r} I_n(\tau r) b_n^{(1)} \right] F_n \quad (\text{A } 37)$$

$$H_z^{(1)} = [-I_n(\tau r) b_n^{(1)}] F_n \quad (\text{A } 38)$$

Region 2

$$E_r^{(2)} = \left[\frac{i\beta}{\tau} I_n'(\tau r) a_n^{(2)} - \frac{\mu\omega n}{\tau^2 r} I_n(\tau r) b_n^{(2)} + \frac{i\beta}{\tau} K_n'(\tau r) c_n^{(2)} - \frac{\mu\omega n}{\tau^2 r} K_n(\tau r) d_n^{(2)} \right] F_n \quad (\text{A } 39)$$

$$E_{\theta}^{(2)} = \left[\frac{-n\beta}{\tau^2 r} I_n(\tau r) a_n^{(2)} - \frac{i\mu\omega}{\tau} I_n'(\tau r) b_n^{(2)} - \frac{n\beta}{\tau^2 r} K_n(\tau r) c_n^{(2)} - \frac{i\mu\omega}{\tau} K_n'(\tau r) d_n^{(2)} \right] F_n \quad (\text{A } 40)$$

$$E_z^{(2)} = [-I_n(\tau r) a_n^{(2)} - K_n(\tau r) c_n^{(2)}] F_n \quad (\text{A } 41)$$

$$H_r^{(2)} = \left[\frac{n\omega\varepsilon}{\tau^2 r} I_n(\tau r) a_n^{(2)} + \frac{i\beta}{\tau} I_n'(\tau r) b_n^{(2)} + \frac{n\omega\varepsilon}{\tau^2 r} K_n(\tau r) c_n^{(2)} + \frac{i\beta}{\tau} K_n'(\tau r) d_n^{(2)} \right] F_n \quad (\text{A } 42)$$

$$H_{\theta}^{(2)} = \left[\frac{i\omega\varepsilon}{\tau} I_n'(\tau r) a_n^{(2)} - \frac{n\beta}{\tau^2 r} I_n(\tau r) b_n^{(2)} + \frac{i\omega\varepsilon}{\tau} K_n'(\tau r) c_n^{(2)} - \frac{n\beta}{\tau^2 r} K_n(\tau r) d_n^{(2)} \right] F_n \quad (\text{A } 43)$$

$$H_z^{(2)} = [-I_n(\tau r) b_n^{(2)} - K_n(\tau r) d_n^{(2)}] F_n \quad (\text{A } 44)$$

Region 3

$$E_r^{(3)} = \left[\frac{i\beta}{\tau} K_n'(\tau r) a_n^{(3)} - \frac{\mu\omega n}{\tau^2 r} K_n(\tau r) b_n^{(3)} \right] F_n \quad (\text{A } 45)$$

$$E_{\theta}^{(3)} = \left[\frac{-n\beta}{\tau^2 r} K_n(\tau r) a_n^{(3)} - \frac{i\mu\omega}{\tau} K_n'(\tau r) b_n^{(3)} \right] F_n \quad (\text{A } 46)$$

$$E_z^{(3)} = [-K_n(\tau r) a_n^{(3)}] F_n \quad (\text{A } 47)$$

$$H_r^{(3)} = \left[\frac{n\omega\varepsilon}{\tau^2 r} K_n(\tau r) a_n^{(3)} + \frac{i\beta}{\tau} K_n'(\tau r) b_n^{(3)} \right] F_n \quad (\text{A } 48)$$

$$H_{\theta}^{(3)} = \left[\frac{i\omega\varepsilon}{\tau} K_n'(\tau r) a_n^{(3)} - \frac{n\beta}{\tau^2 r} K_n(\tau r) b_n^{(3)} \right] F_n \quad (\text{A } 49)$$

$$H_z^{(3)} = [-K_n(\tau r) b_n^{(3)}] F_n \quad (\text{A } 50)$$

In general, to get the full expression of the fields, should summing over all values of n and β for all the fields of the components set forth in the above equations. However, since

the boundary conditions for the sheath helices model are the same for θ e z , the orthogonality in θ and z allows to the boundary conditions to be met for each n e β .

The boundary conditions are applied as follows:

- The field component E , parallel to the direction of conduction, is null
- The component of the field E perpendicular to the direction of conduction must be continuous across the boundary
- The component of the field H , orthogonal to the direction of conduction, must be continuous across the boundary

These conditions are written as follows:

- Per $r = r_1$

$$E_z^{(1)} + E_\theta^{(1)} \cot \psi_1 = 0 \quad (\text{A } 51)$$

$$E_\theta^{(1)} - E_\theta^{(2)} = 0 \quad (\text{A } 52)$$

$$E_z^{(1)} - E_z^{(2)} = 0 \quad (\text{A } 53)$$

$$[H_z^{(1)} - H_z^{(2)}] + [H_\theta^{(1)} - H_\theta^{(2)}] \cot \psi_1 = 0 \quad (\text{A } 54)$$

- Per $r = r_2$

$$E_z^{(3)} + E_\theta^{(3)} \cot \psi_2 = 0 \quad (\text{A } 55)$$

$$E_\theta^{(2)} - E_\theta^{(3)} = 0 \quad (\text{A } 56)$$

$$E_z^{(2)} - E_z^{(3)} = 0 \quad (\text{A } 57)$$

$$[H_z^{(2)} - H_z^{(3)}] + [H_\theta^{(2)} - H_\theta^{(3)}] \cot \psi_2 = 0 \quad (\text{A } 58)$$

Making appropriate substitutions, a system of equations linearly dependent is obtained

$$I_{n1}(1 + A_1 \cot \psi_1) a_n^{(1)} + c \cot \psi_1 I'_{n1} b_n^{(1)} = 0 \quad (\text{A } 59)$$

$$A_1 I_{n1} a_n^{(1)} + c I'_{n1} b_n^{(1)} - A_1 I_{n1} a_n^{(2)} - c I'_{n1} b_n^{(2)} - A_1 K_{n1} c_n^{(2)} - c K'_{n1} d_n^{(2)} = 0 \quad (\text{A } 60)$$

$$I_{n1} a_n^{(1)} - I_{n1} a_n^{(2)} - K_{n1} c_n^{(2)} = 0 \quad (\text{A } 61)$$

$$B \cot \psi_1 I'_{n1} a_n^{(1)} - I_{n1}(1 + A_1 \cot \psi_1) b_n^{(1)} - B \cot \psi_1 I'_{n1} a_n^{(2)} + I_{n1}(1 + A_1 \cot \psi_1) b_n^{(2)} - B \cot \psi_1 K'_{n1} c_n^{(2)} + K_{n1}(1 + A_1 \cot \psi_1) d_n^{(2)} = 0 \quad (\text{A } 62)$$

$$K_{n2}(1 + A_2 \cot \psi_2) a_n^{(3)} + c \cot \psi_2 K'_{n2} b_n^{(3)} = 0 \quad (\text{A } 63)$$

$$A_2 I_{n2} a_n^{(2)} + c I'_{n2} b_n^{(2)} + A_2 K_{n2} c_n^{(2)} + c K'_{n2} d_n^{(2)} - A_2 K_{n2} a_n^{(3)} - c K'_{n2} b_n^{(3)} = 0 \quad (\text{A } 64)$$

$$I_{n2} a_n^{(2)} + K_{n2} c_n^{(2)} - K_{n2} a_n^{(3)} = 0 \quad (\text{A } 65)$$

$$B \cot \psi_2 I'_{n2} a_n^{(2)} - I_{n2}(1 + A_2 \cot \psi_2) b_n^{(2)} + B \cot \psi_2 K'_{n2} c_n^{(2)} - K_{n2}(1 + A_2 \cot \psi_2) d_n^{(2)} - B \cot \psi_2 K'_{n2} a_n^{(3)} + K_{n2}(1 + A_2 \cot \psi_2) b_n^{(3)} = 0 \quad (\text{A } 66)$$

Where:

$$\bullet \quad A_1 = \frac{n\beta}{\tau^2 r_1} \quad (\text{A } 67)$$

- $A_2 = \frac{n\beta}{\tau^2 r_2}$ (A 68)

- $B = \frac{i\omega\varepsilon}{\tau}$ (A 69)

- $c = \frac{i\mu\omega}{\tau}$ (A 70)

- $I_{n1} = I_n(\tau r_1)$ (A 71)

- $K_{n2} = I_n(\tau r_2)$ (A 72)

The only possible non-trivial solution for this system of linearly dependent equations, , is provided by forcing the determinant of the system is equal to zero. The determinant of the system is the following:

$$\begin{aligned}
\mathbf{A} = & \begin{vmatrix}
I_{n1}(1 + A_1 \cot \psi_1) & c \cot \psi_1 I'_{n1} & 0 & 0 & 0 & 0 & 0 & 0 \\
A_1 I_{n1} & c I'_{n1} & -A_1 I_{n1} & -c I'_{n1} & -A_1 K_{n1} & -c K'_{n1} & 0 & 0 \\
I_{n1} & 0 & -I_{n1} & 0 & -K_{n1} & 0 & 0 & 0 \\
B \cot \psi_1 I'_{n1} & -I_{n1}(1 + A_1 \cot \psi_1) & -B \cot \psi_1 I'_{n1} & I_{n1}(1 + A_1 \cot \psi_1) & -B \cot \psi_1 K'_{n1} & K_{n1}(1 + A_1 \cot \psi_1) & 0 & 0 \\
0 & 0 & 0 & 0 & 0 & 0 & K_{n2}(1 + A_2 \cot \psi_2) & c \cot \psi_2 K'_{n2} \\
0 & 0 & A_2 I_{n2} & c I'_{n2} & A_2 K_{n2} & c K'_{n2} & -A_2 K_{n2} & -c K'_{n2} \\
0 & 0 & I_{n2} & 0 & K_{n2} & 0 & -K_{n2} & 0 \\
0 & 0 & B \cot \psi_2 I'_{n2} & -I_{n2}(1 + A_2 \cot \psi_2) & B \cot \psi_2 K'_{n2} & -K_{n2}(1 + A_2 \cot \psi_2) & -B \cot \psi_2 K'_{n2} & +K_{n2}(1 + A_2 \cot \psi_2)
\end{vmatrix} \\
\mathbf{X} = & \begin{vmatrix}
a_n^{(1)} \\
b_n^{(1)} \\
a_n^{(2)} \\
b_n^{(2)} \\
c_n^{(2)} \\
d_n^{(2)} \\
a_n^{(3)} \\
b_n^{(3)}
\end{vmatrix}
\end{aligned}$$

So, the system can be written as

$$A X = 0$$

Coefficients of the Fields of concentric helices

$$b_n^{(1)} = \frac{I_{n1} a_n^{(1)} (A_1 \cot \psi_1 + 1)}{I'_{n1} c \cot \psi_1} \quad (\text{A } 73)$$

$$a_n^{(2)} = \frac{A_1 I_{n1} a_n^{(1)} \cot \psi_1 - \frac{A_1 K_{n1} \left(\frac{I_{n1} \sigma_1}{\sigma_2} + \frac{A_1 I_{n1} \cot \psi_1 \sigma_1}{\sigma_2} \right)}{BI'_{n1}}}{A_1 I_{n1} \cot \psi_1} \quad (\text{A } 74)$$

$$b_n^{(2)} = - \frac{A - \frac{K'_{n1} c \cot \psi_1 (BI_{n1} I'_{n2} a_{n1} \cot \psi_2 - A' + A_1 BI_{n1} I'_{n2} \cot \psi_1 \cot \psi_2 - A_2 BI'_{n1} I_{n2} a_{n1} \cot \psi_1 \cot \psi_2)}{A_2 I_{n1} K_{n2} \cot \psi_2 - A_2 I_{n2} K_{n1} \cot \psi_2 + A_1 A_2 I_{n1} K_{n2} \cot \psi_1 \cot \psi_2 - A_1 A_2 I_{n2} K_{n1} \cot \psi_1 \cot \psi_2 - BI'_{n1} K'_{n2} c \cot \psi_1 + BI'_{n2} K'_{n1} c \cot \psi_1 \cot \psi_2}}{I'_{n1} c \cot \psi_1} \quad (\text{A } 75)$$

Where

$$A = I_{n1} a_{n1} + A_1 I_{n1} a_{n1} \cot \psi_1$$

$$A' = \frac{BI'_{n1} K_{n2} \cot \psi_1 (CC - DD + EE - FF)}{GG + HH - II}$$

$$CC = I'_{n2} K_{n2} a_{n1} \cot \psi_2 A_1^2 I_{n1}^2 \cot^2 \psi_1$$

$$DD = I_{n2} I'_{n2} K_{n1} a_{n1} \cot \psi_2 A_1^2 I_{n1} \cot^2 \psi_1$$

$$EE = 2I'_{n2} K_{n2} a_{n1} \cot \psi_2 A_1 I_{n1}^2 \cot \psi_1$$

$$FF = 2I_{n2} I'_{n2} K_{n1} a_{n1} \cot \psi_2 A_1 I_{n1} \cot \psi_1 + I'_{n2} K_{n2} a_{n1} \cot \psi_2 I_{n1}^2 - I_{n2} I'_{n2} K_{n1} a_{n1} \cot \psi_2 I_{n1} - BI_{n2} K'_{n2} a_{n1} c \cot \psi_2 I_{n1}^2 \cot^2 \psi_1 + BI_{n2} I'_{n2} K'_{n1} a_{n1} c \cot \psi_2 I'_{n1} \cot^2 \psi_1$$

$$GG = I_{n1} I'_{n1} K_{n2}^2 \cot \psi_1 + A_1 I_{n1} I'_{n1} K_{n2}^2 \cot^2 \psi_1 - I'_{n1} I_{n2} K_{n1} K_{n2} \cot \psi_1 + A_2 I_{n1} I'_{n1} K_{n2}^2 \cot \psi_1 \cot \psi_2 - A_1 I'_{n1} I_{n2} K_{n1} K_{n2} \cot^2 \psi_1$$

$$HH = A_1 A_2 I_{n1} I'_{n1} K_{n2}^2 \cot^2 \psi_1 \cot \psi_2 - B I_{n1}'^2 K_{n2} K'_{n2} c \cot^2 \psi_1 \cot \psi_2 - A_2 I'_{n1} I_{n2} K_{n1} K_{n2} \cot \psi_1 \cot \psi_2$$

$$II = A_1 A_2 I'_{n1} I_{n2} K_{n1} K_{n2} \cot^2 \psi_1 \cot \psi_2 + B I'_{n1} I'_{n2} K'_{n1} K_{n2} c \cot^2 \psi_1 \cot \psi_2$$

$$c_n^{(2)} = \frac{\frac{I_{n1} \sigma_1 + A_1 I_{n1} \cot \psi_1}{\sigma_2}}{B I'_{n1} \cot \psi_1} \quad (A 76)$$

$$b_n^{(3)} = -\frac{K_{n2} (A_2 \cot \psi_2 + 1) (LL + MM)}{K'_{n2} c \cot \psi_2 (NN - OO)} \quad (A 77)$$

Where

$$LL = I'_{n2} K_{n2} a_{n1} \cot \psi_2 A_1^2 I_{n1}^2 \cot^2 \psi_1 - I_{n2} I'_{n2} K_{n1} a_{n1} \cot \psi_2 A_1^2 I_{n1} \cot^2 \psi_1 + 2 I'_{n2} K_{n2} a_{n1} \cot \psi_2 A_1 I_{n1}^2 \cot \psi_1 - 2 I_{n2} I'_{n2} K_{n1} a_{n1} \cot \psi_2 A_1 I_{n1} \cot \psi_1$$

$$MM = I'_{n2} K_{n2} a_{n1} \cot \psi_2 I_{n1}^2 - I_{n2} I'_{n2} K_{n1} a_{n1} \cot \psi_2 I_{n1} - B I_{n2} K'_{n2} a_{n1} c \cot \psi_2 I_{n1}'^2 \cot^2 \psi_1 + B I_{n2} I'_{n2} K'_{n1} a_{n1} c \cot \psi_2 I_{n1}' \cot^2 \psi_1$$

$$NN = I_{n1} I'_{n1} K_{n2}^2 \cot \psi_1 + A_1 I_{n1} I'_{n1} K_{n2}^2 \cot^2 \psi_1 - I'_{n1} I_{n2} K_{n1} K_{n2} \cot \psi_1 + A_2 I_{n1} I'_{n1} K_{n2}^2 \cot \psi_1 \cot \psi_2 - A_1 I'_{n1} I_{n2} K_{n1} K_{n2} \cot^2 \psi_1 + A_1 A_2 I_{n1} I'_{n1} K_{n2}^2 \cot^2 \psi_1 \cot \psi_2$$

$$OO = -B I_{n1}'^2 K_{n2} K'_{n2} c \cot^2 \psi_1 \cot \psi_2 - A_2 I'_{n1} I_{n2} K_{n1} K_{n2} \cot \psi_1 \cot \psi_2 - A_1 A_2 I'_{n1} I_{n2} K_{n1} K_{n2} \cot^2 \psi_1 \cot \psi_2 + B I'_{n1} I'_{n2} K'_{n1} K_{n2} c \cot^2 \psi_1 \cot \psi_2$$

$$d_n^{(2)} = -\frac{B I_{n1} I'_{n2} a_{n1} \cot \psi_2 - \frac{B I'_{n1} K_{n2} \cot \psi_1 PP}{QQ} + A_1 B I_{n1} I'_{n2} a_{n1} \cot \psi_1 \cot \psi_2 - A_2 B I'_{n1} I_{n2} a_{n1} \cot \psi_1 \cot \psi_2}{A_2 I_{n1} K_{n2} \cot \psi_2 - A_2 I_{n2} K_{n1} \cot \psi_2 + A_1 A_2 I_{n1} K_{n2} \cot \psi_1 \cot \psi_2 - A_1 A_2 I_{n2} K_{n1} \cot \psi_1 \cot \psi_2 - B I'_{n1} K'_{n2} c \cot \psi_1 \cot \psi_2 + B I'_{n2} K'_{n1} c \cot \psi_1 \cot \psi_2} \quad (A 78)$$

Where:

$$PP = \left(I'_{n2} K_{n2} a_{n1} \cot \psi_2 A_1^2 I_{n1}^2 \cot^2 \psi_1 - I_{n2} I'_{n2} K_{n1} a_{n1} \cot \psi_2 A_1^2 I_{n1} \cot^2 \psi_1 + 2 I'_{n2} K_{n2} a_{n1} \cot \psi_2 A_1 I_{n1}^2 \cot \psi_1 - 2 I_{n2} I'_{n2} K_{n1} a_{n1} \cot \psi_2 A_1 I_{n1} \cot \psi_1 + I'_{n2} K_{n2} a_{n1} \cot \psi_2 I_{n1}^2 \right. \\ \left. - I_{n2} I'_{n2} K_{n1} a_{n1} \cot \psi_2 I_{n1} - B I_{n2} K'_{n2} a_{n1} c \cot \psi_2 I_{n1}'^2 \cot^2 \psi_1 + B I_{n2} I'_{n2} K'_{n1} a_{n1} c \cot \psi_2 I_{n1}' \cot^2 \psi_1 \right)$$

$$QQ = n1 I'_{n1} K_{n2}^2 \cot \psi_1 + A_1 I_{n1} I'_{n1} K_{n2}^2 \cot^2 \psi_1 - I'_{n1} I_{n2} K_{n1} K_{n2} \cot \psi_1 + A_2 I_{n1} I'_{n1} K_{n2}^2 \cot \psi_1 \cot \psi_2 - A_1 I'_{n1} I_{n2} K_{n1} K_{n2} \cot^2 \psi_1 + A_1 A_2 I_{n1} I'_{n1} K_{n2}^2 \cot^2 \psi_1 \cot \psi_2 \\ - B I_{n1}'^2 K_{n2} K'_{n2} c \cot^2 \psi_1 \cot^2 \psi_2 - A_2 I'_{n1} I_{n2} K_{n1} K_{n2} \cot \psi_1 \cot \psi_2 - A_1 A_2 I'_{n1} I_{n2} K_{n1} K_{n2} \cot^2 \psi_1 \cot \psi_2 + B I'_{n1} I'_{n2} K'_{n1} K_{n2} c \cot^2 \psi_1 \cot \psi_2$$

$$a_n^{(3)} = \frac{RR+SS I'_{n1} \cot^2 \psi_1}{TT-BI'_{n1}{}^2 K_{n2} K'_{n2} c \cot^2 \psi_1 \cot \psi_2 - A_2 I'_{n1} I_{n2} K_{n1} K_{n2} \cot \psi_1 \cot \psi_2 - A_1 A_2 I'_{n1} I_{n2} K_{n1} K_{n2} \cot \psi_2 \cot^2 \psi_1 + BI'_{n1} I'_{n2} K'_{n1} K_{n2} c \cot^2 \psi_1 \cot \psi_2} \quad (\text{A } 79)$$

$$\begin{aligned} RR &= I'_{n2} K_{n2} a_{n1} \cot \psi_2 A_1^2 I_{n1}^2 \cot^2 \psi_1 - I_{n2} I'_{n2} K_{n1} a_{n1} \cot \psi_2 A_1^2 I_{n1} \cot^2 \psi_1 + 2 I'_{n2} K_{n2} a_{n1} \cot \psi_2 A_1 I_{n1}^2 \cot \psi_1 - 2 I_{n2} I'_{n2} K_{n1} a_{n1} \cot \psi_2 A_1 I_{n1} \cot \psi_1 \\ SS &= I'_{n2} K_{n2} a_{n1} \cot \psi_2 I_{n1}^2 - I_{n2} I'_{n2} K_{n1} a_{n1} \cot \psi_2 I_{n1} - B I_{n2} K'_{n2} a_{n1} c \cot \psi_2 I_{n1}^2 \cot^2 \psi_1 + B I_{n2} I'_{n2} K'_{n1} a_{n1} c \cot \psi_2 \\ TT &= I_{n1} I'_{n1} K_{n2}^2 \cot \psi_1 + A_1 I_{n1} I'_{n1} K_{n2}^2 \cot^2 \psi_1 - I'_{n1} I_{n2} K_{n1} K_{n2} \cot \psi_1 + A_2 I_{n1} I'_{n1} K_{n2}^2 \cot \psi_1 \cot \psi_2 - A_1 I'_{n1} I_{n2} K_{n1} K_{n2} \cot^2 \psi_1 + A_1 A_2 I_{n1} I'_{n1} K_{n2}^2 \cot^2 \psi_1 \cot \psi_2 \end{aligned}$$

Where the $a_n^{(1)} = a_{n1}$ is defined. Normalizing constants so that the relationship is valid:

$$\sqrt{a_n^{(1)2} + b_n^{(1)2} + a_n^{(2)2} + b_n^{(2)2} + c_n^{(2)2} + d_n^{(2)2} + a_n^{(3)2} + b_n^{(3)2}} = 1 \quad (\text{A } 80)$$

Then all the constants that determine the components of the fields are obtained.

REFERENCES

[RD.01]	SATELLITE COMMUNICATIONS PAYLOAD AND SYSTEM - Teresa M. Braun – Third edition – 2012 – Wiley
[RD.02]	SATELLITE COMMUNICATIONS SYSTEMS - Gerard Maral – Fifth Edition – 2009 – Wiley
[RD.03]	Vander Haagen, G.A., "The electrical tuning of helical resonators", microwave J., Vol. 10, 1967
[RD.04]	Solfrey, W., "Wave propagation in helical wire", J. Appl. Phys., Vol. 22, 1951
[RD.05]	Pierce, J., "Travelling-Wave Tubes," The Bell System Technical Journal, Vol. 29, No. 1, pp. 1–59
[RD.06]	MacAlpine, W.W., R.O Schildknecht, "Coaxial Resonator with Helical Inner Conductor" Proc. IRE, Vol. 47, 1959
[RD.07]	Zverev, A.I., and H.J. Blinchikoff, "Realization of a Filter with Helical Components", IRE Trans. Comp. Parts, Vol. CP-8, 1961
[RD.08]	L. F. Lind and R. E. Massara, "Generalised interdigital helical filter," Electronics Letters, vol. 8, p. 525, 1972.
[RD.09]	Dishal, M., "Alignment and Adjustment of Synchronously Tuned Multiple Resonant Circuit Filters", Elect. Commun., 1952
[RD.10]	Cohen, M., "Design Techniques Utilizing Helical Line Resonator", Microwave J., Vol. 8, 1965
[RD.11]	Cutler, C.C., "Experimental Determination of Helical Wave properties", Proc. IRE, Vol. 36, 1948
[RD.12]	Sichak, W., "Coaxial Line with Helical Inner Conductor", Proc. IRE, Vol. 42, 1954
[RD.13]	Bryant, J.H., "Some Wave properties of Helical Conductors", Elect. Commun., Vol. 31, 1954
[RD.14]	Miley, D.J., and J.B. Beyer, "Field Analysis of helical resonators with constant bandwidth filter applications", IEEE Trans. Parts, Material and Packaging, Vol. PMP-5, 1969
[RD.15]	B. Rawat and R. Miller, "Improved design of a helical resonator filter for 450-500 MHz band land mobile communication," IEEE Transactions on Vehicular Technology, vol. 33, no. 1, pp. 32–36, 1984.
[RD.16]	J. Everard, K. Cheng, and P. Dallas, "High-Q helical resonator for oscillators and filters in mobile communications systems," Electronics Letters, vol. 25, p. 1648, 1989.
[RD.17]	Filters with Helical and Folded Helical Resonators – Peter Vizmuller – First edition – 1987 – Artech House Microwave Library
[RD.18]	Filter Design for Satellite Communications: Helical Resonator Technology - Efstratios Doumanis, George Goussetis, Savvas Kosmopoulos – First edition – 2014 – Artech House Microwave Library
[RD.19]	R.S. Kwok ; S.J. Fiedziuszko, Dual-mode helical resonators; IEEE Microwave Theory and Techniques Society, Page(s): 474 - 477
[RD.20]	R.E. Hayes, Higher Order Modes in Coupled Helices (Correspondence), IEEE Page(s): 119 – 120
[RD.21]	J. S. Cook, R. Kompfner, C. F. Quate, "Coupled helices", Bell Sys. Tech. J., vol. 35, 1956
[RD.22]	J. A. Straton, Electromagnetic Theory, N. Y., New York: McGraw-Hill Book Co. - 1941.
[RD.23]	S.F. Paik, "Design formulas for helix dispersion shaping", IEEE Transactions on Electron Devices, Vol. 16, 1969
[RD.24]	Microwave Engineering – David M. Pozar – Fourth Edition – 2011 -Wiley
[RD.25]	Numerical Techniques in Electromagnetics – Matthew N.O. Sadiku – Second edition – 2000 – CRC Press
[RD.26]	Handbook of Filter Synthesis – Anatol L. Zverev – First edition – 2005 - Wiley

[RD.27]	Atia, A.E., and A.E. Williams, "Measurements of Intercavity Couplings", IEEE Trans. Microwave Theory Tech. Vol. MTT-23, 1975
[RD.28]	Microstrip Filters for RF / Microwave Applications - Jia-Shen G. Hong, M. J. Lancaster – Second edition – 2001 – Wiley
[RD.29]	Microwave Filters: Fundamentals, Design and Applications - Cameron, Kudsia, Mansour – First edition – 2007 – Wiley
[RD.30]	A John B. Ness, Unified Approach to the Design, Measurement, and Tuning of Coupled-Resonator Filters IEEE transactions on microwave theory and techniques, vol. 46, no. 4
[RD.31]	Ming Yu, "Power-Handling Capability for RF Filters", IEEE Microwave magazine, 2007
[RD.32]	S.J.G Strijk, "ESA/ESTEC Multipactor calculator manual / help file", (issue 1.6), ESA/ESTEC Noordwijk, The Netherlands, April 2007
[RD.33]	E. Dumanis, G. Goussetis, W. Steffe, D. Maiarelli, S.A. Kosmopoulos, "Helical Resonator Filters with Improved Power Handling Capabilities for Space Applications," IEEE Microwave and Wireless Components Letters, Vol. 20, No. 11, pp. 568-600, November 2010.
[RD.34]	G. Salza, Savvas A. Kosmopoulos, George Goussetis "PSEUDO-ELLIPTIC HELICAL RESONATOR FILTERS WITH IMPROVED POWER HANDLING CAPABILITY" ESA Contract No 4000107834/13/NL/CO
[RD.35]	G. Salza, G. Goussetis, E. Dumanis, C. Vicente, M. Reglero, M. Taroncher, V. Boria, J. Galdeano, M. Guglielmi, S. Kosmopoulos, "Helical Resonator with Modulated Radius for Improved Multipactor Threshold: Numerical and Experimental Results," 46 European Microwave Week, London, 3-7 October 2016
[RD.36]	Rodney M. Vaughan, "Multipactor", IEEE Trans. Electron Devices, vol. 35, No 7, July 1988
[RD.37]	A. Dexter, R. Seviour, "Rapid generation of multipactor charts by numerical solution of the phase equation", Journal of Physics D: Applied Physics, vol. 38, 2005.
[RD.38]	Technical Datasheet Rexolite - www.laminatedplastics.com/rexolite.pdf
[RD.39]	B. J. McMurtry, "Fundamental interaction impedance of a helix surrounded by a dielectric and a metal shield", IRE Trans. Electron Devices, vol. ED-9, 1962.
[RD.40]	Khosro Shamsaifar, Troy Rodriguez, and James Haas, "High-Power Combline Diplexer for Space", IEEE transactions on microwave theory and techniques, Year 2013
[RD.41]	http://www.microwavefilter.com/MCcomblin.htm
[RD.42]	Rodney M. Vaughan, "Multipactor", IEEE Trans. Electron Devices, vol. 35, No 7, July 1988
[RD.43]	David A. Constable; Paul McElhinney; Chris Lingwood; Graeme Burt; Giuseppe Salza; George Goussetis, "Analytical and numerical simulation of multipactor within a helical resonant filter", Eighteenth International Vacuum Electronics Conference (IVEC), 2017
[RD.44]	A. A. San Blas; B. Gimeno; V. E. Boria; E. Bronchalo, "Analysis of the multipactor effect by means of the 3D BI-RME method", Progress In Electromagnetics Research Symposium, 2017
[RD.45]	"Carlos Vicente, ""Multipactor and corona discharge: Theoretical fundamentals and analysis with CST and SPARK3D software tools""
[RD.46]	IEEE International Symposium on Electromagnetic Compatibility & Signal/Power Integrity (EMCSI), 2017"
[RD.47]	http://riccimicrowave.com/portfolio_page/waveguide_filters/
[RD.48]	http://www.klfilterwizard.com